NASA CR 165250
PWA-5684-19

NASA

(NASA-CR-165250) COMBUSTOR LINER DURABILITY ANALYSIS Final Report (Pratt and Whitney Aircraft Group) 84 p HC A05/MF A01 CSCL 21E

N81-17079

Unclas
G3/07 41090

COMBUSTOR LINER DURABILITY ANALYSIS

by

V. MORENO

February 1981

UNITED TECHNOLOGIES CORPORATION
Pratt & Whitney Aircraft Group
Commercial Products Division

Prepared for

NATIONAL AERONAUTICS AND SPACE ADMINISTRATION
NASA-Lewis Research Center
Contract NAS3-21836

1. Report No.	2. Government Accession No.	3. Recipient's Catalog No.
NASA CR-165250		

4. Title and Subtitle	5. Report Date
Combustor Liner Durability Analysis	February 1981
	6. Performing Organization Code

7. Author(s)	8. Performing Organization Report No.
V. Moreno, Program Manager	PWA-5684-19
	10. Work Unit No.

9. Performing Organization Name and Address	11. Contract or Grant No.
United Technologies Corporation Pratt & Whitney Aircraft Group - CPD East Hartford, Connecticut 06108	NAS3-21836
	13. Type of Report and Period Covered
12. Sponsoring Agency Name and Address	Final Report
National Aeronautics and Space Administration Lewis Research Center 21000 Brookpark Road, Cleveland, Ohio 44135	14. Sponsoring Agency Code

15. Supplementary Notes

NASA Project Manager, Dr. G. R. Halford; Technical Advisor, Mr. A. Kaufman,
NASA-Lewis Research Center
Cleveland, Ohio 44135

16. Abstract

The results of the 18 month Combustor Liner Durability Analysis Program (NAS3-21836) performed by Pratt & Whitney Aircraft are presented. The objective of the program is to evaluate the use of advanced three-dimensional transient heat transfer and non-linear stress-strain analyses for modeling the cyclic thermomechanical response of a simulated combustor liner specimen. Cyclic life prediction technology for creep/fatigue interaction is evaluated for a variety of state-of-the-art tools for crack initiation and propagation. The sensitivity of the initiation models to a change in the operating conditions is also assessed.

17. Key Words (Suggested by Author(s))	18 Distribution Statement
o Combustor Liner o Thermomechanical Fatigue o Non-linear Analysis o Life Prediction	

19 Security Classif. (of this report)	20 Security Classif. (of this page)	21 No. of Pages	22 Price*
Unclassified	Unclassified	87	

* For sale by the National Technical Information Service, Springfield, Virginia 22161

FOREWORD

The work described in this report was performed by Pratt & Whitney Aircraft Group, Commercial Products Division for the National Aeronautics and Space Administration, under Contract NAS3-21836. The Principal Investigator was Mr. V. Moreno, with technical assistance provided by Mr. G. J. Meyers and Mr. B. C. Schlein. The NASA Technical Project Manager was Dr. G. R. Halford, with Mr. A. Kaufman serving as Technical Advisor.

TABLE OF CONTENTS

	Page
1.0 Summary	1
2.0 Introduction	2
3.0 Task I - Hot Section Component Selection	4
3.1 Combustor Liner Rig	4
3.2 Cyclic Thermal Loading and Failure Data	4
4.0 Task II - Heat Transfer and Stress-Strain Analysis	10
4.1 Heat Transfer Analysis	10
4.1.1 Thermal Analysis Method	10
4.1.2 Model Description	10
4.1.3 Thermal Boundary Conditions	10
4.1.4 Results of Heat Transfer Analysis	12
4.2 Stress-Strain Analysis	13
4.2.1 Non-Linear Structural Analysis Method	13
4.2.2 Louver Finite Element Model	14
4.2.3 Material Model Strategy	17
4.2.4 Results of Three Dimensional Non-Linear Analysis	19
4.2.5 Thermomechanial Specimen Test	22
4.2.6 Linear Elastic Analysis	24
5.0 Task III - Cyclic Life Prediction and Sensitivity Analysis	54
5.1 Introduction	54
5.2 Crack Initiation Analyses	54
5.2.1 Strain Range Partitioning Method	54
5.2.2 Pratt & Whitney Aircraft - Commercial Products Division Combustor Life Prediction Method	56
5.2.3 Continuous Damage Method	58
5.3 Crack Propagation Analysis	63
5.4 Sensitivity Analysis	64
6.0 Discussion of Results and Conclusions	74
7.0 References	77
Distribution	79

1.0 SUMMARY

The results of the 18 month Combustor Liner Durability Analysis Program (NAS3-21836) performed by Pratt & Whitney Aircraft are presented. The objective of the program is to evaluate the use of advanced three-dimensional transient heat transfer and non-linear stress-strain analyses for modeling the thermomechanical response of a simulated combustor liner specimen. Cyclic life prediction technology for creep/fatigue interaction is evaluated for a variety of state-of-the-art tools for crack initiation and propagation. The sensitivity of the initiation models to systematic changes in the operating conditions is also assessed.

The selected component for the program is a simulated combustion chamber outer liner. Testing under accelerated cyclic thermal loading provided the structural response and failure data for comparison with the analytical simulations.

Transient and steady state three dimensional heat transfer analyses were conducted using a finite difference solution. Good correlation with measured temperature response was obtained. The greatest area of uncertainty in the analysis was in the calculation of the heat transfer coefficients. Modification of the initial values was required to match the steady state temperature distribution.

Results of the transient heat transfer analysis were used to create an incremental temperature file for the three dimensional non-linear finite element analysis of a segment of the combustor liner.

The three dimensional non-linear finite element analysis was conducted with the MARC computer code. The analysis used existing time independent classical plasticity theory with a Von Mises yield surface and the combined (isotropic-kinematic) hardening rule. A constant rate creep model was used to account for instantaneous time dependent plasticity effects. Both the plasticity and creep models were calibrated to isothermal Hastelloy X material response data. Results of the analysis indicates that this material model does not accurately predict the stress-strain response under thermomechanical loading conditions. The prediction shows continued cyclic hardening while experimental data suggests that the response is stable after several loading cycles.

Three existing state-of-the-art crack initiation models were considered for prediction of the combustor liner fatigue life. The Strain Range Partitioning method overpredicted the observed cracking by more than a factor of 2. This calculation is sensitive to the definition of the generic fatigue curves and the prediction of the inelastic strain components. A Pratt & Whitney Aircraft (Commercial Products Division) developed Combustor Life Prediction Method also overpredicted the crack initiation life. This method is similar to Strain Range Partitioning but differs in the definition of the inelastic strain components and the basic fatigue curves. In actual design practice, this procedure is used along with extensive experimental and field service data to provide a realistic estimate of overall service life. The third method, the Continuous Damage Approach, underpredicted the observed cracking by more than a factor of 2. It does not appear to be suited to the prediction of thermomechanical fatigue of highly rate dependent materials (e.g. Hastelloy X).

A linear elastic fracture mechanics approach is used to predict the crack growth observed in the combustor liner. All calculations predict a slower crack growth rate than observed.

2.0 INTRODUCTION

The overall operating cost of the modern gas turbine engine is significantly affected by the durability and efficiency of the major hot section components. These are the combustor and turbine structures in the engine. During each flight cycle, these components undergo large thermally induced stress and strain cycles which include significant amounts of creep and relaxation. Primary responsibilities of the combustor, in the engine cycle, are gas temperature level and pattern control, required for efficient turbine operation, and exhaust emission control at the various flight operating conditions. These goals are accomplished by the precise metering of air throughout the combustor structure. The high pressure and high combustion gas temperature characteristic of this environment require that the combustor liner be cooled for durability. These requirements for control of exit gas temperature, emissions, and metal temperature generate an intense competition for utilization of combustor airflow. The more aggressive performance, efficiency, and emission goals set for current and future engines emphasize the need for development of durable combustor structures which can operate with reduced levels of cooling air. This requires detailed knowledge of the operating environment and the ability to accurately predict structural response for these loadings.

Current structural technology activities for hot section component design and life prediction seek to exploit major advances that have been made in nonlinear structural analysis capabilities. Large, general purpose finite element programs such as the MARC code have been developed expressly for nonlinear structural analysis. These programs involve sophisticated computational algorithms and advanced finite element formulations, yet rely on material models whose applicability to the hot section component environment is questionable. Of primary concern is the response of materials to cyclic loading involving simultaneous creep and plastic behavior. A major need is the development of appropriate hot section component structural response data, sufficient to evaluate the advanced structural analysis capabilities with emphasis on the effectiveness of the material models.

Adequate prediction of the nonlinear stress (strain) response of the hot section component also requires good prediction of the thermal load history. Such predictions must be capable of modeling both spatial and temporal response, suitable for life prediction purposes. Creep-fatigue life prediction for hot section components is currently calibrated to simplified models for predicting the local cyclic hysteresis response to thermal-mechanical loading. Further, these models generally lack calibration to well-controlled hot section component fatigue test data. Thus, a second major need is for the evaluation of life prediction models for creep-fatigue response of hot section components using the results of nonlinear stress (strain) analysis and well-controlled component response data.

The use of advanced nonlinear models for three-dimensional stress (strain) analysis of hot section components poses major burdens in terms of engineering and computing times. Design of these components requires cost effective, shortcut tools which can evaluate the effects of design changes on component

life without the use of full three dimensional analyses. Calibration of such tools is required by reference to both the nonlinear finite element results and the component response data.

The 18 month program addressed a critical issue in the development of advanced life prediction technologies -- the need to establish the limitations of current nonlinear structural modeling and creep/fatigue life prediction schemes for a major hot section component. In order to make a critical evaluation of these tools, a well-controlled component simulation test served as the calibration data source for the program. The component test uses a prototypical combustor liner specimen constructed in an identical configuration with current combustor liners in engine service. The combustor liner rig data and supporting isothermal constitutive/fatigue data has been generated under existing Pratt & Whitney Aircraft company-funded programs and made available for use in this contract.

3.0 TASK I - HOT SECTION COMPONENT SELECTION

3.1 Combustor Liner Rig

At Pratt & Whitney Aircraft, simulated combustor liners have been evaluated in a specially constructed experimental rig. Cyclic engine level temperatures and thermal gradients are generated on simulated combustor liners by a 250 kW, 450 kHz induction heater used in conjunction with controlled cooling air temperature and flow rate. A schematic drawing of the rig showing the principal components is shown in Figure 1.

Cooling air is supplied to the lower plenum of the rig from a non-vitiated upstream air heater at temperatures up to 538°C (1000°F). The air in the lower plenum is then directed through flow straightener plates to the upper flow divider plate which permits ratioing shroud-side airflow to hot-side flow. Shroud-side air provides the total cooling air supplied to the specimen which is discharged into the hot-side flow annulus and then, together with the metered hot-side flow, ejected to ambient.

The specimen is inductively heated by power supplied from a 250 kW, 450kHz induction heater. High frequency (450 kHz) heating has been chosen to minimize the depth of penetration of the induced current (heat) in the test specimen to best simulate the thermal surface loadings (radiative/conductive) experienced by combustor liners in engine operation.

The induction coil is supported on a framework of glass-bonded mica which is transparent to the induction field. A 48.3 cm (19 in) diameter quartz cylinder (also transparent to the field) is positioned between the coil and the specimen to form the inner boundary of the hot-side flow annulus. The quartz cylinder is retained in position by a 45.4 kg (100 lb). quartz cover. The test specimen selected for this program simulates a combustor outer liner and incorporates five (5) sheet metal Hastelloy-X louvers. Prior to testing, the test section, transition pieces and top shroud cover are assembled as a unit. This provides a permanent instrumentation installation and facilitates frequent inspection during testing. The assembled louver test specimen and cover are shown in Figure 2A. Fine wire chromel-alumel thermocouples are used to determine temperature distributions during testing. Typical thermocouple locations are shown in Figure 2B.

3.2 Cyclic Thermal Loading and Failure Data

For this program, results of a single cyclic test were used to provide the temperature and failure data for the thermal/structural analysis and life predictions. All information from the test was taken from the third (center) louver of the test specimen.

The test program consisted of a ninety (90) second thermal cycle in which the rig cooling air was maintained at a constant temperature and flow rate (504°C-2.5 kg/sec (940°F-5.5 lb./sec.)) while cycling power from the induction heater. A representative transient and steady state temperature distribution measured on the center (third) louver is shown in Figure 3. The

cycle consists of a twenty (20) second transient from an isothermal (504°C (940°F)) to maximum temperature distribution, a forty (40) second steady state portion, and a cool down back to the original isothermal condition.

During the testing, a maximum circumferential temperature difference of 44°C (80°F) was recorded at any time point in the cycle. For purposes of the thermal and structural analyses, measurements were averaged to provide a circumferentially uniform temperature profile.

A total of 1730 cycles were accumulated on the test specimen. Inspection for cracking using eddy current and fluoropenetrant (zyglo) techniques started at cycle 500 and continued in intervals of 125 or 250 cycles. The accepted limit of the smallest detectable crack that the eddy current method can reliably determine on the test specimen was 0.0254 cm (0.010 in). Once the location of a crack was determined, crack lengths were measured using the zyglo technique.

At cycle 1000, detectable cracks were discovered at the edge of the louver lip. Subsequent cycling and inspection revealed additional crack initiation origins at various circumferential locations at the edge of the lip, while earlier discovered cracks showed an axial propagation growth mode. A typical crack location observed during testing is shown in Figure 4. Representative crack length data for four crack locations are shown in Figure 5. No other crack initiation locations were observed during the test. Metallurgical examination of the fracture surfaces revealed predominantly a transgranular crack growth mechanism. Oxidation of the surfaces prevented further examination of the crack behavior.

Based on these results, axial lip cracking was identified as the key failure mechanism and location which would be addressed by the structural analysis and life prediction.

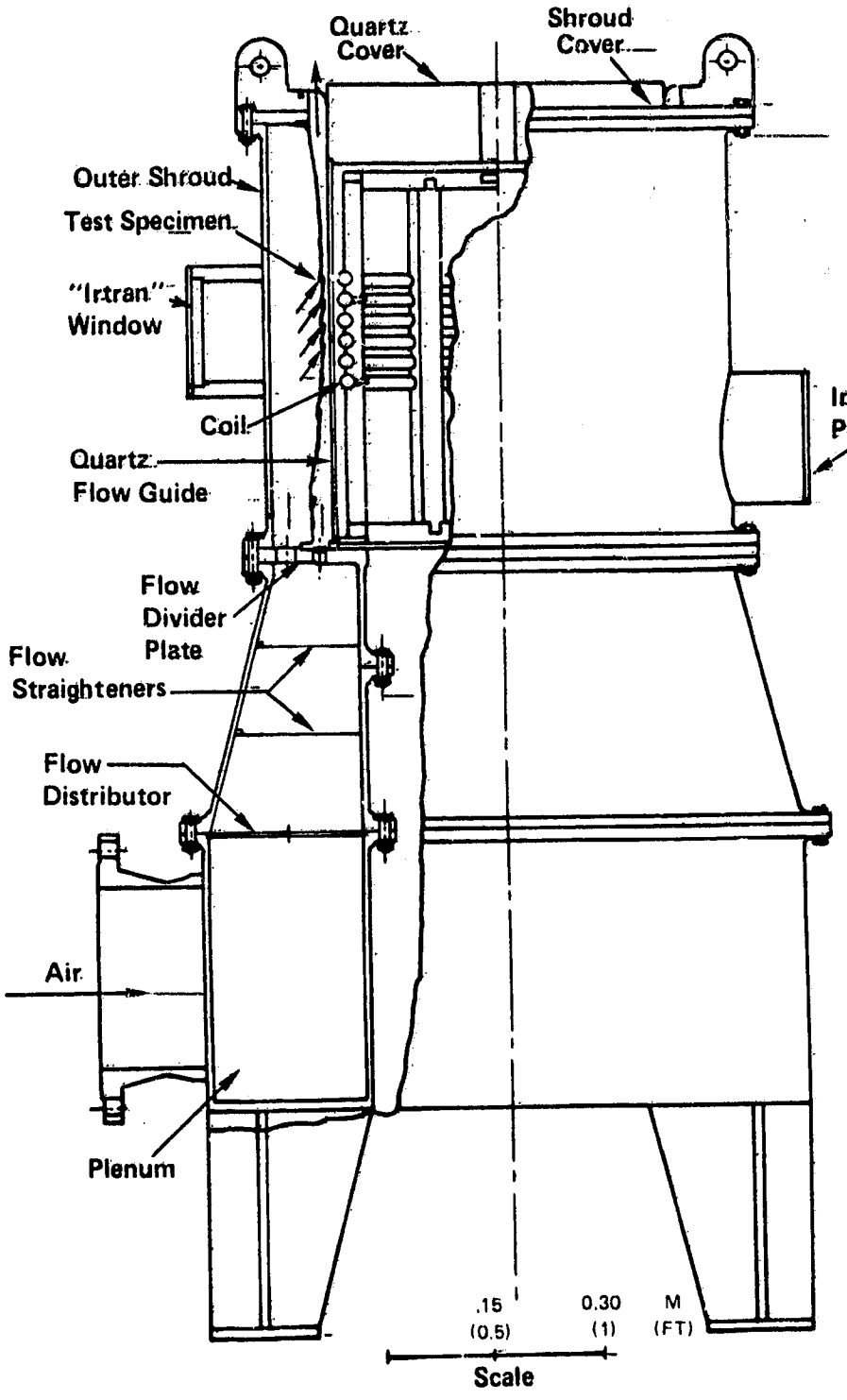

Figure 1 Combustor Liner Induction Heated Test Rig

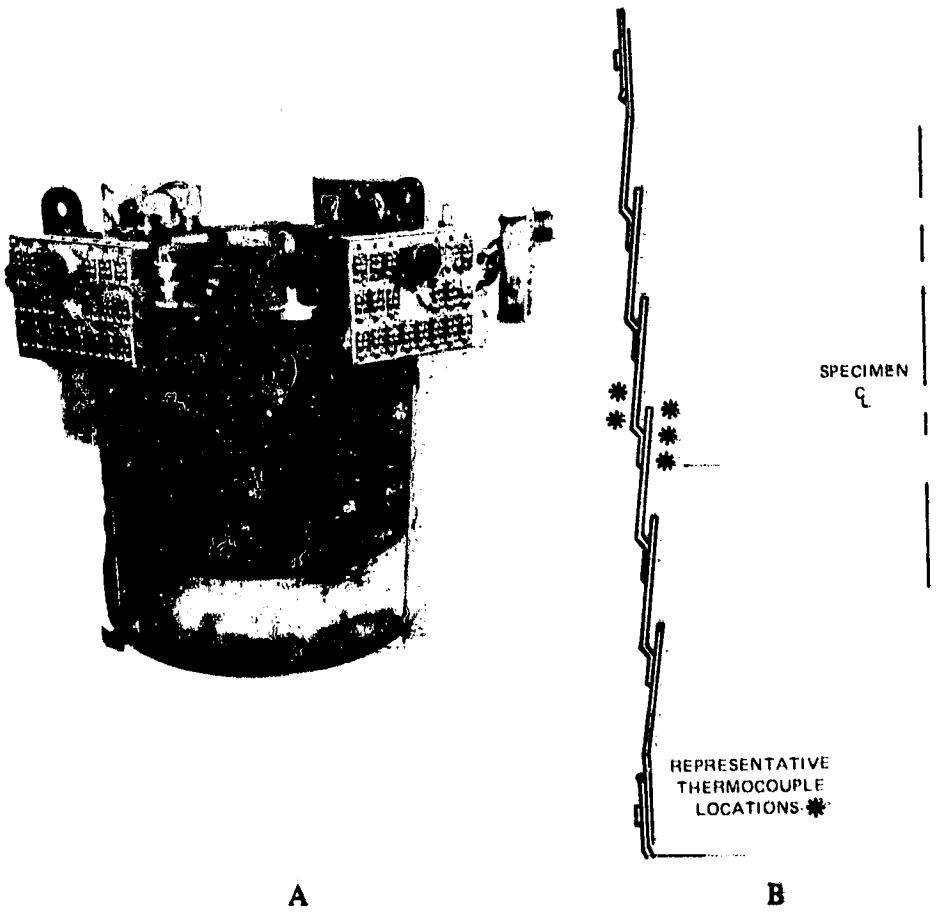

Figure 2 Assembled Liner Test Specimen and Cover (A) and 5-Louver Test Section (B)

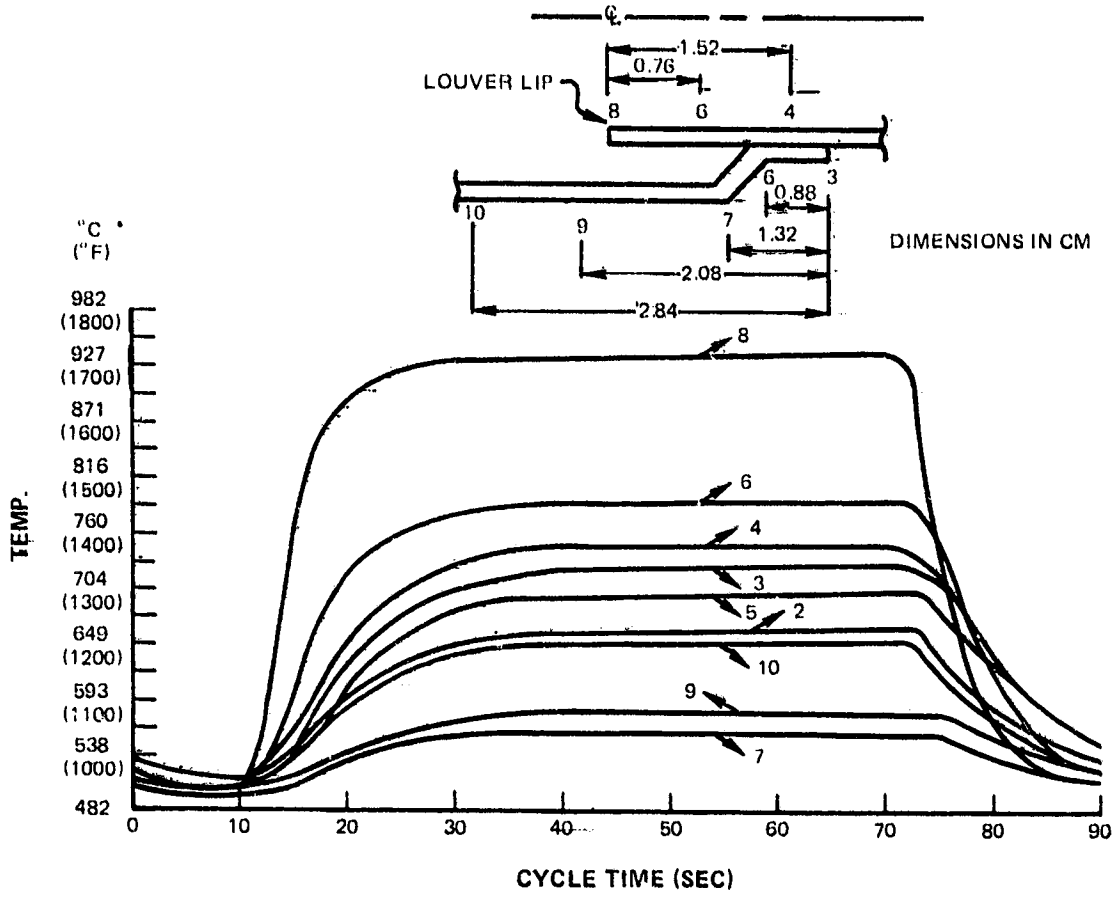

Figure 3 Measured Thermal Response

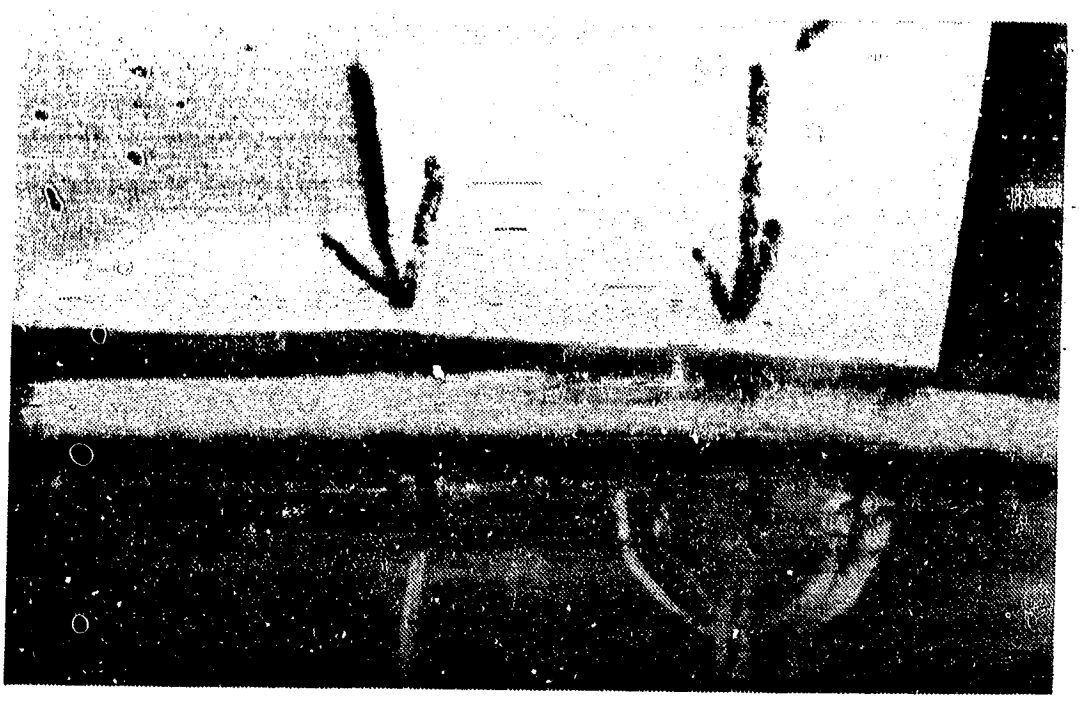

Figure 4 Combustor Louver Lip Cracks

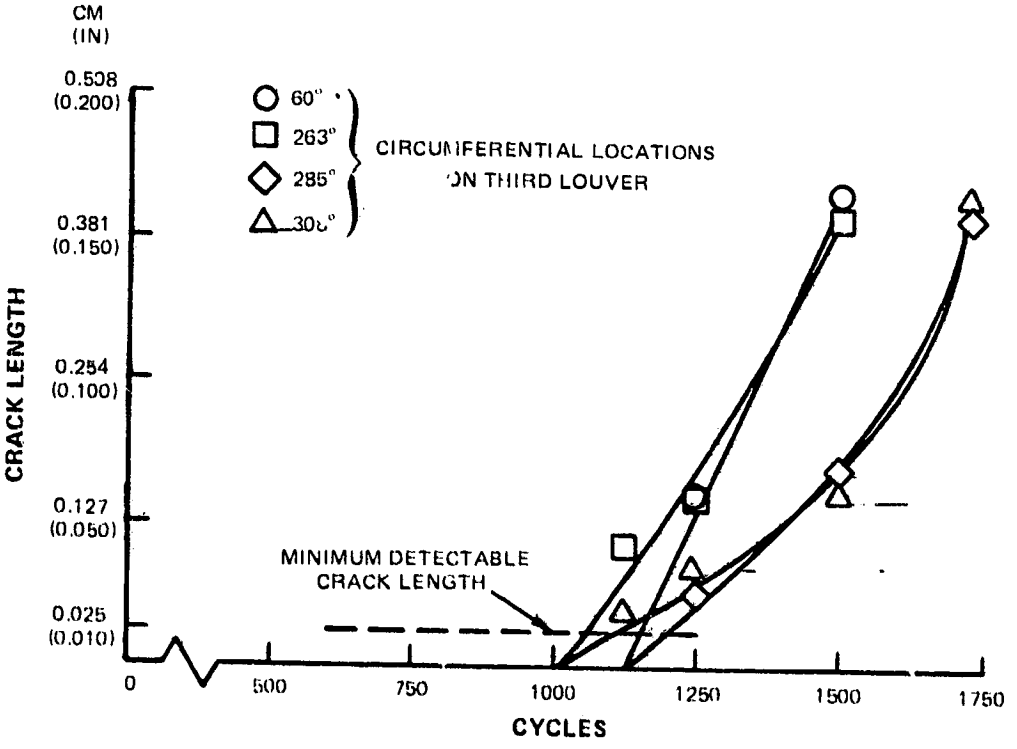

Figure 5 Crack Initiation and Propagation Data

4.0 TASK II - HEAT TRANSFER AND STRESS-STRAIN ANALYSIS

4.1 Heat Transfer Analysis

4.1.1 Thermal Analysis Method

Transient three-dimensional heat transfer analysis of the induction rig louver test specimen was conducted to provide detailed temperature information for the structural analysis and life prediction portions of the program. The analysis was performed using a Pratt & Whitney Aircraft developed thermal analysis system. The major elements of this system include a geometric breakup preprocessor which provides a discretization of a section of the louver into a series of individual thermal elements, whose properties are associated with a centroidal nodal point. A boundary condition preprocessor specifies environmental temperature, heat loads, and heat transfer coefficients along the surfaces of the model. For transient thermal analyses, both the internal properties at the nodes (thermal conductivity, specific heat and heat generation) and the external boundary conditions (film coefficients, environmental temperature, fluid temperature, fluid flow rates and heat generation) were specified as functions of time. The temperature at the nodes was then obtained through a finite difference solution of the heat balance equation at each internal point. Surface temperatures were determined from the internal temperature solutions and the local environmental conditions. Compatibility with the structural finite element model (discussed in section 4.2.2) was maintained, to a large extent, to ensure accurate detailed temperature distributions in areas of rapidly changing temperature gradients. The interpolation of the predicted temperatures onto the structural analysis map is discussed in section 4.2.2.

4.1.2 Model Description

The discretized section of the third louver is shown in Figure 6. The size and dimensions of the model were established based on the closest geometric symmetry planes (to minimize computer run times) and the fact that the measured circumferential temperature distributions in the louver lip were quite uniform. The model contains 496 internal nodes in two layers per sheet metal thickness. The nodal density in the lip region and around the cooling holes is higher than the remainder of the model.

In the weld region, perfect contact between the upper and lower sheets is assumed over the middle half of the weld region (0.53 cm (0.21 in)). An air gap is assumed to separate the upper and lower sheet nodes over the initial and final 0.22 cm (0.085 in) in the weld region.

4.1.3 Thermal Boundary Conditions

Convection

There is convective heat loss from the test specimen to the cooling air around the entire contour, including cooling holes. The only exception is at the end points of the model, where the actual test specimen is connected to up and

downstream louvers. In order to provide a continuous conduction path without having to model all the louvers in the test specimen, the corresponding upstream and downstream nodes are thermally connected.

Convective heat transfer coefficients for the hot and cold sides, lip cavity and cooling holes were calculated with the channel flow equation:

$$N_{NU} = .023\ N_{Re}^{0.8} N_{PR}^{0.3}$$

where N_{NU} = Nussult number
N_{PR} = Prandtl number
N_{Re} = Reynolds number

The hot side coefficient was based upon the cooling flow and slot dimensions determined by the distance between the hot side of the specimen and the quartz liner. The heat transfer on the cold side of the lip is enhanced by the impingement flow. An empirically determined cross flow impingement correlation was used to calculate the heat transfer coefficients in this region.

Radiation

In addition to the convective heat transfer, the upper and lower surface nodes radiate to the rig walls at the cooling temperature. The shape factor was calculated from the equation for concentric cylinders. The emissivity of the test specimen and outer rig wall was assumed to be 0.8 while the quartz inner wall was taken as 0.9. No radiation is assumed from one part of the model to the other, such as within the lip cavity.

Heat generation was assumed to be circumferentially uniform. Therefore, there was no heat transfer into or out of the model in a circumferential direction. The only circumferential variation introduced is by the cooling hole geometry.

Power Input

Determination of the heat flux on the louver was accomplished by a separate experiment. With the cooling air turned off, the specimen was subjected to a rapid step increase in power from the induction heater. A high speed recorder was used to monitor the initial thermocouple response. By assuming no heat loss from the specimen at the thermocouple location, either through convection or conduction, the rate of temperature rise was related to the heat flux by:

$$q = \rho c_p \ell \frac{dT}{d\theta}$$

where c_p = metal heat capacity (joule/kg ^{o}C)
q = heat flux (WATT/m^2)
T = metal temperature (^{o}C)
ℓ = metal thickness (cm)
θ = time (sec)
ρ = metal density (kg/m^3)

The measured heat flux values from the experiment were then used to calculate a flux distribution along the louver during the actual cyclic test. This distribution is shown in Figure 7. In the thermal analysis, the heat flux was introduced to the specimen through the hot side surface nodes. This is a good approximation of high frequency induction heating where the power input falls rapidly with distance into the specimen.

The variation of input power (heat flux) with time for the cyclic fatigue test was controlled by a DATATRAK system. This variation with time is shown in Figure 8. During the transient heat transfer analysis the flux was applied in a similar manner.

4.1.4 Results of Heat Transfer Analysis

The heat transfer analysis of the louver section was completed in two stages. Initially, a steady state calculation was performed using the heat transfer coefficients and heat flux values determined by the methods discussed in section 4.1.3. These results indicated that the predicted temperatures were cooler than the averaged thermocouple data. The greatest difference between the prediction and the data at any one location was 36°C (65°F). In this analysis, the greatest degree of uncertainty was associated with the prediction of the heat transfer coefficients. Since greater accuracy was required for the structural analysis and life prediction, modification of the initial heat transfer coefficient values was made to improve the agreement. A local average increase of 50% over the originally computed values was required to match the measured temperatures. The final distribution of heat transfer coefficients used in the analysis is shown in Figure 9. A comparison of the steady state prediction and thermocouple data is shown in Figure 10. The distribution shows a large temperature gradient along the outer half of the lip length and a comparable temperature difference between the weld and colder regions in the area of the cooling holes.

For the transient analysis, the modified heat transfer values were assumed to remain constant throughout the transient cycle. This is a reasonable assumption since the cooling air temperature and flow rate remained constant during the cycling. The comparison of the predicted transient temperature response and the measured data is shown in Figure 11. The analysis accurately predicts the transient response at all locations within the louver. The major features of the thermal cycle include the maximum temperature gradient occurring early in the cycle (10 sec.) and the inverse temperature gradient between the edge of the louver lip and the weld regions during the cool down portion of the cycle. After the initial heatup on cycle 1, all subsequent thermal cycles were predicted to be identical.

The final results of the transient heat transfer solution were used to create an incremental temperature file for the structural analysis.

4.2 Stress-Strain Analysis

4.2.1 Non-Linear Structural Analysis Method

The MARC general purpose finite element program (Reference 1) was used to predict the response of the louver component to the thermal and mechanical loads. In evaluating the response the program assumes that the loading history is divided into a number of incrementally applied loading steps. Each load step is then sequentially analyzed as a linear problem using an appropriate stiffness matrix and load vector.

The plasticity algorithm in MARC uses a tangent stiffness approach, in which the stiffness matrix is updated and reassembled for every plastic loading increment. An iterative scheme is then used to calculate the response of the structure to each individual load increment. When the strains used to estimate the stiffness matrix in the assembly phase are equal, within a user specified tolerance, to the strains obtained in the solution phase, the iteration is terminated and the program proceeds to the next loading increment. If convergence is not obtained within a number of cycles specified by the user, the program will terminate with an appropriate error message. In order to ensure that the solution does not drift away from a state of equilibrium as loading progresses, the applied incremental load vector, ΔP, is modified by the addition of a residual load correction vector, P-I. This residual load vector is obtained by taking the sum of the internal reactions, I, and subtracting this vector from the total external load vector, P. The residual load vector from the (n-1)th increment is then used to augment the applied incremental load vector in the nth increment.

For general use in structures undergoing small deformation, the program uses the Prandtl-Reuss stress-strain equations of classical plasticity with a Von-Mises yield surface. The yield surface may be assumed to expand isotropically using the ISOTROPIC option. This option allows the material to harden, but due to the equality of the yield condition for tension and compression, it does not allow for a Bauschinger effect. The KINEMATIC option allows the yield surface to translate without expansion but predicts a closed hysteresis loop after the first cycle under strain control. The COMBINED hardening option allows the yield surface to expand and translate and was considered as the best model to represent the cyclic material response. A piecewise linear representation of the monotonic stress-strain curves was provided through the MARC user subroutine WKSLP.

The nonlinear algorithm employed in the program assumes that the total strain may be additively split into elastic, plastic, and creep components. The plastic strain ϵ_{pl} is determined during the plastic loading phase according to rate-independent plasticity theory. It is assumed that the prior creep strain ϵ_{cr} does not affect the subsequent plastic response, so that no interaction effects are included in the constitutive theory.

The creep option allows time dependent effects to be included by assuming that the creep response equations are constitutive equations which are valid not only for constant stress histories, but for general stress histories. The creep strain is assumed to be independent of prior plastic deformation. The program algorithm assumes that the nonlinearities due to the creep "constitutive relation" may be incorporated into a suitable load vector and treated by an initial strain technique. Thus, during small deformation creep the stiffness matrix remains constant and only the load vector is changed on an incremental basis. Since the stiffness matrix is constant, the reassembly of this matrix is avoided and the program solves for the incremental displacements by matrix back substitution. It has been demonstrated that this results in typical incremental computer times which are about 50% of the computer time required for the assembly and solution required in a plastic loading increment. An automatic time stepping scheme is incorporated into the solution algorithm to take advantage of the diffusive nature of the creep process. The description of the material creep response for this analysis was incorporated within the MARC user subroutine CRPLAW.

Under the high temperatures encountered during the thermal loading cycle the material will exhibit time dependent plastic behavior - the material "creeps" during the plastic loading phase. In order to properly account for such behavior a time dependent plasticity theory is needed. In default of such a theory the behavior was approximated in the MARC program by applying increments of creep and plasticity alternately.

4.2.2 Louver Finite Element Model

The three dimensional (3D) finite element model of the louver used in the structural analysis is shown in Figure 12. The model contains an included angle of 0.577^{0} which represents the distance between the radial symmetry planes of two adjacent cooling holes. This small model size was selected because of the circumferentially uniform temperatures in the louver lip region and to minimize computer run time. Aspects of the modeling philosophy, which had to be established prior to the complete analysis, are discussed separately.

Element Type

As shown, the model consists of 30 elements. Twenty-one (21) of the elements are the 20 node isoparametric element with reduced integration using 8 Gauss points (MARC element #57). Since it is known that some reduced integration point elements are unreliable if distorted shapes are used, the full 27 integration point element (MARC element #21) was used around the cooling holes. Selection of the reduced integration point elements was based on initial estimates of the savings in run time over the full integration point element, and to minimize the required spatial temperature interpolation between the heat transfer and structural analysis meshes.

Boundary Conditions

The effect of the complete shell structure was simulated by the appropriate boundary conditions. Along the radial planes AC and BD (Figure 12), only radial displacement was permitted. This was accomplished by use of the TRANSFORMATION option to transform the global degrees of freedom in these planes to the local coordinate systems. Along the planes AB AND CD the effect of the fore and aft louvers was simulated by requiring that the radial displacements of nodal points on each plane were related by the equation:

$$\delta_{AB} = \delta_{CD} \times \frac{R_{AB}}{R_{CD}}$$

where: R_{AB} original radial coordinate on AB

R_{CD} original radial coordinate on CD

An additional condition equated the axial slopes along these planes. These conditions were prescribed by the user subroutine UFORMS. The fact that a series of louvers may be represented by this technique had been demonstrated in previous elastic shell of revolution analyses.

Double Precision

Numerical accuracy problems associated with the small included angle were investigated with a simple two element model having an included angle equal to the louver model. An initial analysis with this model did produce unacceptably large stresses when run in an isothermal condition. In this problem, the radial displacements, due to the free thermal growth, were several orders of magnitude larger than the circumferential displacements. Circumferential (hoop) stresses were produced as a result of the numerical round-off during the solution. Using a double precision version of MARC significantly reduced the round-off error to produce an acceptable isothermal solution.

Performance of the reduced integration point element in double precision was further verified with a linear temperature distribution. In this analysis, boundary conditions were applied simulating a section of a long cylinder with a through thickness temperature distribution. The results of the linear elastic solution indicate almost exact agreement with the known elasticity solution.

Mesh Density

An element mesh density study was conducted to identify an optimum mesh along the louver lip. This was initially considered necessary because of the large temperature gradient along the lip. The study was conducted using a linear elastic axisymmetric representation of the 3D louver model. A temperature distribution associated with the maximum lip to weld temperature difference (10 sec) was used in all analyses. A total of four (4) element meshes were

considered. The results of the analyses (shown in Figure 13) indicate little sensitivity of the predicted hoop (circumferential) mechanical strain distribution to the number of elements in the model. Based on these results the eight element mesh (mesh #1) was selected for the 3D louver model.

Weld Simulation

In the actual louver, the seam weld extends only over a portion of the overlapping sheets (see Figure 6). During the heat-up portion of the test cycle the hotter louver lip wants to expand radially a larger amount than the colder knuckle and cooling hole region. This results analytically in overlapping of the structure in this region (an impossibility). Analyses conducted using the TYING option in MARC to prevent the overlapping of these nodes indicated a 13% increase in hoop mechanical strain relative to the case where overlapping was allowed to occur.

The philosophy used for the 3D model was to tie the nodes to prevent overlapping during the heat-up and steady state portions of the cycle and then use the TYING CHANGE option to untie the nodes during the cool-down portion of the cycle.

Initial Verification of 3D Model

Prior to running the complete thermal cycle, the 3D louver model was run with isothermal and pressure loading conditions to verify the construction and modeling assumptions. The free thermal (isothermal) test case, with all required boundary conditions, transformations, and ties required for the small included angle model, predicted essentially zero stress throughout the structure. The second test case was run with a uniform pressure load (2.67×10^4 N/m^2 (4 psi)) simulating the actual pressure drop that occurred in the combustor liner test. Results of this analysis indicated a maximum hoop stress of -6.89 MPA (-1 KSI) and are in good agreement with the predicted stresses obtained from an axisymmetric louver analysis with the same pressure loading. Based on these two cases, the construction of the model was verified.

In the final form, the 3D model required 640K double precision words of storage on the IBM 370/3033 system.

Thermal Increment File

The loading sequence for the louver analysis consisted of initally applying the mechanical pressure load followed by the temperature increments as determined from the heat transfer analysis. The thermal loading cycle was repeated as required. As discussed in Section 4.1.1, the heat transfer finite difference map was determined based on locating a temperature solution point as close as possible to the finite element integration point. Thus the 4:1 element relationship between the two meshes shown in Figures 6 and 12. The results of the transient heat transfer analysis discussed in Section 4.1.1 were used to define the temperature history throughout the louver model. With-

in the MARC program, the allowable temperature increment size is estimated from the relation:

$$\Delta T \leq F \frac{\sigma_y}{E\alpha}$$

where:
- ΔT = temperature increment (°C)
- σ_y = yield stress (MPA)
- E = Young's Modulus (MPA)
- α = coefficient of thermal expansion ($^oC^{-1}$)
- F = factor based on in-house experience (0.30 in this analysis)

This guideline is used to prevent excessive strain (stress) changes occurring during a loading increment possibly effecting the stability of the solution. Generation of the temperature increment file and required spatial interpolation between the heat transfer and finite element meshes was accomplished by the general interpolator described in Reference 2. Initial experience for the 3D model with this interpolation was not successful, particularly in the area of the overlapping sheets. The final thermal file required a considerable amount of manual modification of the temperature increments to obtain temperatures at all integration points to within 3°C (5°F) of the desired value from the thermal analysis. In the complete analysis, the successive temperature increments were obtained from the thermal file with the MARC subroutine CREDE.

4.2.3 Material Model

Cyclic Plasticity Model

The combustor liner specimen, discussed in Section 3.2 was constructed of Hastelloy X sheet material. This is a fine grained nickel base alloy which has relatively low strength but high ductility at elevated temperatures. It is representative of the combustor liner materials used in the gas turbine industry. Previous experimental testing conducted, both internally by P&WA and under Reference 3, have shown that this material is highly strain rate (time) sensitive at elevated temperature, i.e., creep and plasticity occur simultaneously. The temperatures attained in the cyclic louver test are well into the range where time dependent plasticity will comprise a significant portion of the structural response. In addition, the differential heating and cooling of the louver produces a variable strain rate throughout the loading cycle. The general material model available in the MARC code (and most other non-linear codes) is based on classical time independent plasticity theory with a Von Mises yield criterion. Cyclic plasticity is considered by either the isotropic, kinematic, or combined hardening rules. For the louver analyses, a cyclic plasticity model consistent with an estimated average strain rate was used together with a creep simulation to account for time dependence at the lower strain rates.

The development of the Hastelloy X material plasticity model considered a tri-linear representation of the monotonic tensile curves and the COMBINED cyclic hardening rule. The criteria for development of the model was based on prediction of the cyclic inelastic strain range observed during stabilized isothermal strain controlled testing at representative strain rates. In constructing a monotonic curve for each temperature within the analysis the elastic modulus, work hardening slope and stress level (at large strains) was chosen based on previous testing conducted at 0.008 min^{-1}. The yield point was determined using the tangency point of the actual stress-strain curve and by equating the areas under the experimental and analytical curves. Figure 14 shows a representative construction. Using this approach, the monotonic stress-strain curves for temperatures between 427°C (800°F) and 982°C (1800°F) were constructed and incorporated into the MARC WKSLP user subroutine. The complete stress-strain description used in the louver analysis is presented in Figure 15.

A series of isothermal, uniaxial simulations were run to verify the accuracy of the representation under monotonic and cyclic loading. Figures 16A through 16C show the predicted results at 760°C (1400°F), 871°C (1600°F) and 982°C (1800°F) for cyclic strain controlled loading between ±0.6% strain. Shown are the stable 5th cycle MARC results vs. available cyclic test data for two representative strain rates ($\dot{\epsilon} = 2.4 \times 10^{-2}$ MIN^{-1} and $\dot{\epsilon} = 2.4 \times 10^{-3}$ MIN^{-1}). As shown, the stable stress values and the cyclic plastic strain range (width of the loop) are consistent relative to the test data.

Creep Model

A creep solution was included in the analysis to model the time dependent material response at the slower strain rates. This was accomplished using the MARC subroutine CRPLAW and required that the incremental plasticity solution be periodically stopped and "creep allowed to occur."

The final form of the creep simulation incorporated into the CRPLAW subroutine is:

$$\epsilon_{CR} = A\sigma^{n}t$$

ϵ_{CR} = creep strain

where: σ = stress (KSI)
t = time (hrs)
A, n = temperature dependent constants

The simulation of the instantaneous time dependent nature of the high temperature material response required that the constants be determined from short time (< 1 minute), high stress level (σ applied ≥ 0.5 σ yield) Hastelloy X creep data.

The accuracy of this constant rate model was demonstrated by simulation of monotonic stress relaxation tests. Stress relaxation, not creep, is appropriate in judging the model since, with the thermal loading, the time-dependent louver response is predominately stress relaxation. Comparison of these results are shown in Figure 17. Good agreement is obtained with the model, particularly for the higher temperatures ($\geq$871°C (1600°F)).

A piecewise interpolation scheme was developed for the temperature dependence of the constants A and n. In the louver analysis, creep was "allowed" to occur between 1300°F and 1800°F. The values of the constants were determined as:

704°C-871°C (1300°F-1600°F)
$$A = 3.05 \times 10^{-12} \left(\frac{T}{1000}\right)^{17.87} \qquad n = 3.39 \times 10^{-3}(T)$$

871°C-927°C (1600°F-1700°F)
$$A = 9.48 \times 10^{-30} \left(\frac{T}{1000}\right)^{103.64} \qquad n = -1.63 \times 10^{-2}(T) + 31.49$$

927°C-982°C (1700°F-1800°F)
$$A = 2.49 \times 10^{-23} \left(\frac{T}{1000}\right)^{75.78} \qquad n = -1.27 \times 10^{-2}(T) + 25.39$$

where T = metal temperature (°F)

4.2.4 Results of the 3D Non-Linear Analysis

The fatigue critical location of the combustor liner specimen is the edge of the louver lip. The observed failure mode is axial crack propagation from the edge toward the weld. Results of the structural analysis indicated that this location experiences essentially a uniaxial (circumferential/hoop) stress field. In the following discussion, the predicted hoop stress/strain components at the element integration point closest to the edge have been used to define the response.

The predicted results for the first two thermal loading cycles are shown in Figure 18. A representative temperature history used in this analysis for three locations in the louver model (end of the lip, weld, and knuckle) is shown in Figure 19. Referring to the letter designations and the temperatures, the response at the end of the lip throughout the two loading cycles can be followed.

A - (0 sec - 504°C (940°F)) Start of cycle 1

B - (5 sec - 732°C (1350°F)) Initial yield point

C - (12.5 sec - 921°C (1690°F))	Beginning of first creep increment. The increase in mechanical strain from B to C is produced by the increasing temperature difference throughout the louver. The reduction in stress level is associated with the temperature dependence of the stress-strain curves used in the analysis.
D - (60 sec - 954°C (1750°F))	End of the heating portion of the thermal cycle. Temperature between C and D remain essentially constant. The response between C and D consists of creep/relaxation and elastic unloading. Rationale for three (3) creep increments used is discussed below.
E - (66 sec - 760°C (1400°F))	Reverse yield point during cool down.
F - (78 sec - 513°C (955°F))	Minimum strain point.
A' - (90 sec - 504°C (940°F))	End of cycle 1, beginning of cycle 2.

Due to the tensile residual stress at the end of cycle 1, subsequent loading in cycle 2 requires more thermal loading increments to produce re-yielding of the louver lip (point B'). The rapid temperature rise in the heatup portion of the cycle results in this yield point occurring at 893°C (1640°F) vs 732°C (1350°F) as in cycle 1. The lower stress level at B' 159 MPA (23 KSI)) reflects the temperature dependence of the stress-strain curves in the analysis. The remaining points in the second cycle (C' - F') occur at similar times as in the first cycle.

As discussed previously, the analysis was conducted with the time-independent plasticity formulation in the MARC code. The stress-strain curves that are used were generated at a strain rate representative of the expected average rate experienced during the loading cycle. To account for the actual time dependent material response, a creep solution was included in the thermal loading cycle. In attempting to determine the amount of creep time and at what point in the loading cycle it should be included, the variation in strain rate throughout the cycle was considered. Figure 20 shows the predicted variation in strain rate at the end of the louver lip for a portion of the first thermal loading cycle. The strain rate was evaluated based on the predicted mechanical strain increments and the time associated with the temperature change for that increment. The results show a rapid ($>.01$ min^{-1}) initial strain rate, a peak value occurring at 6 sec and a dramatic drop in strain rate after 10 sec. Since the predicted response during most of the first 10 sec of the cycle is elastic loading (A - B, A' - B') and not generally rate sensitive, only the remaining 50 sec of the heat-up was considered for the creep simulation. The 50 sec of creep time was arbitrarily divided into 3 segments and applied as follows:

5 sec (10 - 15 sec) applied at the 12.5 sec point
15 sec (15 - 30 sec) applied at the 20 sec point
30 sec (30 - 60 sec) applied at the 45 sec point

As shown in Figure 18, the three (3) creep solutions produce both a reduction in stress (relaxation) and an increase in strain. Elastic unloading follows each creep solution. The sensitivity of these results to the creep modeling was investigated by including all of the creep time (50 sec) at the 60 second point in a separate loading cycle. The results indicated a small change (6%) in the total inelastic (plastic and creep) strain predicted for the cycle.

The second cycle (and all remaining cycles) required 78 MARC increments as follows:

60 thermal loading (35 heat-up, 25 cool down)
14 creep
1 tying change
3 null (no load to insure equilibrium prior to creep and after the tie change)

Each loading cycle required 45 minutes of CPU time on an IBM 370/3033 computer.

The louver model was finally run through a total of six (6) complete thermal loading cycles. The predicted hoop stress and strain history at the end of the lip for the 6 cycles is shown in Figure 21. As shown, cycles 2-6 have similar stress-strain loops that are moving (ratchetting) in the negative strain direction and show a progressively higher peak tensile stress during the cool down portion of each cycle. Details of the sixth cycle response are shown in Figure 22 and contain the same elastic, plastic and creep regions discussed for cycle 2. The total mechanical strain range is defined as the distance between points C* and F. The analysis required 4 loading cycles for the total strain range to stabilize. This result is shown in Figure 23 where the initial strain range of 0.3406% (cycle 1) increases to 0.3482% by cycle 4 and remains constant for cycles 5 and 6. This small change in the total mechanical strain range with the first 4 loading cycles is apparently produced by a decrease in the stiffness of the louver. With the combined hardening cyclic plasticity model used in the analysis, a number of loading cycles are required to produce a stabilized stress-strain response at each location in the louver. The reduction in local stiffness, associated with the change in slope of the stress-strain curve from the initial to stabilized curve, in combination with the pressure and thermal loads on the louver, produce the 2% change in mechanical strain range.

The results of the first six (6) cycles also show that the cyclic inelastic strain range is decreasing with each cycle. This can be seen in Figure 24 where the individual inelastic strain components are plotted vs. cycle number. The compression going inelastic strain consists of the time-independent plastic strain generated between points B and C and the creep strain produced between points C and D. These individual components occur during the heat-up portion of each cycle and together comprise the total compression going inelastic strain. The tension going inelastic (time-independent) strain occurs

between points E and F during the cool-down portion of each cycle. As shown, the total inelastic strains are not exactly fully reversed which results in the ratchetting of the stress-strain response. The change in inelastic strain range is consistent with the fact that the stress range is increasing in each cycle. From Figure 21, the peak tensile stress produced during the cool portion of each cycle is increasing. With the higher peak tensile stress, the louver lip location now has a longer elastic range to traverse before yielding can occur during heat-up of the next cycle. This requires a larger temperature difference (more loading increments) which reduces the amount of temperature "load" available to produce plastic strain. The high temperature stress levels do not change significantly after cycle 1 because the cyclic stress-strain curves have hardened to their final value. The predicted creep strain per cycle remains essentially constant, consistent with the stable stress levels.

Stress-strain results at other locations throughout the 3D louver model are presented in the following Figures. Results from the 6th loading cycle indicate:

1. The maximum cyclic strain range occurs at the end of the louver lip. Figure 25 indicates a rapid drop off in cyclic strain range along the lip. These results are consistent with the observed fatigue failures originating at the end of the louver lip in the rig test.

2. Cyclic inelastic strain in the lip occurs in only the last 3 elements. Figure 26 shows the 3D louver model with key elements numbered. Figure 27 is a composite stress-strain result for the last 3 lip elements (28, 29, 30). A small amount of inelastic strain is observed in element 28 produced by the creep solution, otherwise the response is elastic.

3. Elements closer to the weld region show reduced values of residual tensile stress. In Figure 28, element 24 shows a completely compressive stress response.

4. Results in the knuckle region (Figure 29) show a peak tensile stress during the heatup portion of the loading cycle and a residual compressive stress at the end of the cycle, as expected. The cyclic strain range at this point is approximately 65% of the cyclic range at the end of the lip.

4.2.5 Thermomechanical Specimen Test

As shown in Section 4.2.4, the predicted stress-strain response at the end of the louver lip had not stabilized after 6 thermal loading cycles. The mean strain and stress values were increasing and the amount of cyclic inelastic strain per cycle was decreasing. Accurate fatigue life prediction for this thermomechanical response requires a detailed knowledge of the history of these and other response parameters. Obviously the selection of the material model (Section 4.2.3) determines, to a large extent, the predicted response. While the modeling assumptions were calibrated with isothermal test data, the actual component response under varying strain rate and temperature conditions may be significantly different. Testing of a smooth, uniaxial, strain control-

led specimen was conducted to provide material response data under the thermomechanical conditions for further model calibration and to define a stable response for the life prediction portion of the program.

Pratt & Whitney Aircraft conducts thermomechanical fatigue testing on a routine basis. The experimental system developed to conduct these tests is based upon standard closed loop servohydraulic test machines using low frequency (10kHz) induction heating and compressed air for temperature control on the specimen (Ref. 4). Specimen temperature measurement is provided by radiation pyrometer and used in conjunction with independently computer controlled preprogrammed mechanical strain and temperature histories. The system is capable of cycling at a positive or negative mean strain, with either stress or strain control and hold times within each cycle. The tubular specimen used for this type of testing is shown in Figure 30. Axial strain is measured from the machined internal ridges utilizing a linear variable differential transformer (LVDT) and a quartz internal extensometer. Load and total strain for this system can be controlled to within 1% and temperature within 2°C (4°F)

The predicted circumferential mechanical strain and temperature histories for the 6th thermal loading cycle at the edge of the louver lip were used to define the specimen test conditions. This is shown in Figure 31 where the letter designations are consistent with the points in the loading cycle described in section 4.2.4. Because the region near the edge of the louver lip experiences a uniaxial stress field, the stress-strain output from the specimen test is considered representative of the actual response producing the fatigue failure.

During the first 14 cycles of the test the strain range was inadvertantly set larger ($\Delta\epsilon$ = .39% vs. $\Delta\epsilon$ = .35%) than the desired value. This resulted in the slightly "fatter" stress-strain loops shown in the data. After cycle 14, the strain range was corrected. A total of 138 cycles was accumulated on the specimen with the "non-linear" strain temperature history. General observations from the test results are:

1. The stress-strain response stabilized within the first complete cycle (cycle #3, cycles 1 and 2 were required for start-up)

2. No appreciable relaxation of the response was observed during the 138 cycles

3. The hold time had essentially no effect on the shape of the response

4. Reverse plasticity is observed during the cool down portion of the cycle

Results from the testing are presented in the following Figures:

Figure 32 - Comparison of cycle 3 vs. cycle 11 indicates a stable response

Figure 33 - Cycle 11 vs. cycle 20 showing the effect of larger strain range during the first 14 cycles

Figure 34 - Cycles 60-70-80 indicates repeatibility of the response

The comparison of the experimental results with the predicted 6th cycle response is shown in Figure 35. In general, the predicted response for this cycle shows qualitative agreement with the experiment. Further investigation of the ability of the material model to reproduce the experimental results was conducted with a one dimensional, strain controlled analytical simulation of the experiment. This analysis used the same material model as the 3D louver analysis and was run through the same mechanical strain-temperature history as the specimen test. The simplicity of the analysis allowed a larger number of cycles to be economically run to evaluate material cyclic response. These results, in conjunction with results from previous isothermal analyses, result in the following conclusions relative to the material model.

1. Under isothermal, strain controlled cycling, the combined (isotropic-kinematic) hardening model will predict a stable stress-strain response. This is demonstrated in Figures 16A, 16B, 16C.

2 The inelastic strain produced by a creep and/or stress relaxation does not increase the size of the yield surface. This may result in an apparent rachetting of the stress-strain response.

3. For the thermomechanical cycle considered, the predicted stress-strain response did not stabilize. This conclusion may be cycle and/or material model dependent.

4. The results in Figure 36 show the cyclic hardening that occurs for the one dimensional analysis during the first 15 loading cycles.

5. The inelastic strain components for cycles 1-15 are shown in Figure 37. As indicated, the creep strain per cycle remains essentially constant while the cyclic plasticity is decreasing. This is consistent with the results from the 3D louver analysis and suggests that additional cycling would have produced a smaller amount of cyclic inelestic strain than predicted for the 6th loading cycle.

6. A comparison between the predicted response for cycle 15 and the results of the specimen test is shown in Figure 38. The prediction has a larger tensile mean stress and a smaller amount of cyclic inelestic strain (defined as the width of the loop across the strain axis).

It appears that further modification to the material model (combined hardening and creep simulation) is required to accurately reproduce the Hastelloy X thermomechanical response.

4.2.6 Linear Elastic Analysis

Within the design process, rigorous non-linear analysis as described in Section 4.2.4 may not be always practical. This is particularly true where several iterations are required to establish the final design geometry. A linear elastic analysis of the 3D louver model was conducted to establish the relationship between the elastic response at the louver lip and the results pre-

dicted by the nonlinear analysis. The results were used to identify a simplified (short cut) approach to qualitatively determine the actual response from the elastic response. The analysis used the same finite element model and incremental temperature loading as the nonlinear analysis. The yield points in the stress strain curve description were set at an arbitrarily high value to prevent yielding during the cycle. The creep simulation was not included in the elastic analysis.

Predicted stress-strain results at the end of the lip are shown in Figure 39. Again using the same letter designation as the non-linear analysis the response can be followed:

- A - Start of cycle
- C* - Minimum mechanical strain point
- D - End of heat-up portion of cycle
- F - Maximum mechanical strain point
- A' - End of cycle

A comparison of these results with the predicted non-linear analysis results indicates:

	Elastic	Non-Linear (6th Cycle)
Max. Strain %	+.0135	-.100
Min. Strain %	-.361	-.448
Strain Range %	.3751	.348
Mean Strain %	-.174	-.274
Mean Stress (MPA)	- 245	+ 138
(KSI)	(- 35.5)	(+ 20.0)

The cyclic strain range predicted with the elastic analysis is within 8% of the value from the 6th cycle of the non-linear analysis. While the peak stress and strain values are different between the analyses, the shapes of the strain-temperature histories are similar. These results, shown in Figure 40, are due to the fact that the louver is primarily a thermally loaded structure and the variation in thermal strain ($\alpha \Delta T$), which produces the stresses, is independent of material stiffness.

The elastic strain-temperature history was used in the development of a qualitative approximation of the non-linear results from the elastic calculations. Refering to Figure 41, the predicted mechanical strain-temperature history and the monotonic stress-strain curves (Figure 15) are used to construct the stress-strain response during the loading (heating) portion of the first load cycle. This corresponds to the minimum strain point (D) in the Figure. Elastic unloading is assumed to occur from this point at an average elastic modulus. Estimation of the reverse yield point is based on two assumptions.

1. All of the mechanical strain generated during the heating portion of the cycle is plastic strain.

2. The size of the yield surface during unloading for each temperature is determined using an isotropic rule.

The reverse yield point is labeled E in Figure 41. Continued unloading (cooling) takes place along an average plastic modulus, determined from the temperatures in this portion of the cycle, to point F (the maximum strain). Reloading for the second cycle again uses an average elastic modulus. The new yield point is determined with the same assumptions, however, the equivalent plastic strain has been increased based on the reversed yielding during the unloading. This produces an additional amount of strain hardening which raises the new yield point for the loading portion of the cycle. Comparison of the cyclic response using this approach with the 2nd cycle response from the non-linear analysis is also shown in the Figure. Further cycling would produce a more elastic response (small inelastic strain range) due to the increased yield stress associated with the isotropic hardening assumption. Strain rachetting cannot occur because the strain history is fixed by the elastic solution. Time dependent (creep) effects have not been included. This approach has produced good qualitative results, for the one dimensional stress state under strain controlled loading, relative to the more rigorous non-linear analysis. It may prove useful for future analysis of this type where an approximation of the response is acceptable.

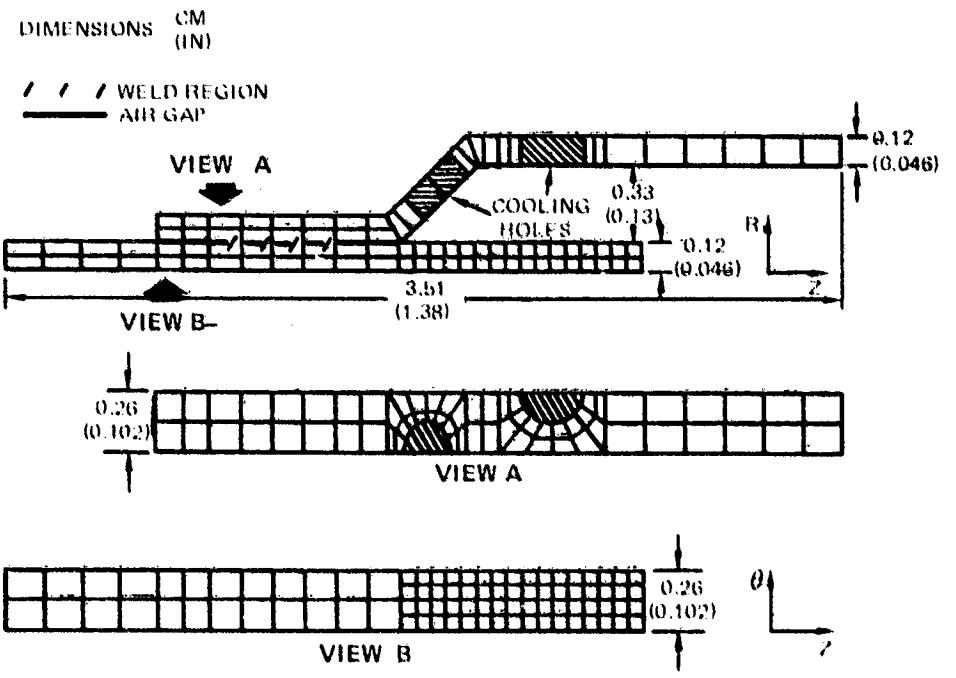

Figure 6 Three-Dimensional Heat Transfer Breakup for Louver

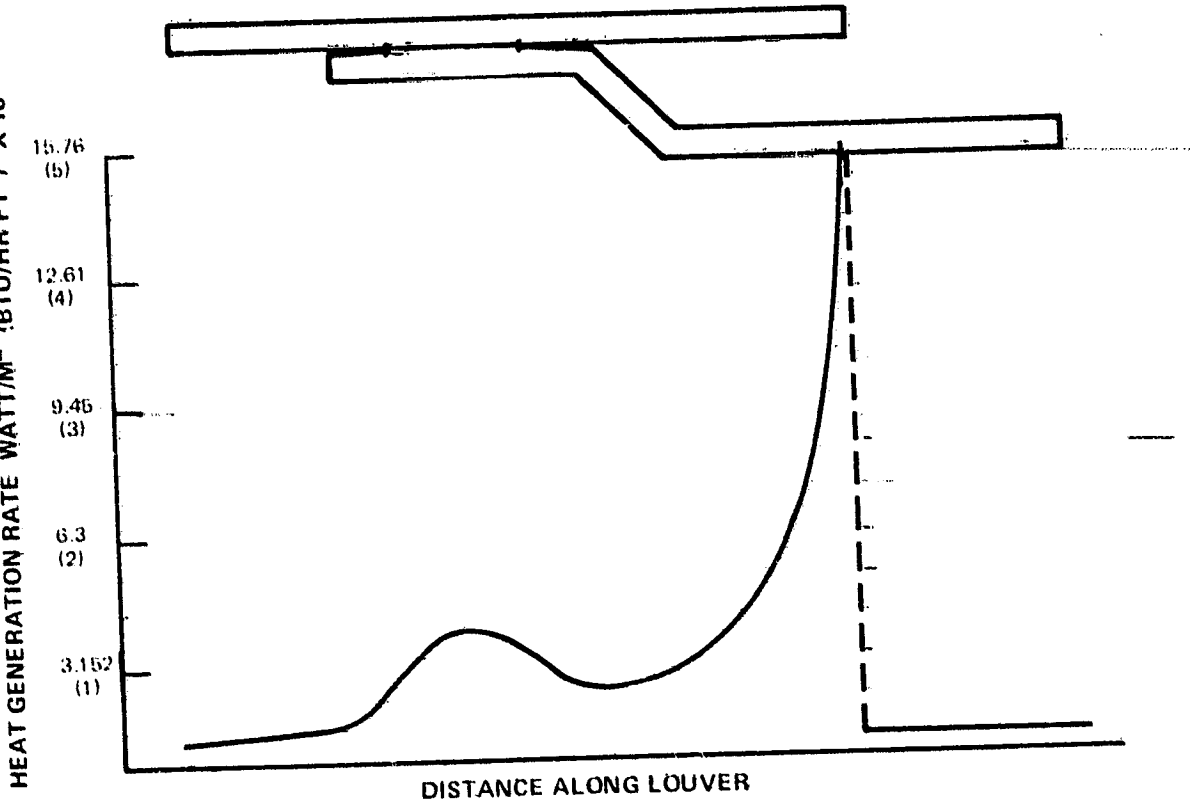

Figure 7 Calculated Heat Flux Distribution

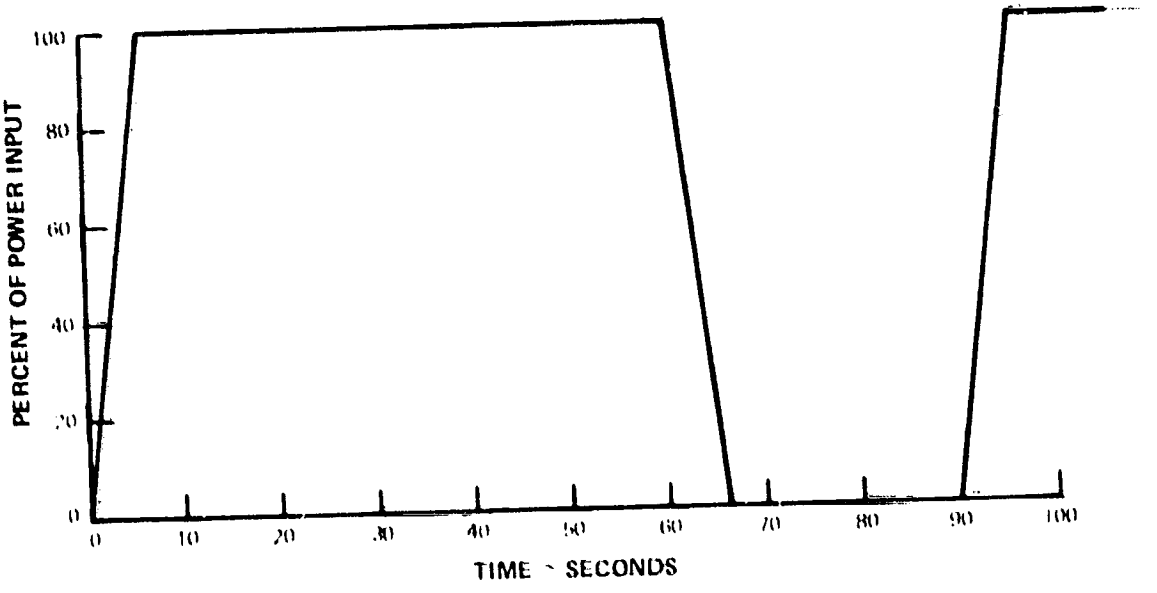

Figure 8 Induction Heater Power Vs. Time for Test Cycle

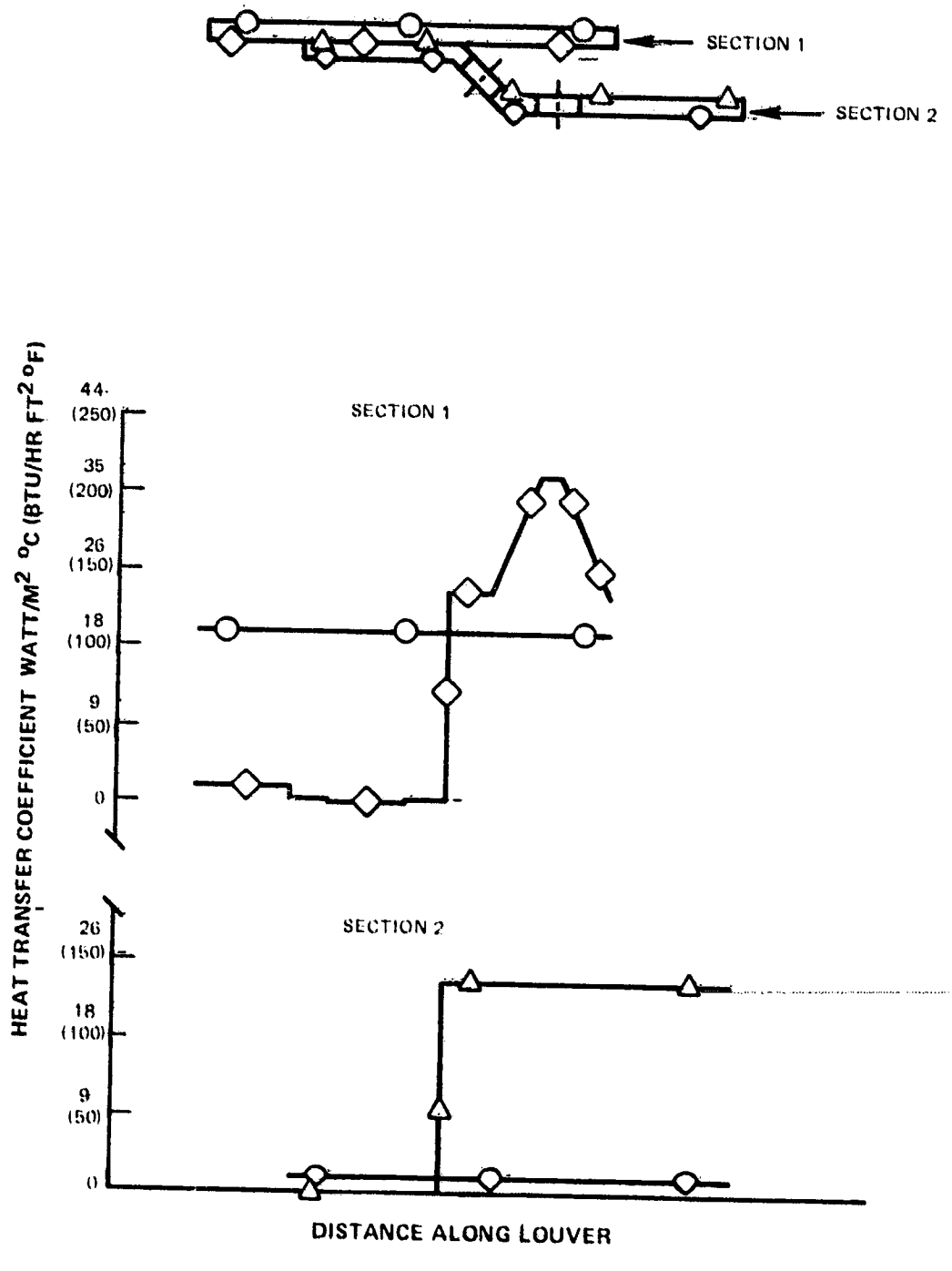

Figure 9 Convective Heat Transfer Coefficient Distribution

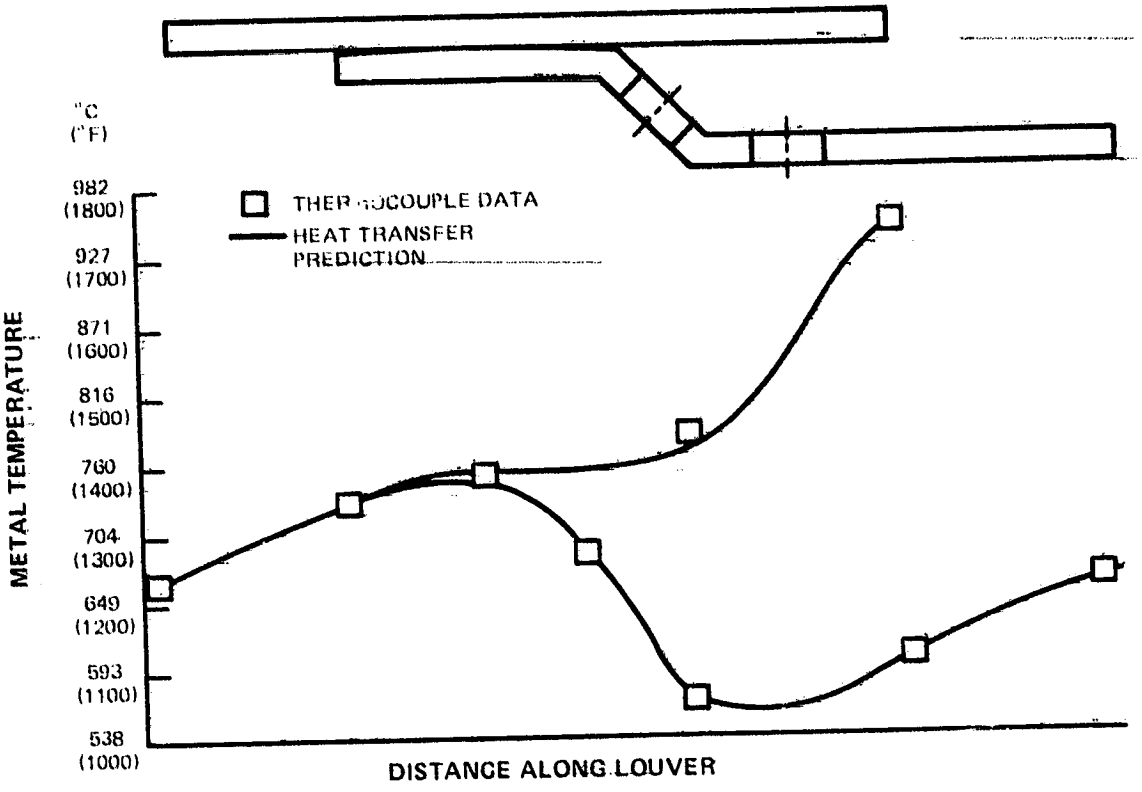

Figure 10 Steady State Temperature Distribution

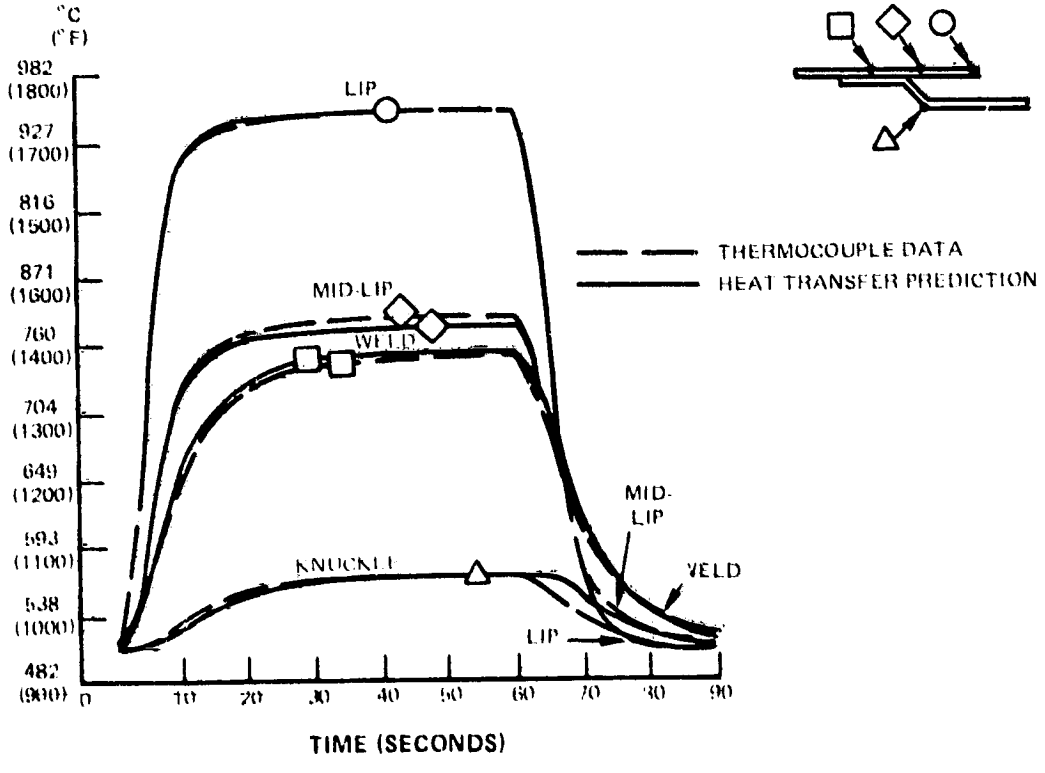

Figure 11 Transient Temperature Response

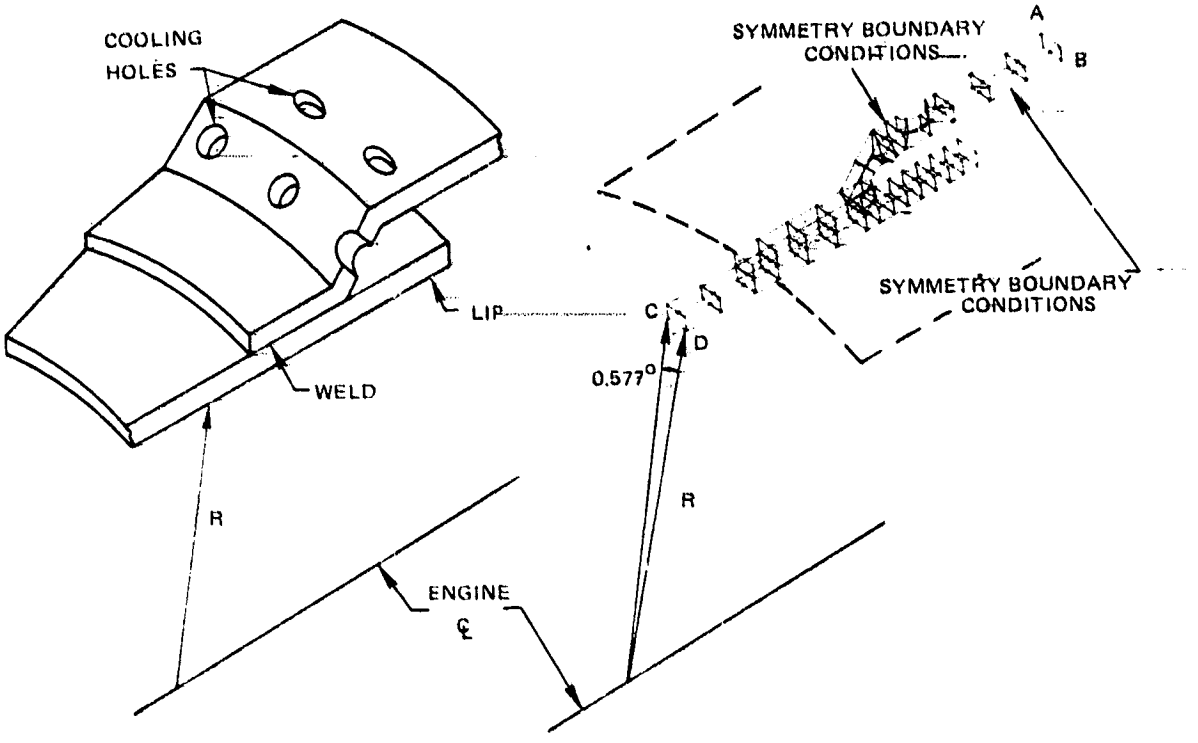

Figure 12 MARC Finite Element Breakup of Combustor for Liner Specimen

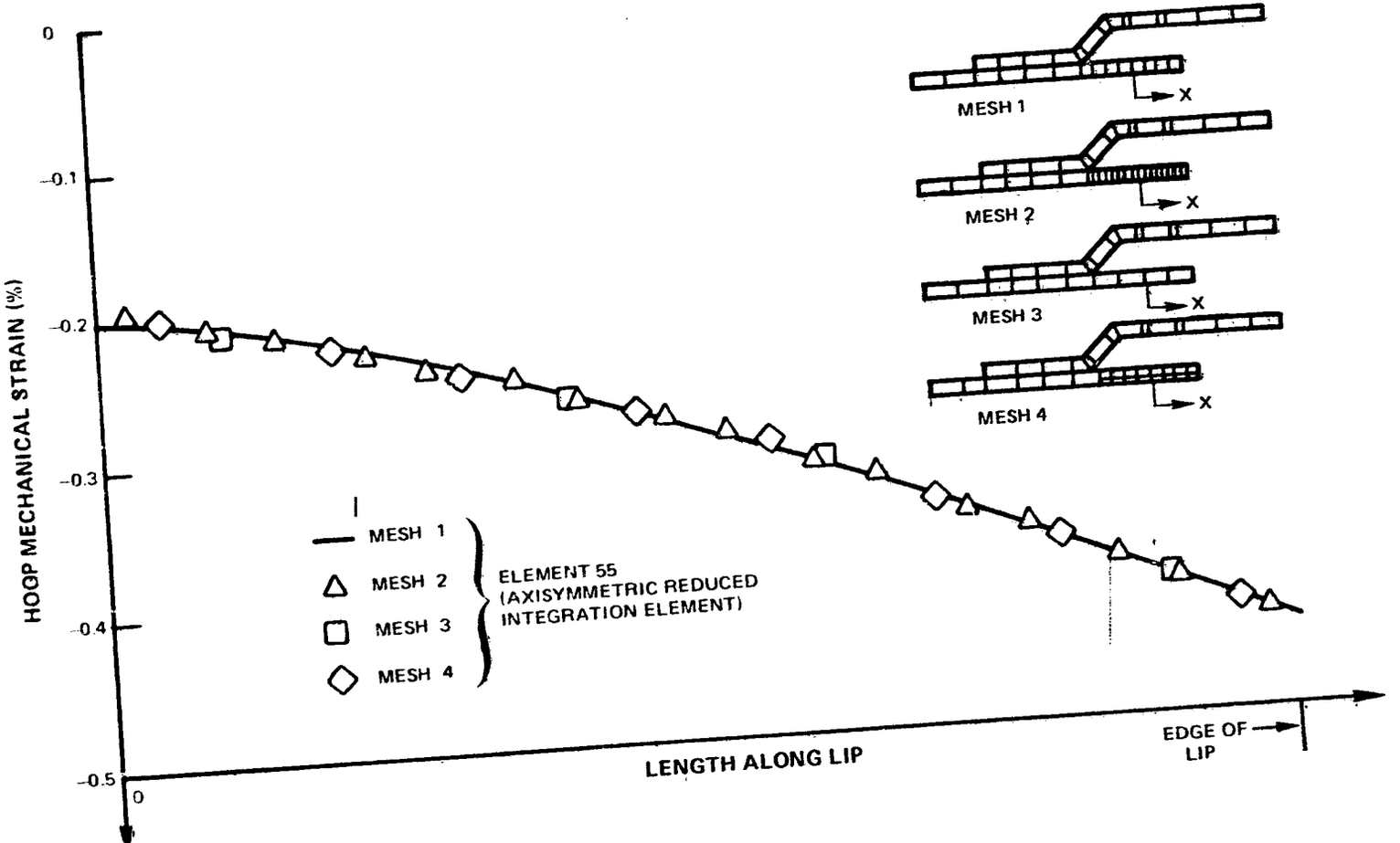

Figure 13 Sensitivity of Strain Distribution to Mesh Density

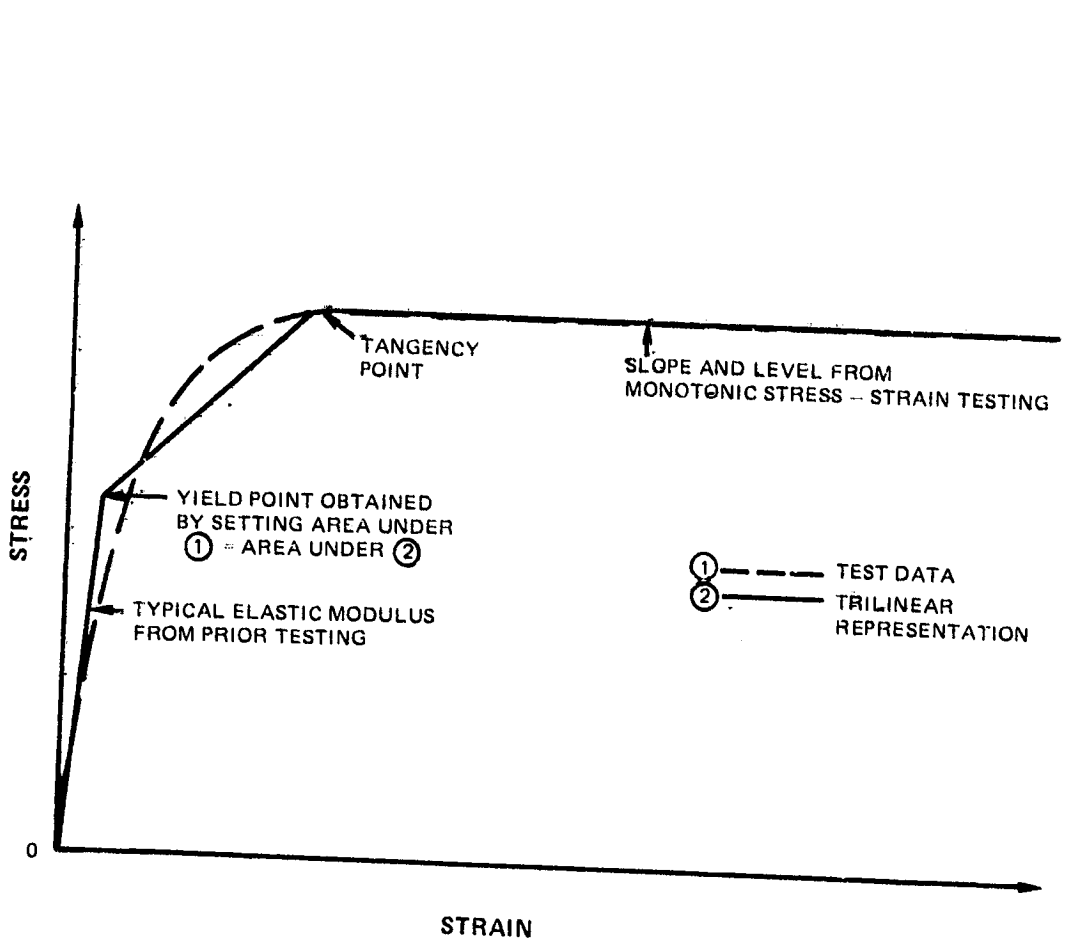

Figure 14 Construction of Stress-Strain Input for Analysis

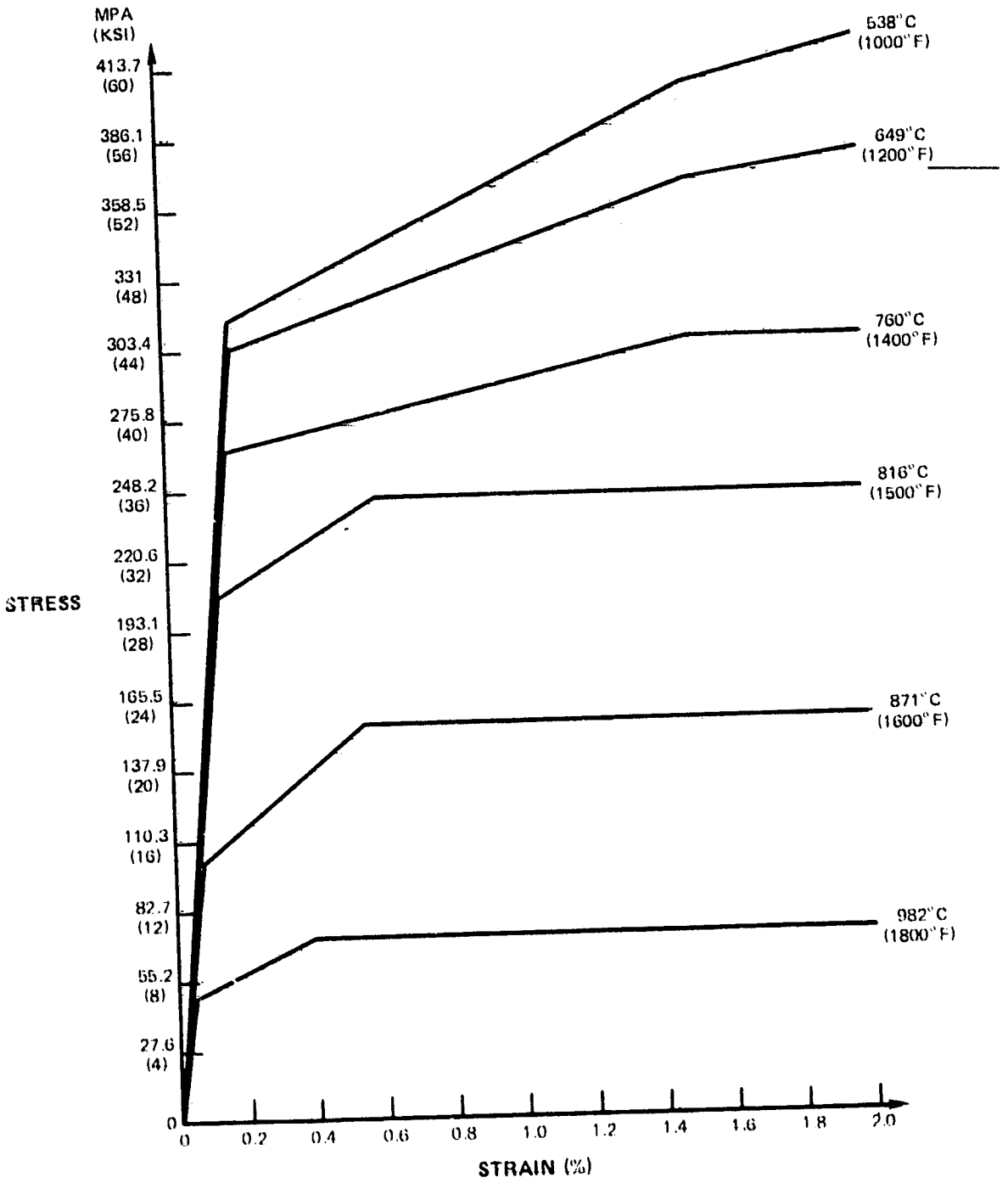

Figure 15 Hastelloy X Stress-Strain Representation for MARC Analysis

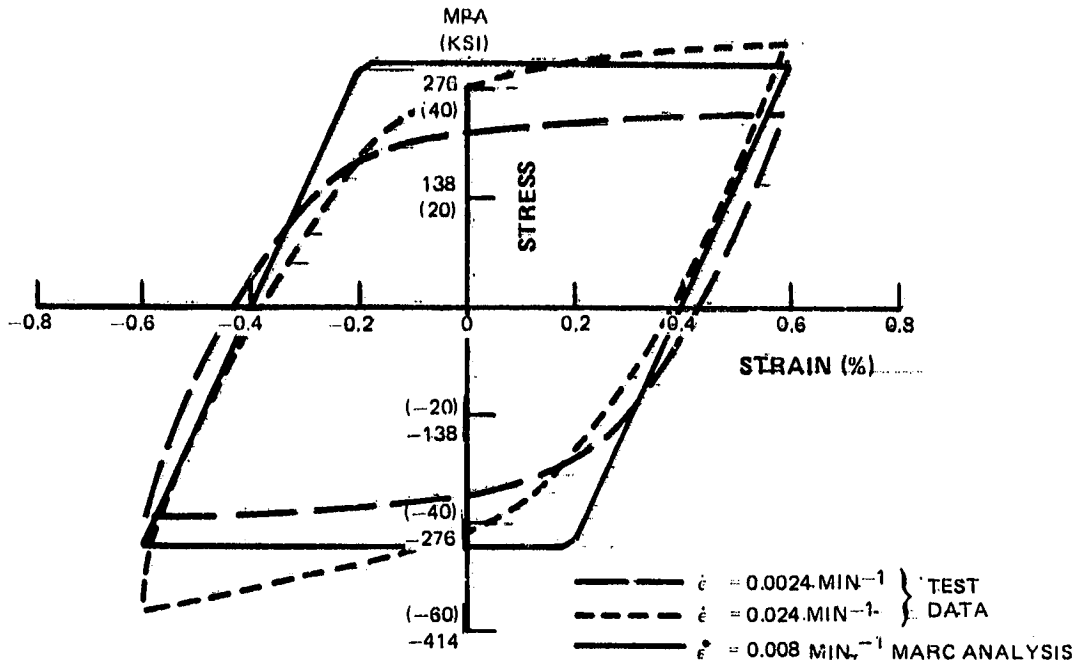

Figure 16A Prediction of Cyclic Response at 760°C (1400°F)

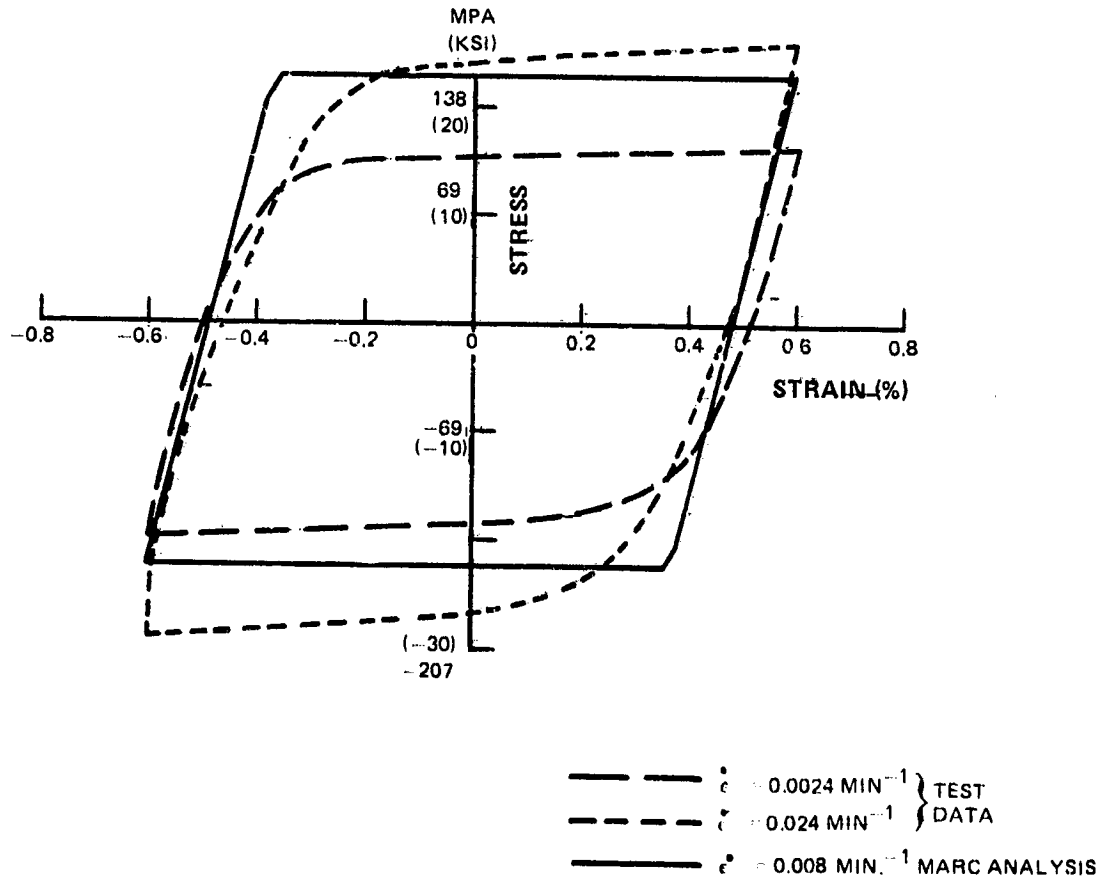

Figure 16B Prediction of Cyclic Response at 871°C (1600°F)

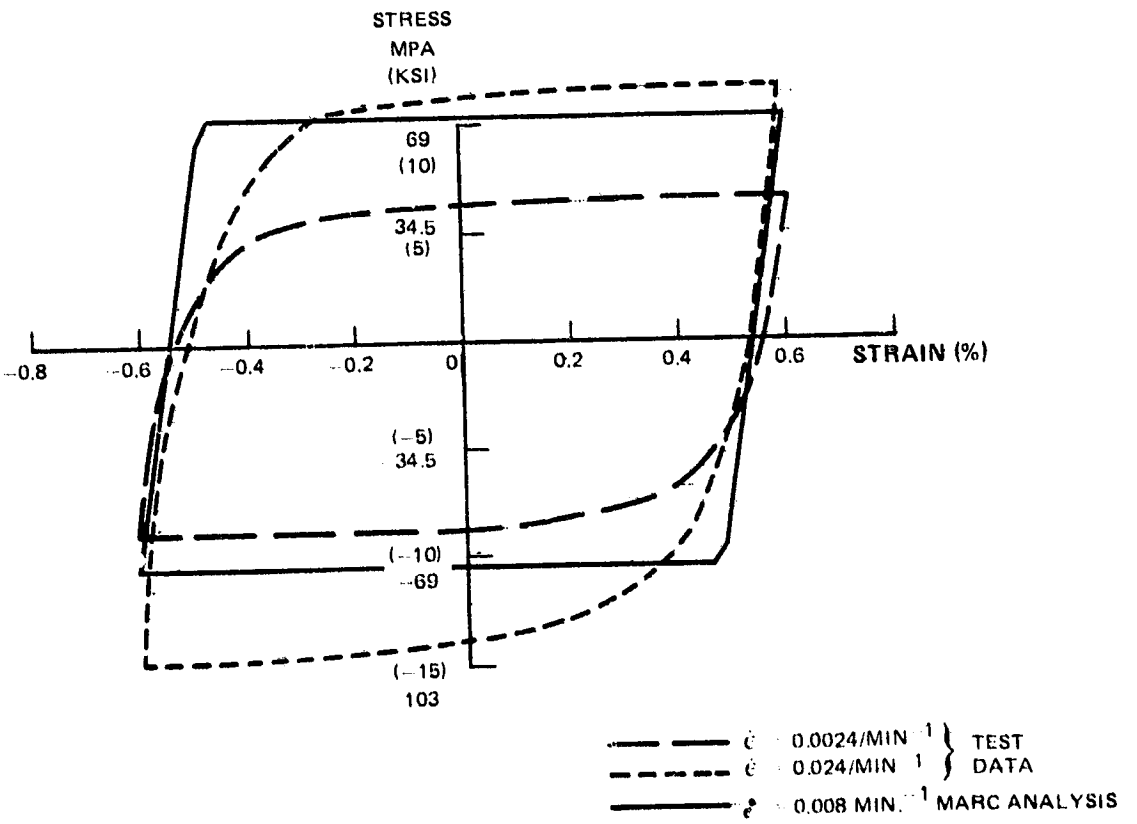

Figure 16C Prediction of Cyclic Response at 982°C (1800°F)

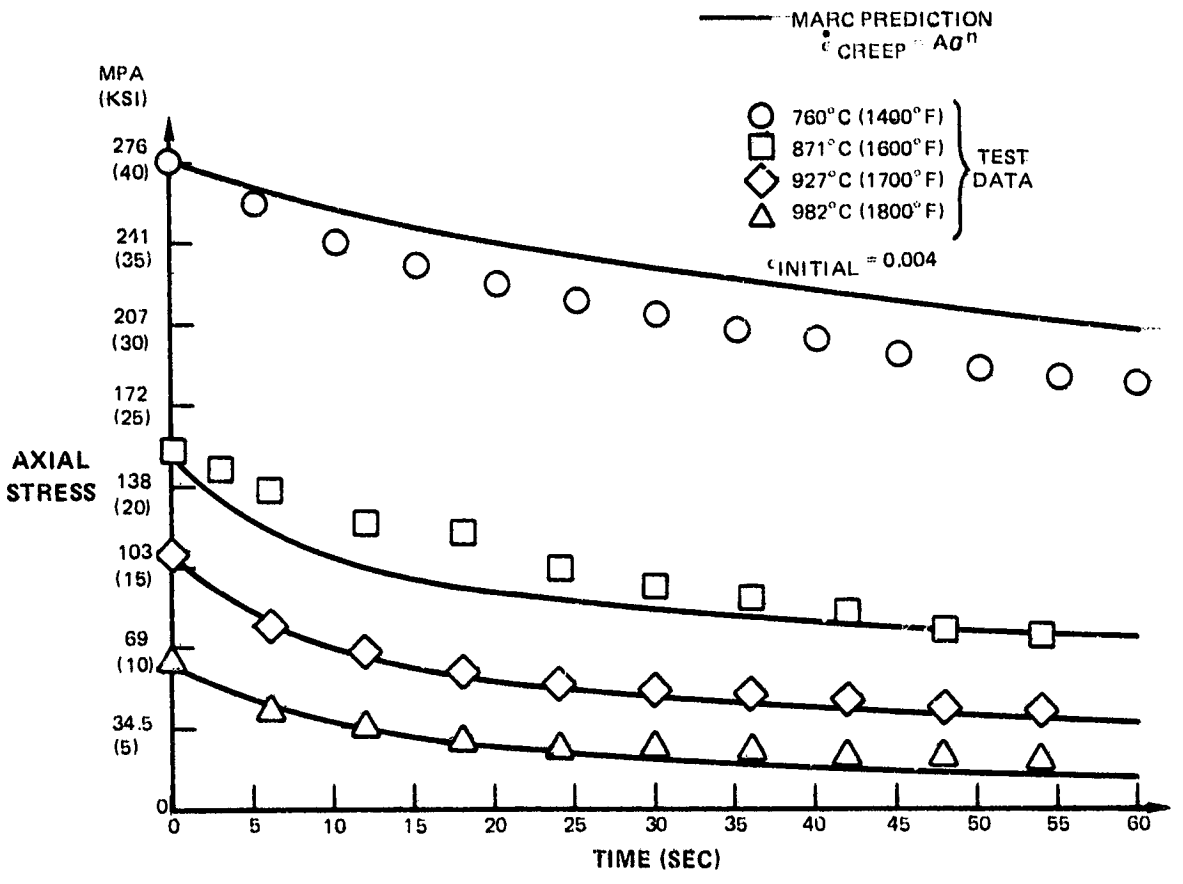

Figure 17 Prediction of Short Time Uniaxial Stress Relaxation Data

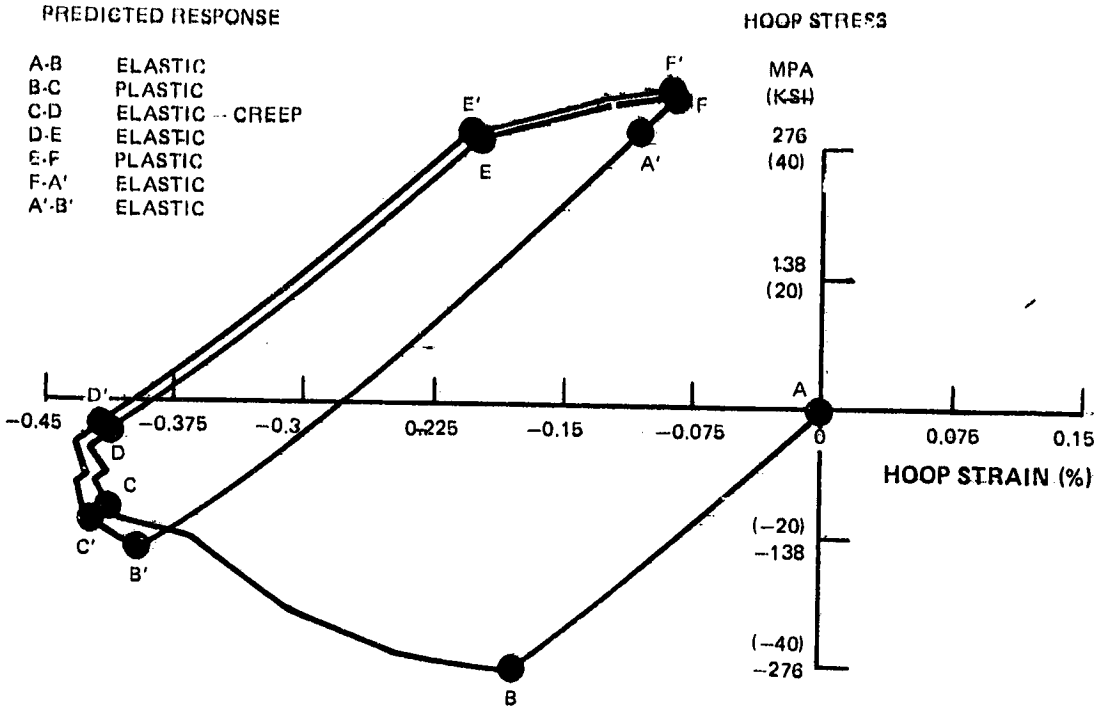

Figure 18 Louver Lip Response for First Two Loading Cycles

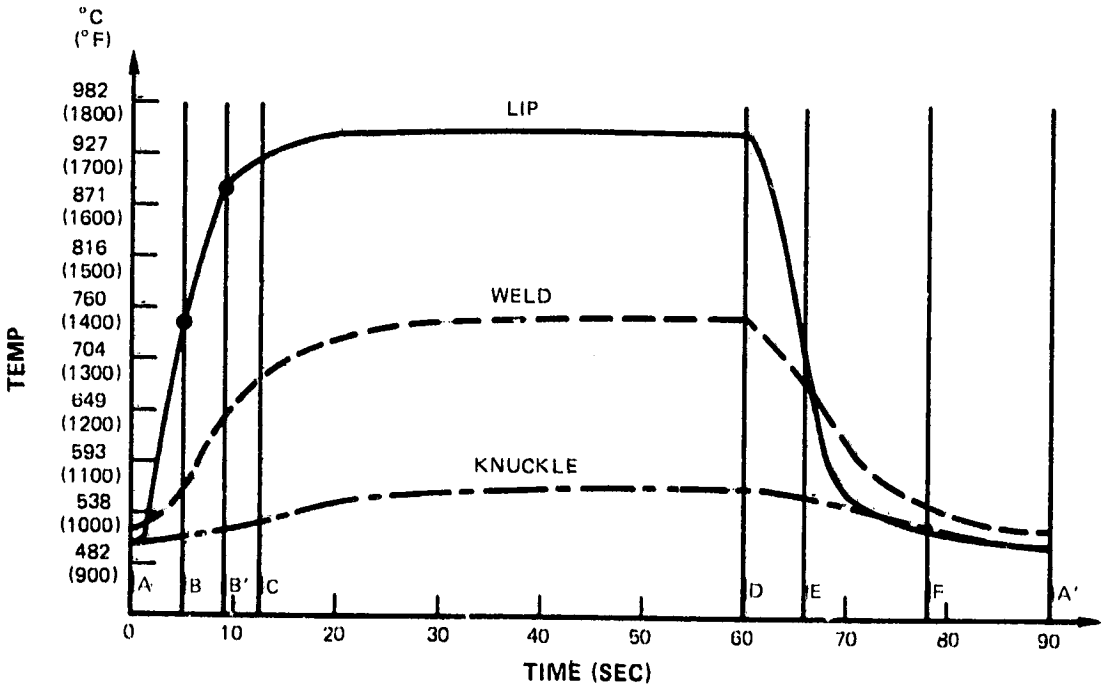

Figure 19 Louver Temperature Response

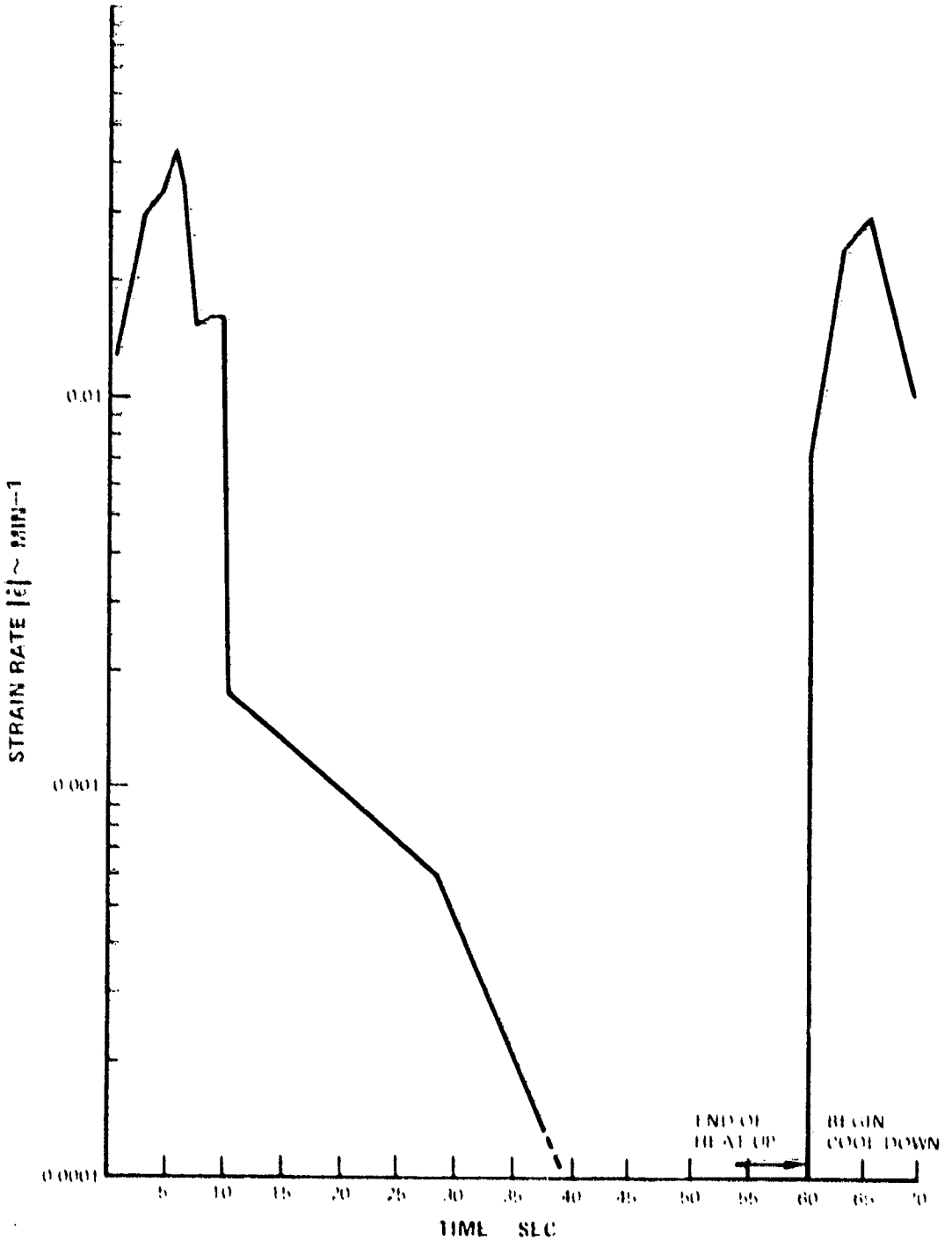

Figure 20 Strain Rate Variation During First Cycle at End of Louver Lip

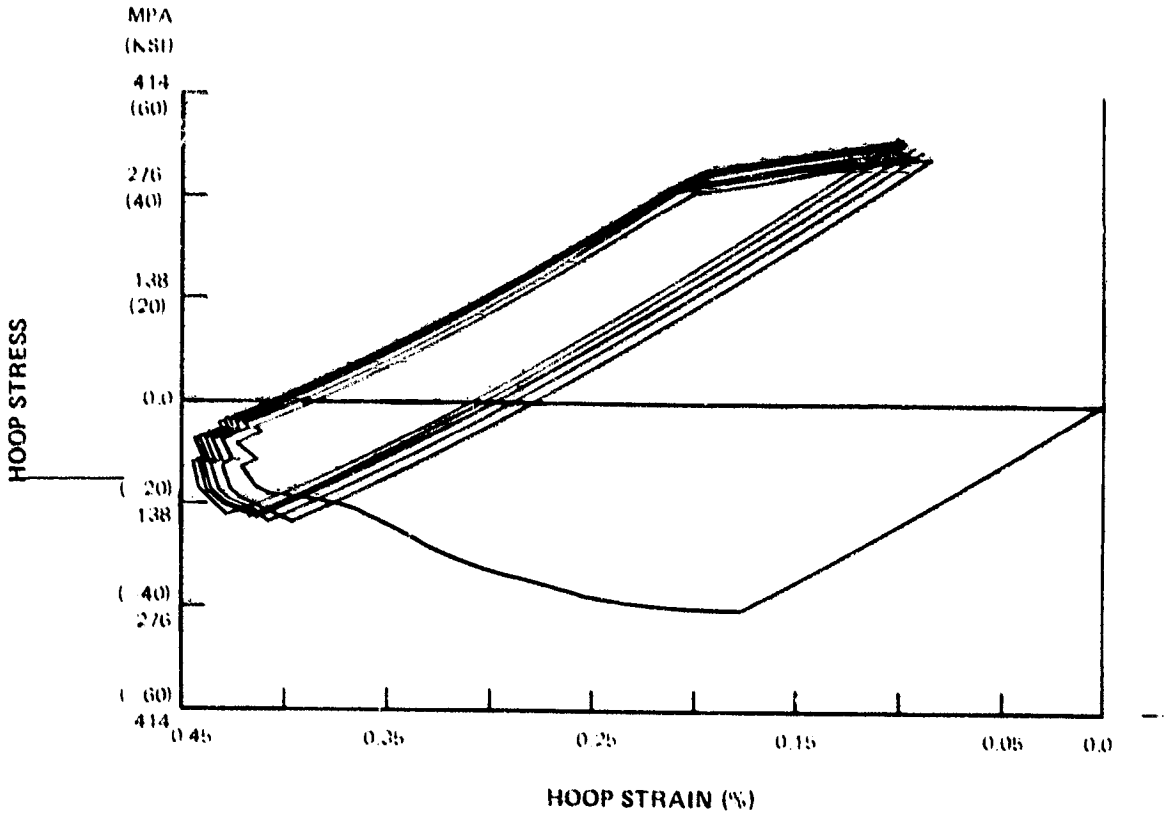

Figure 21 Predicted Louver Lip Response for Six (6) Loading Cycles

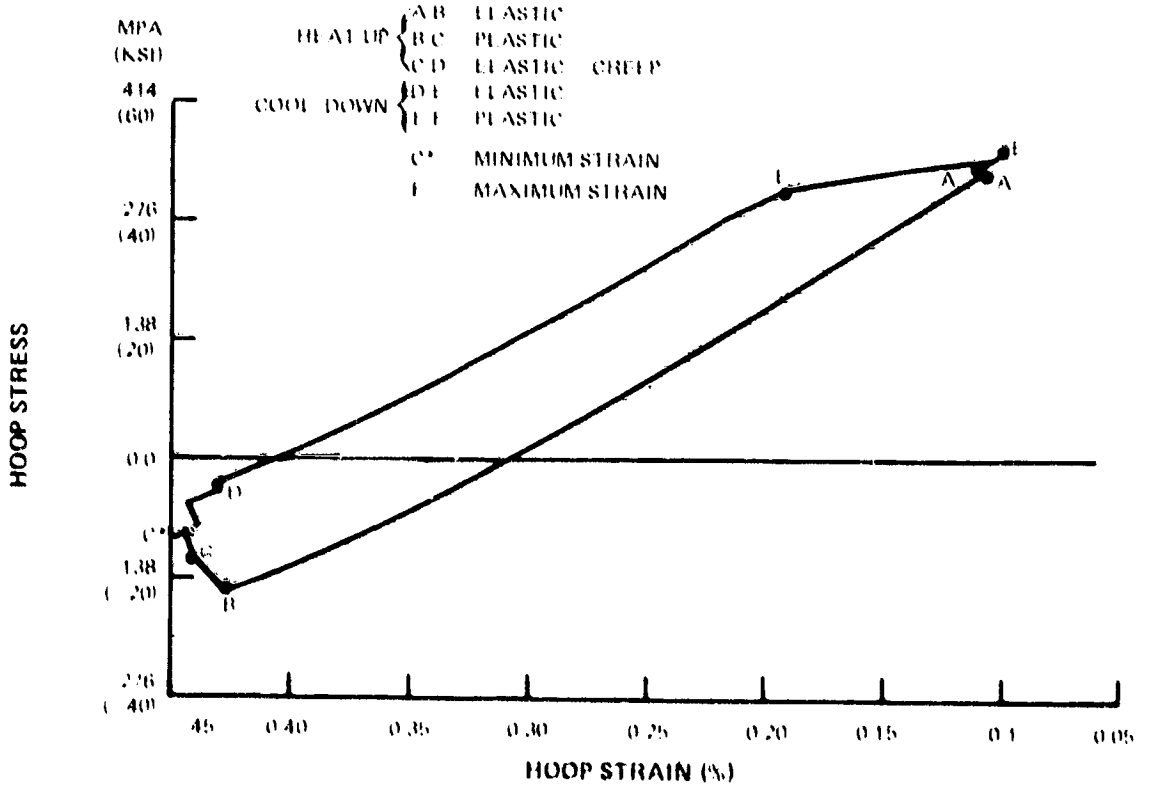

Figure 22 Details of 6th Cycle Response

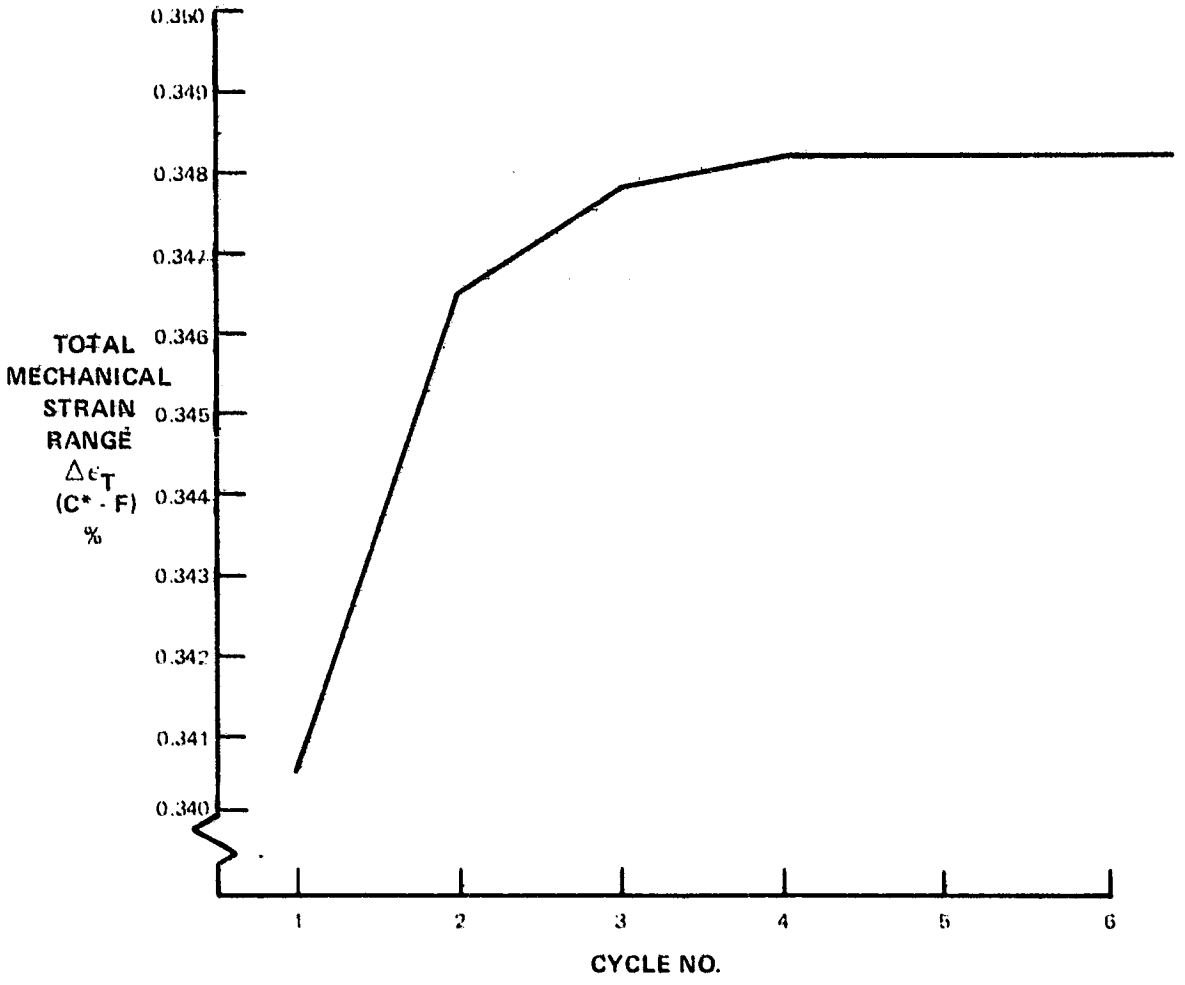

Figure 23 Total Mechanical Strain Range Vs. Cycle Number

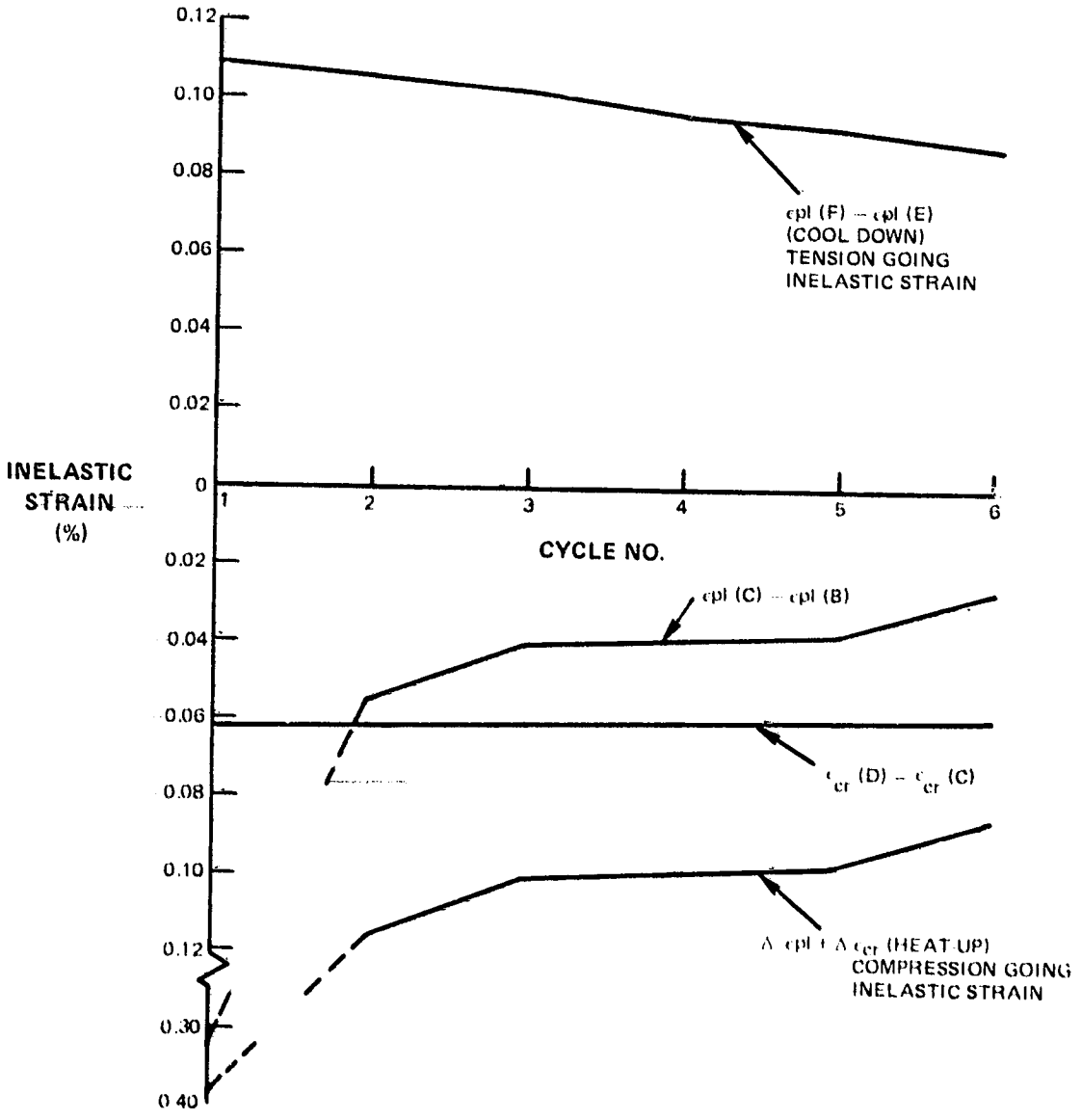

Figure 24 Inelastic Strain Components versus Cycle Number

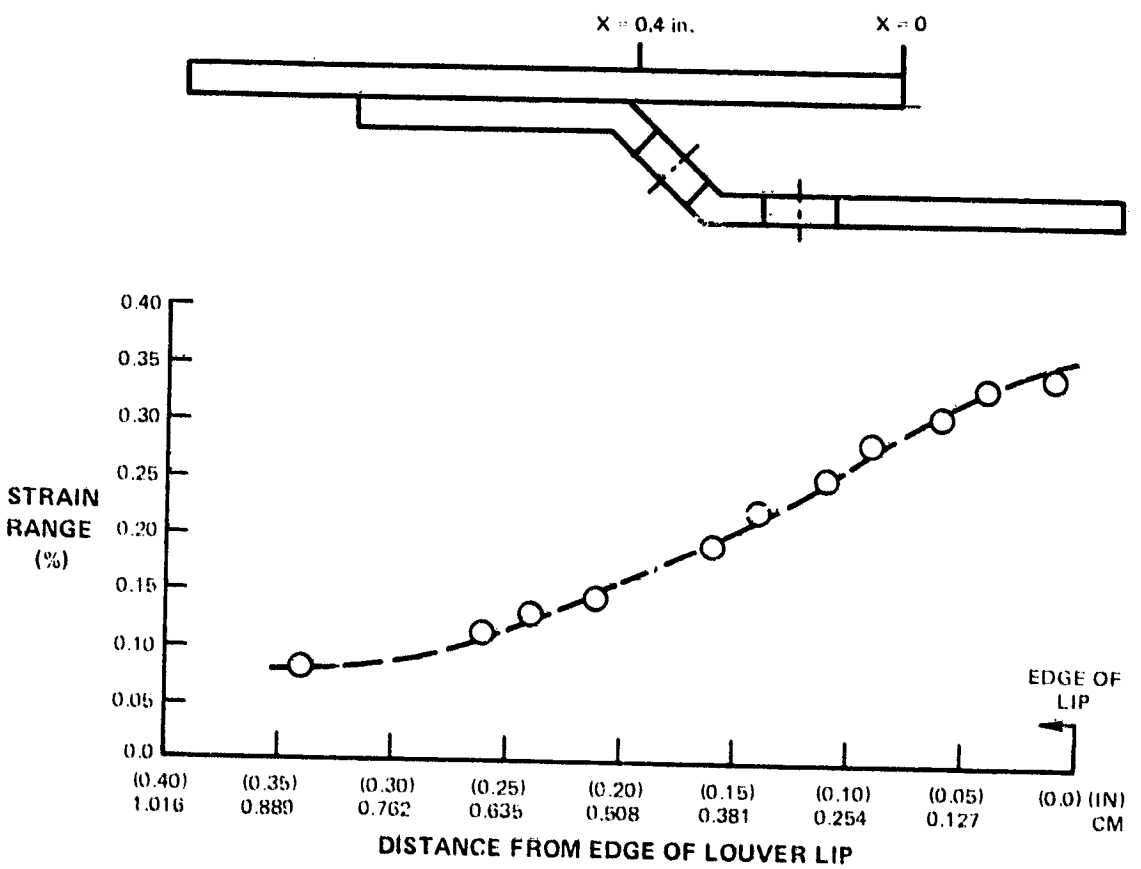

Figure 25 Mechanical Strain Range Distribution Along Louver Lip

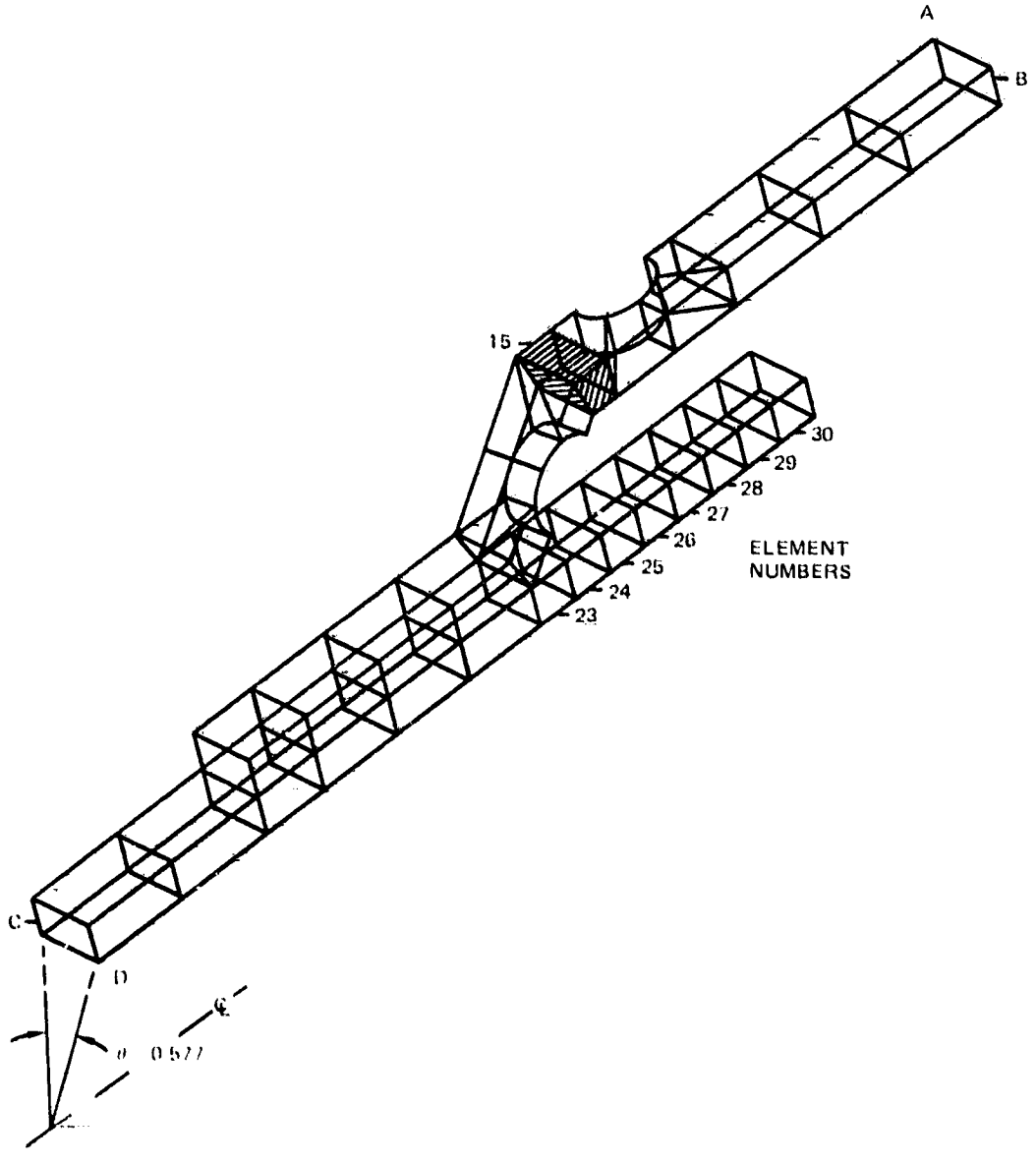

Figure 26 Louver 3-Dimensional Model

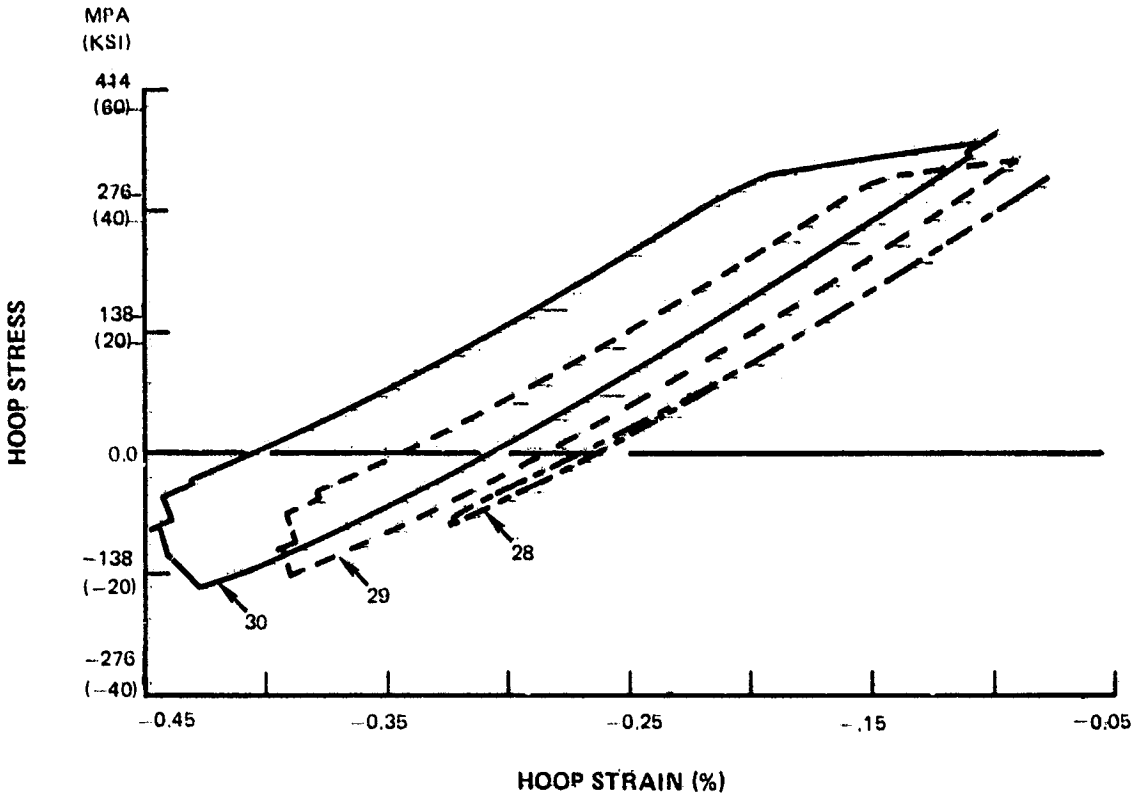

Figure 27 6th Cycle Stress-Strain Results for Last 3 Lip Elements

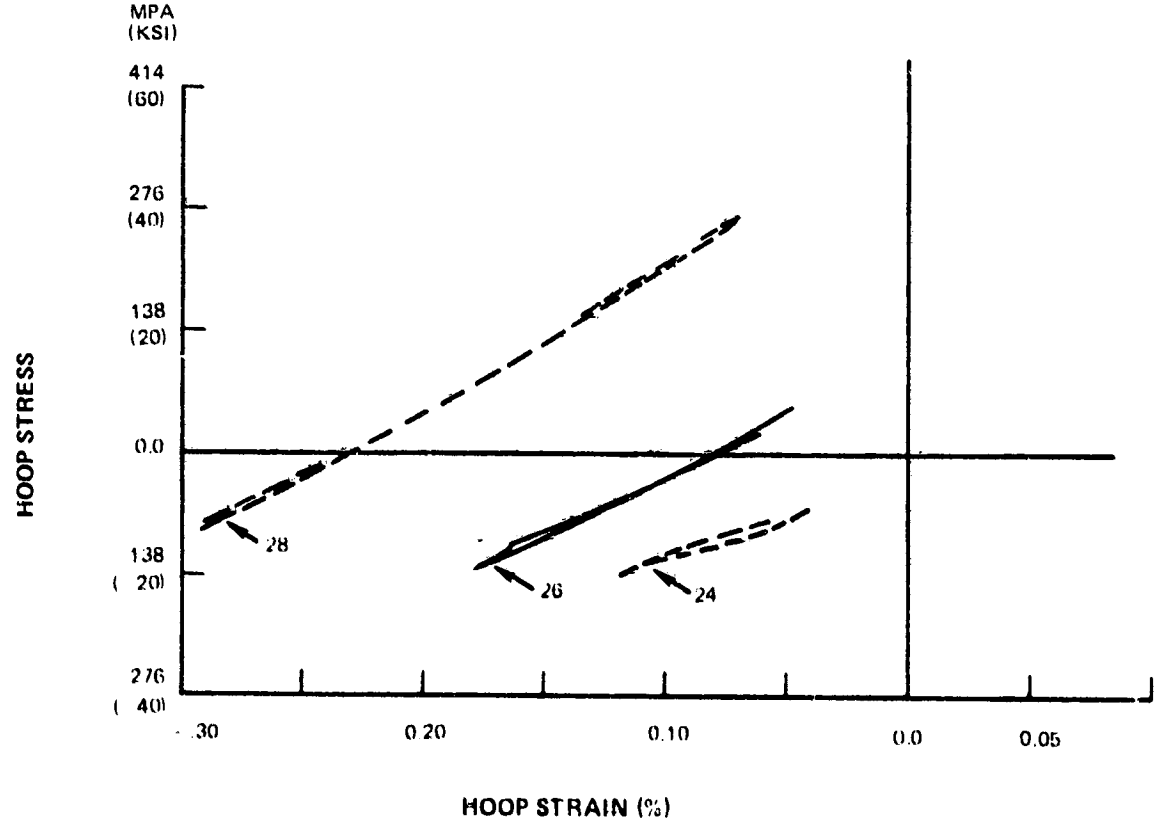

Figure 28 6th Cycle Stress-Strain Results for Lip Elements Approaching Weld Region

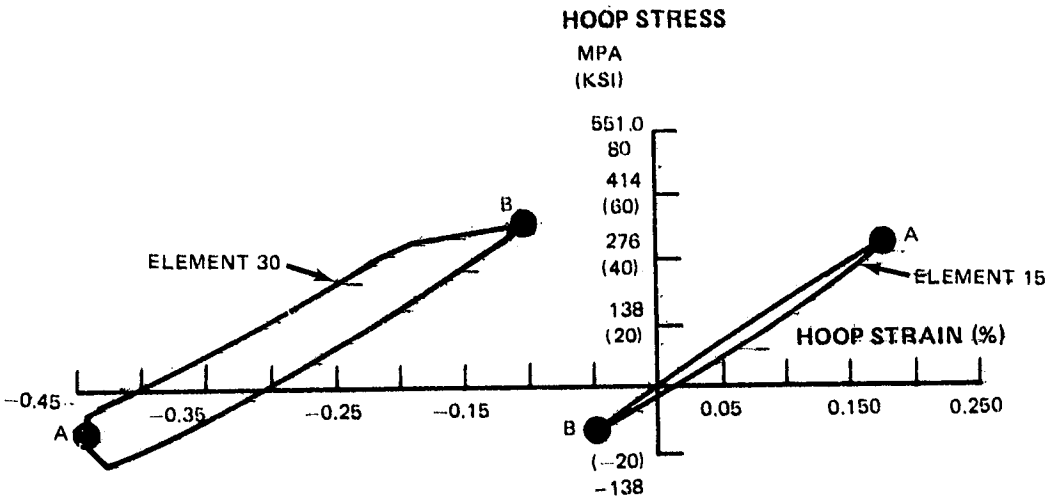

A – MAXIMUM TEMPERATURE

B – MINIMUM TEMPERATURE

Figure 29 6th Cycle Stress-Strain Results for Cooling Hole and End of Lip Regions

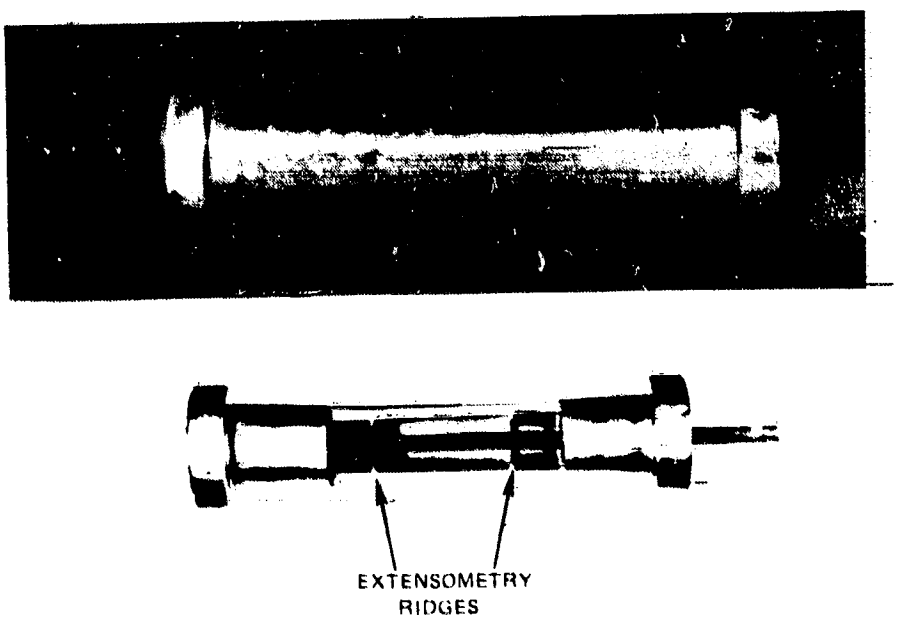

Figure 30 Tubular Specimen for Thermomechanical Testing

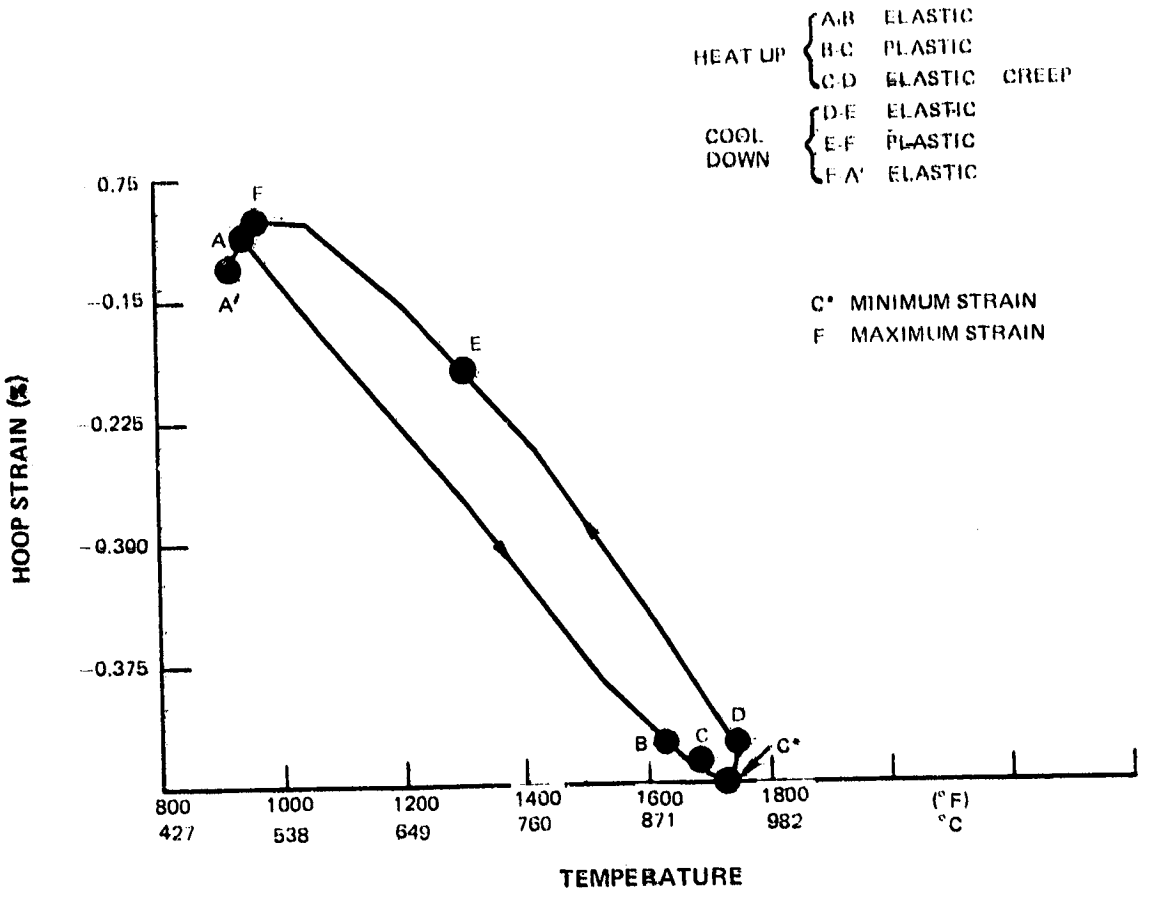

Figure 31 6th Cycle Mechanical Strain-Temperature History

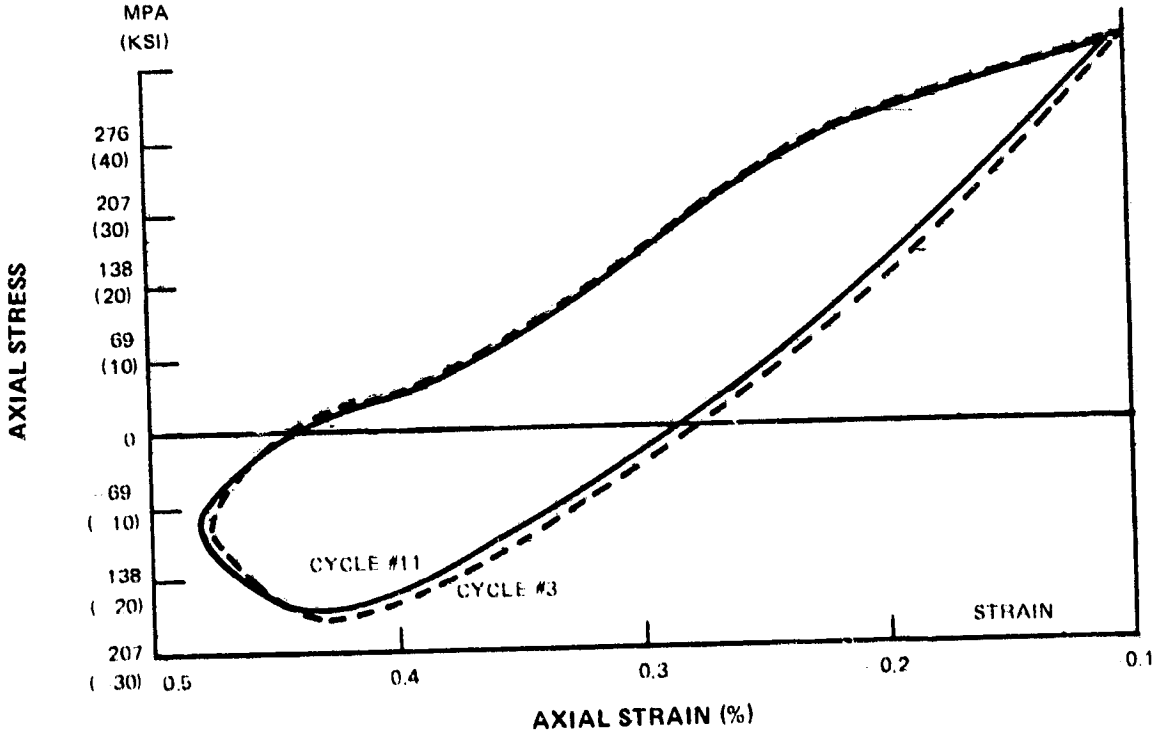

Figure 32 Stable Specimen Response

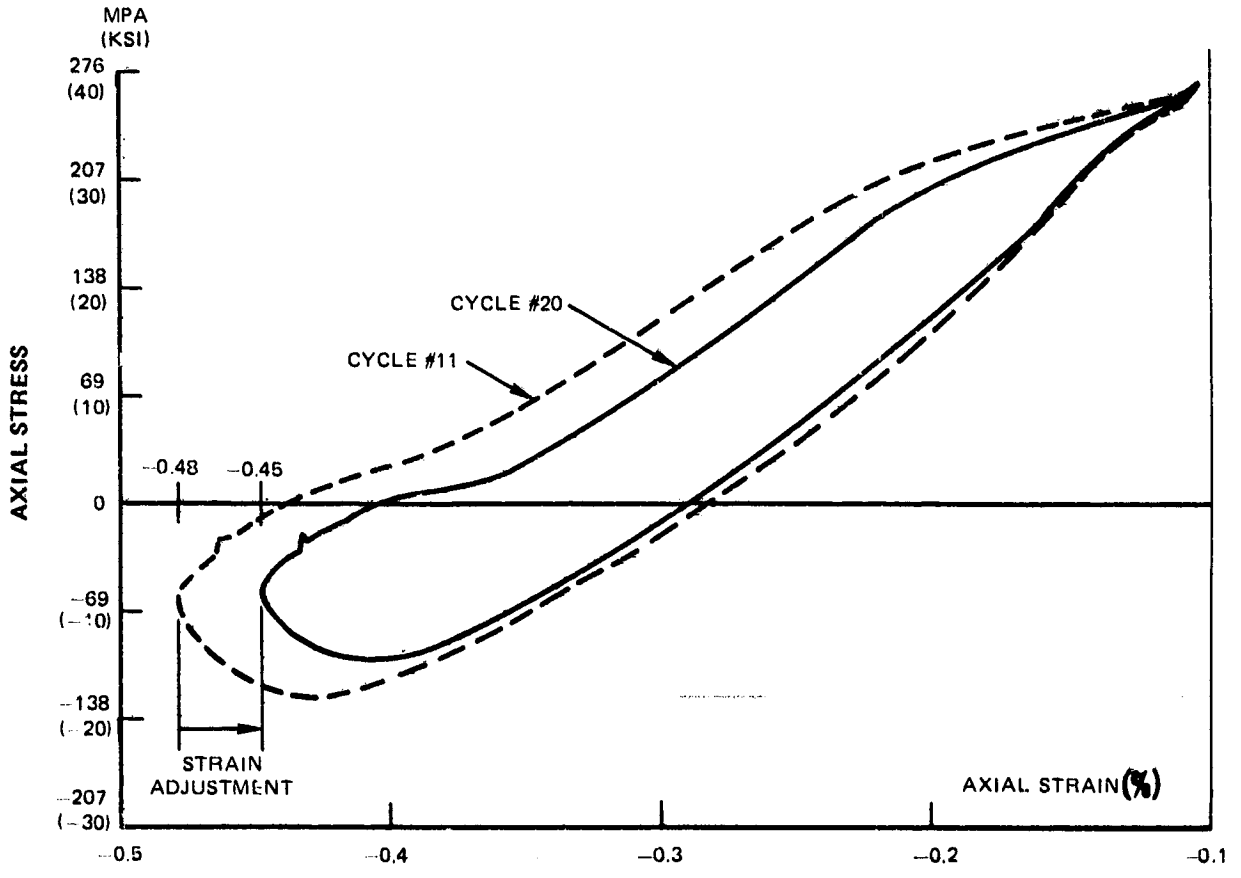

Figure 33 Sensitivity of Specimen Response to Total Strain Range

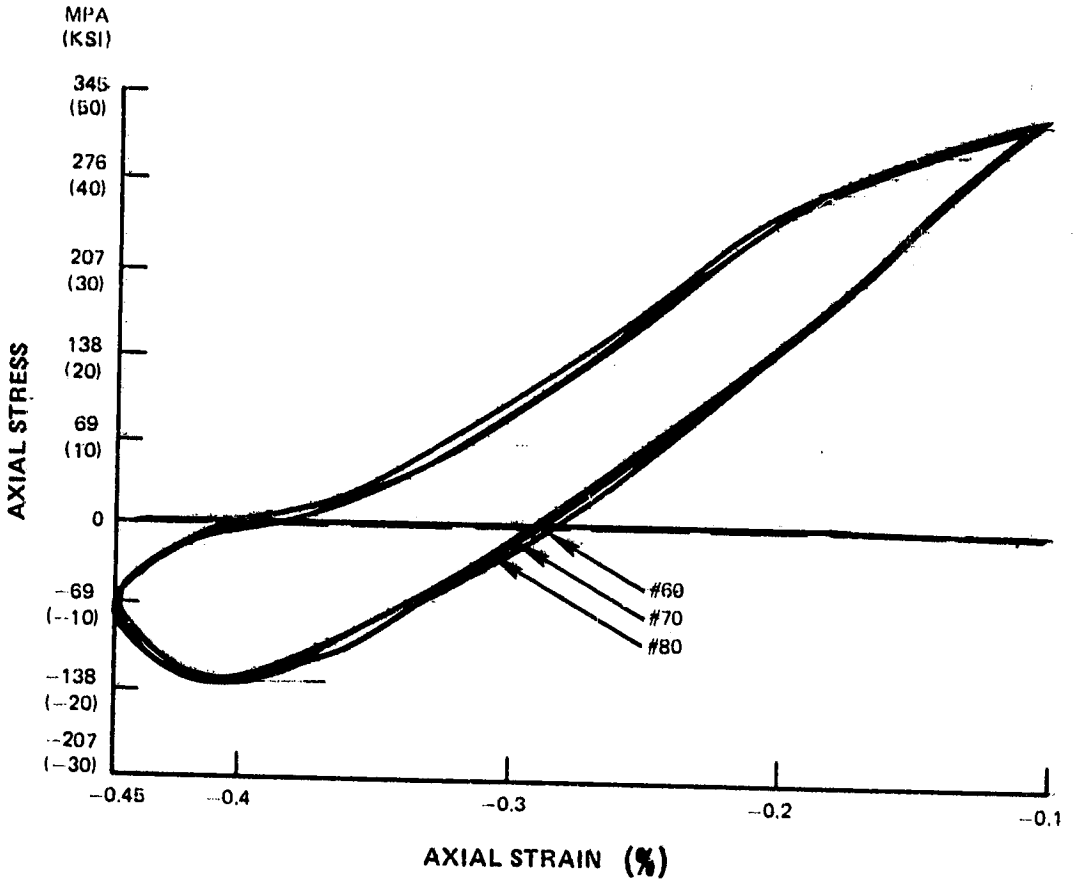

Figure 34 Test Specimen Response at Cycles 60, 70 & 80

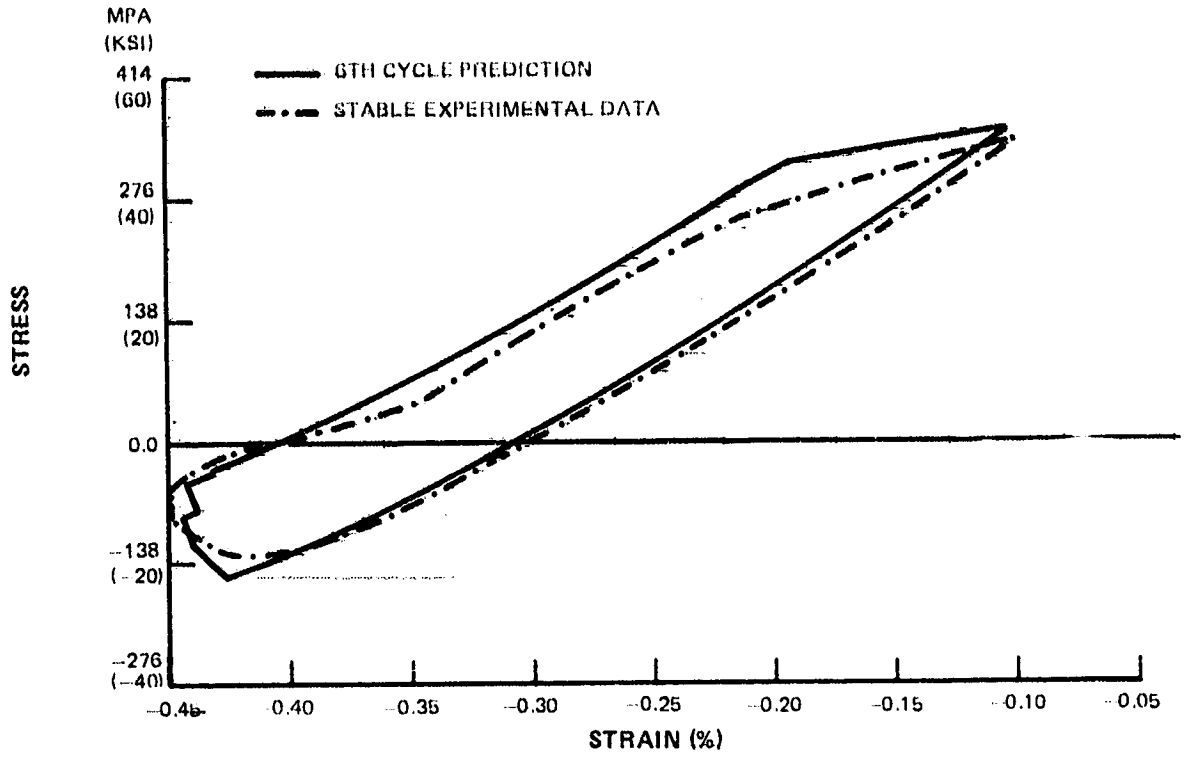

Figure 35 Comparison of Predicted 6th Cycle and Experimental Response

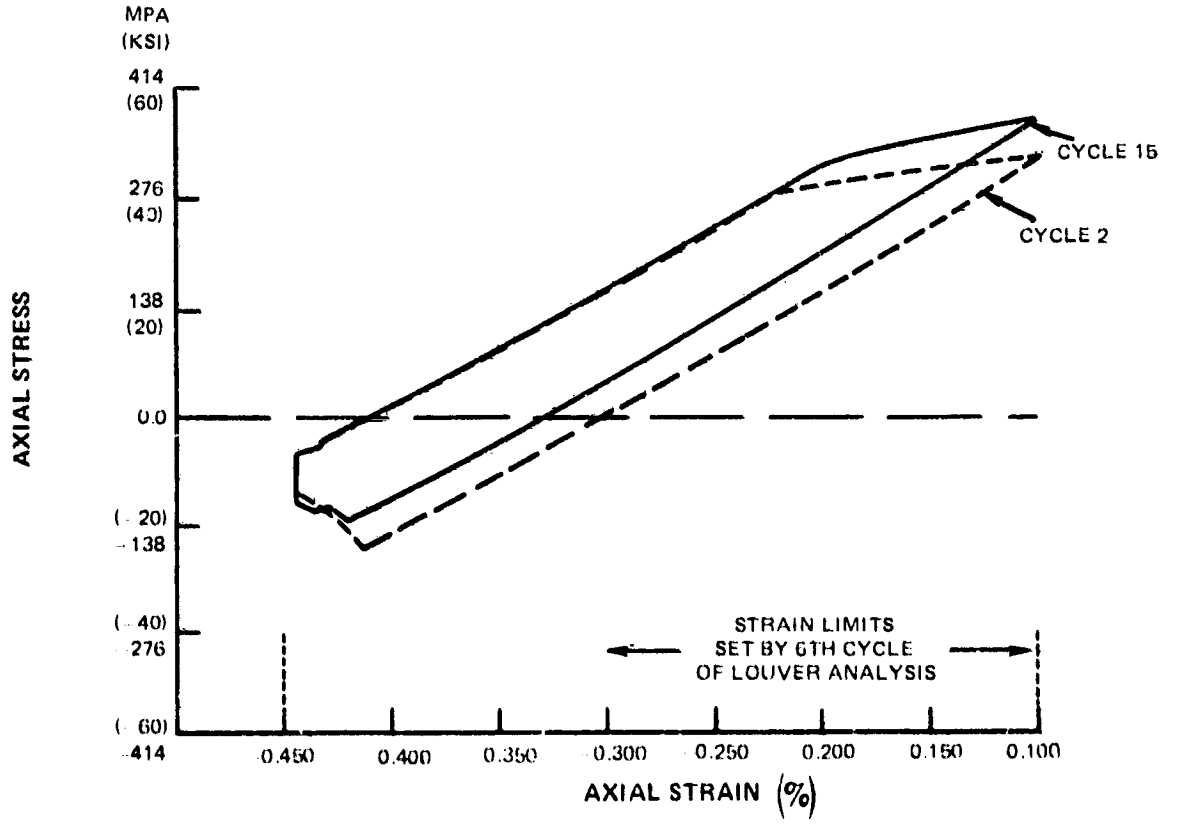

Figure 36 Cyclic Hardening Predicted by One Dimensional Analysis

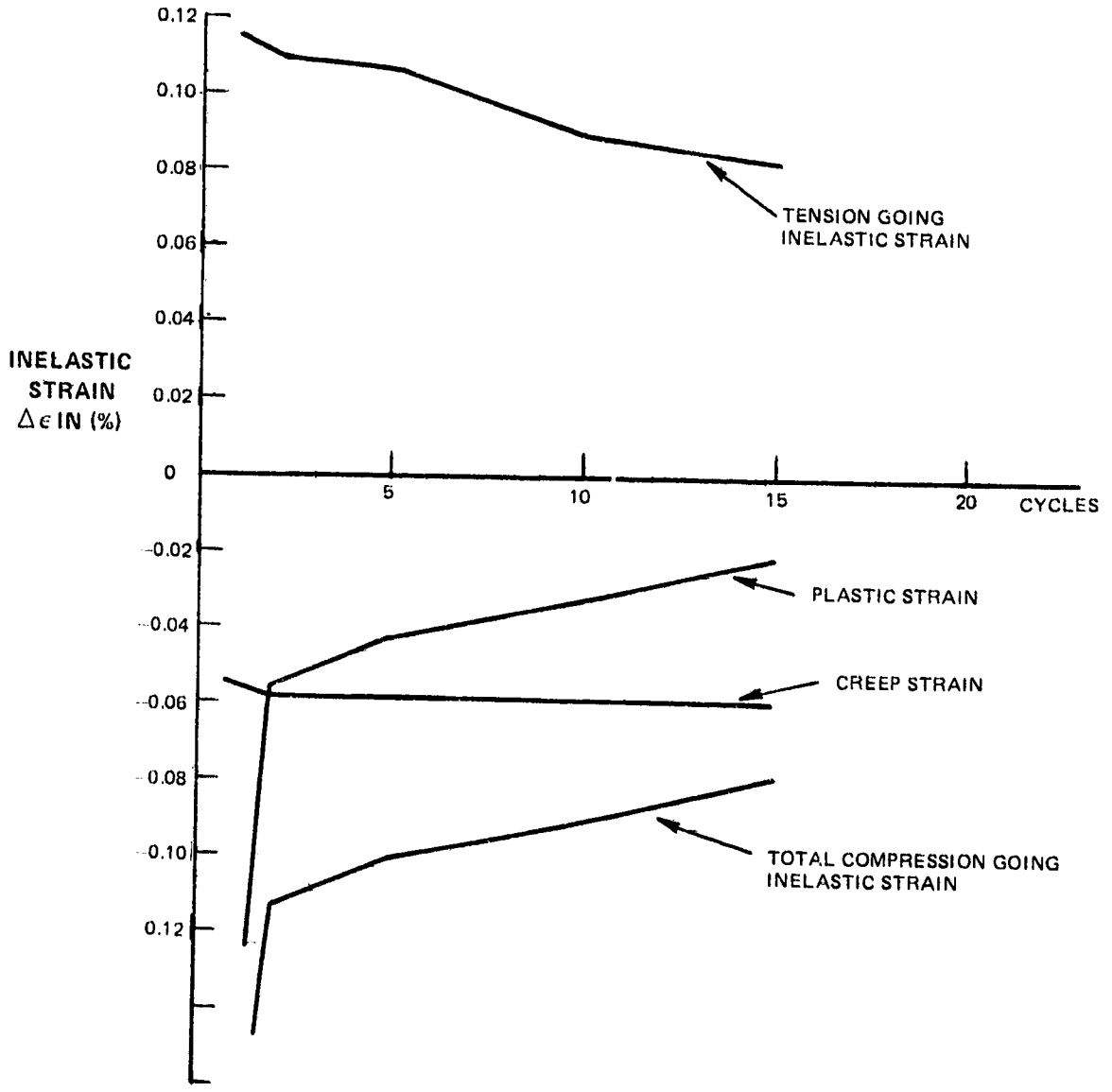

Figure 37 Inelastic Strain Components From One Dimensional Analysis

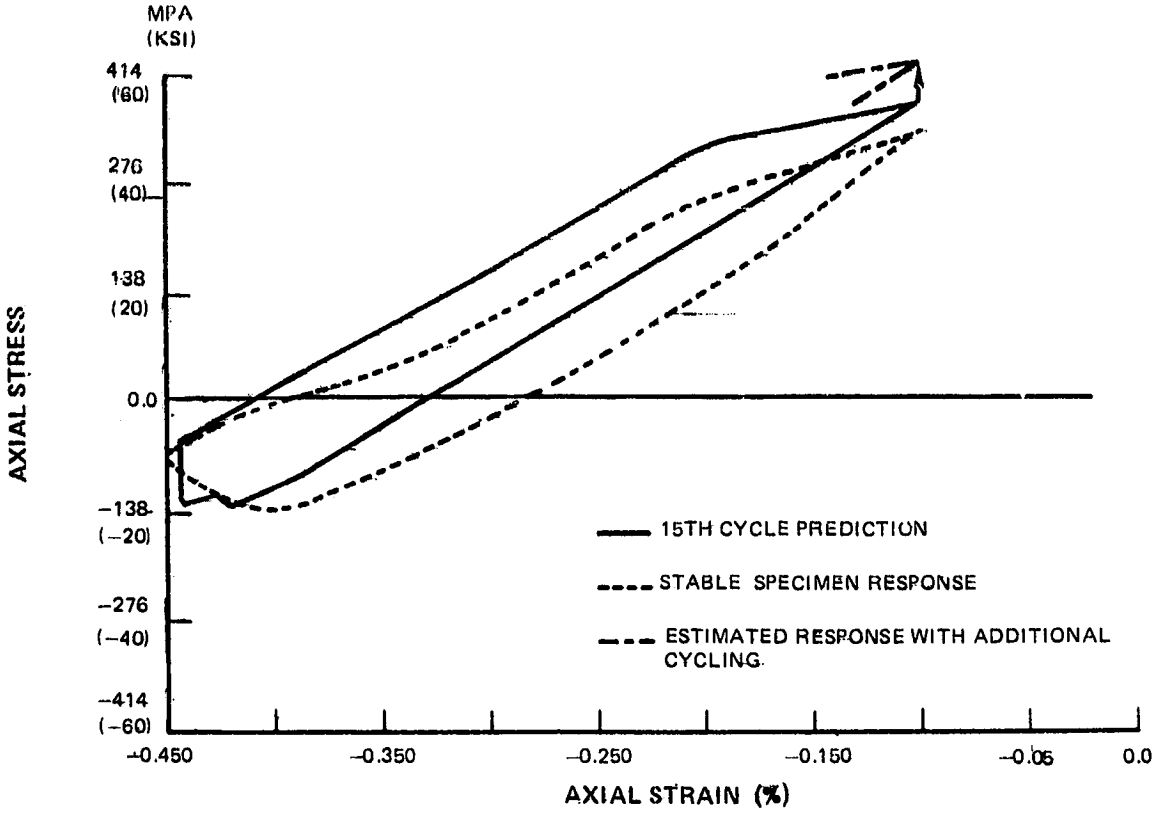

Figure 38 Predicted 15th Cycle and Stable Specimen Response

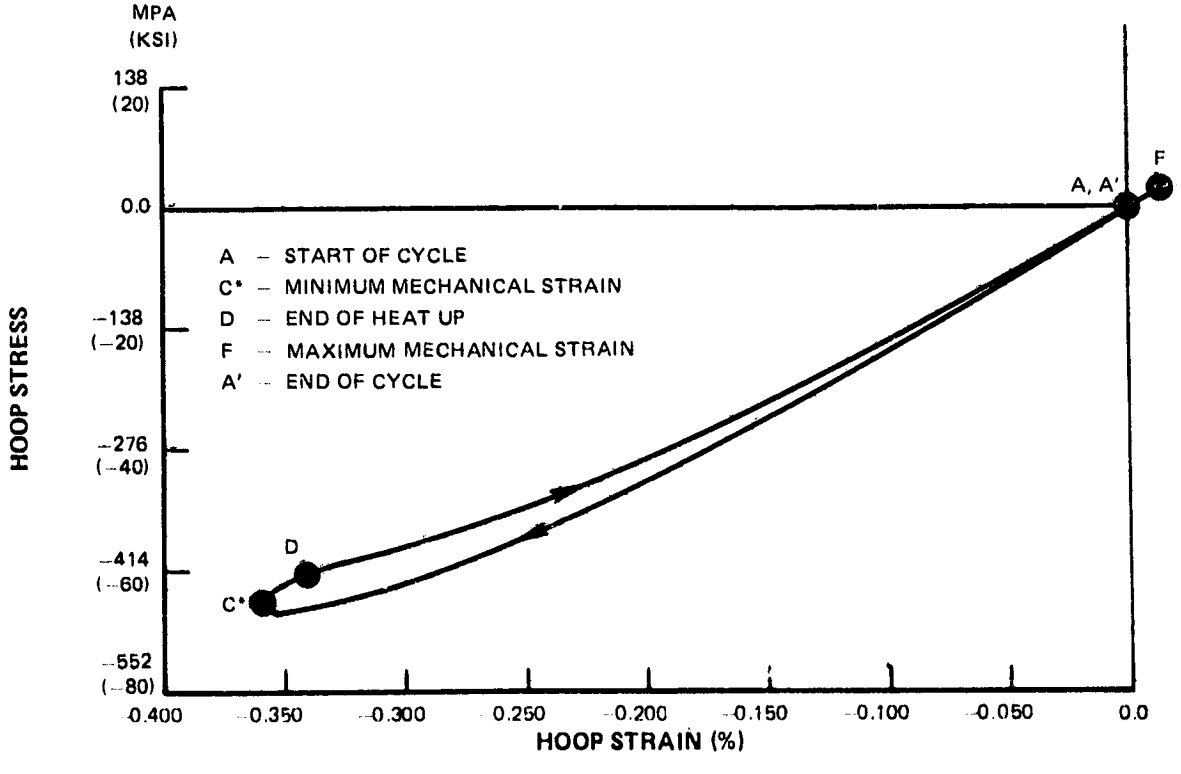

Figure 39 Linear Elastic Louver Lip Stress-Strain Response

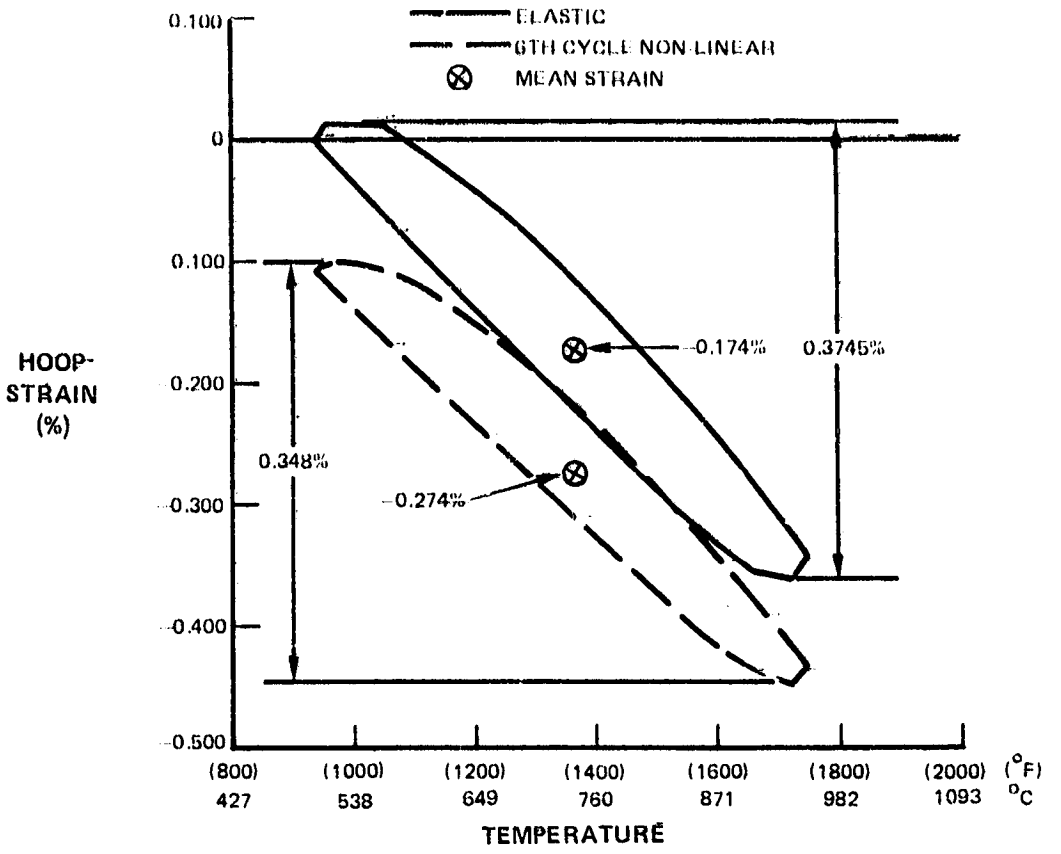

Figure 40 Linear Elastic and 6th Cycle Non-Linear Strain-Temperature Histories

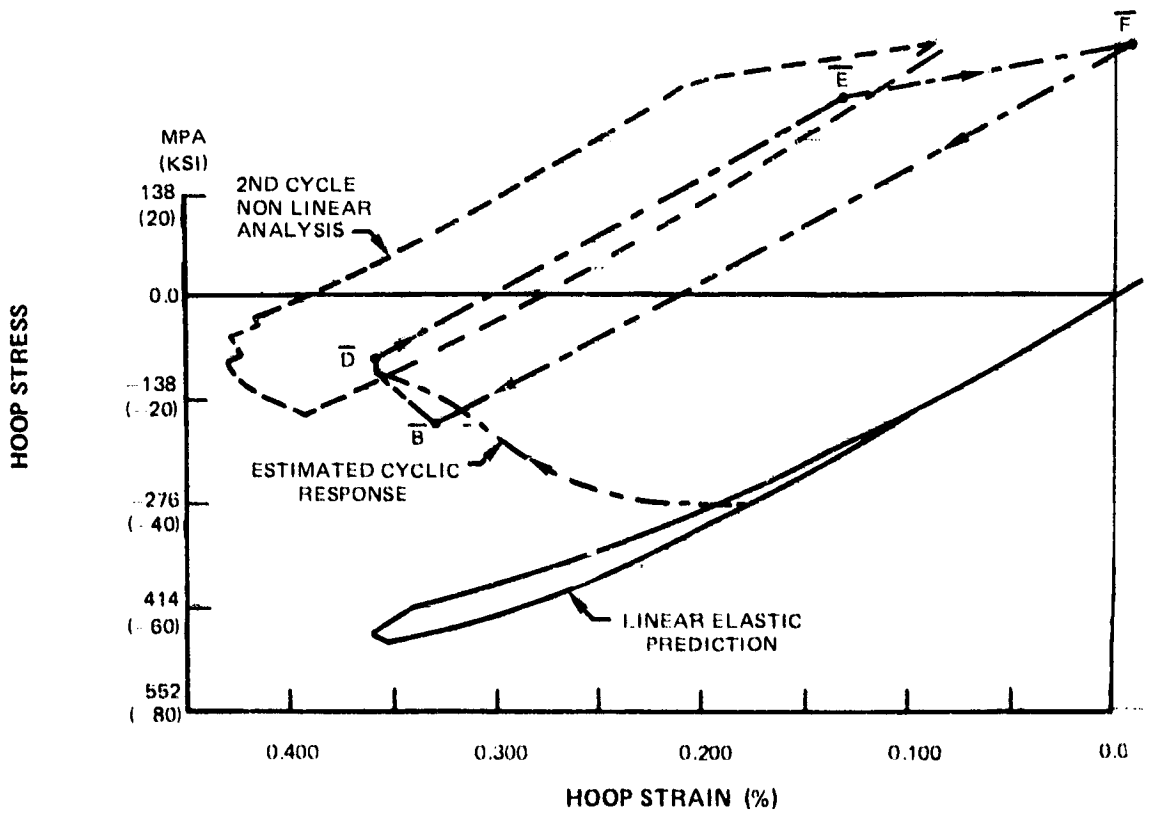

Figure 41 Cyclic Louver Lip Response Estimated From Linear Elastic Analysis

5.0 TASK III CYCLIC LIFE PREDICTION AND SENSITIVITY ANALYSIS

5.1 Introduction

The cyclic thermomechanical loading experienced by the louver component is representative of the loading on many of the structural components in the hot section of the gas turbine engine and is one of the most difficult problems for accurate durability prediction. The well defined experimental and analytical results obtained for the louver component have been used as a basis for the evaluation of several existing life prediction procedures. The failure mode for the louver has been considered as two mechanisms, crack initiation at the edge of the louver lip and axial crack propagation from the edge of the lip toward the weld. Three crack initiation procedures, described in the current literature, were selected and applied to this problem to determine their capability to predict the louver lip crack initiation life. A linear elastic fracture mechanics analysis was conducted and the results compared to the observed life growth data. Finally, a sensitivity analysis was conducted on each of the three crack initiation models.

All of the louver lip information presented in the previous sections has been predicted at the integration point closest to edge of the lip. Previous analysis using an axisymmetric louver model to determine optimum element mesh density indicated that the strain gradient in the lip could be accurately predicted by the 8 reduced integration point elements selected for the analysis. For the crack initiation life predictions, the stress and strain values at the corner of the louver lip were considered as the major "driver" for the initiation process.

The extrapolation procedure used to determine these values was based on the last 3 lip elements and is shown in Figure 42. The average value for each layer of integration points was used with a quadratic extrapolation to determine the surface strains. The two values of surface strain were then linearly extrapolated to the corner of the lip. Using this procedure, the variation between the corner node and the integration point in terms of total mechanical strain range is 7%. A similar procedure for the inelastic strain range (defined as the tension going plastic strain from the MARC analysis) produced a 17.5% increase in the value at the corner relative to the nearest integration point. In the following life prediction calculations the extrapolated corner values are used.

5.2 Crack Initiation Analyses

5.2.1 Strain Range Partitioning Method

Strain Range Partitioning (Reference 5) is a well known approach for the prediction of high temperature (creep/fatigue) crack initiation life. The method is based on the assumption that a structural response contains time independent plastic and time dependent creep components. Under cyclic reversed loading, these components combine to produce four (4) possible types of damage modes:

pp - tensile plasticity reversed by compressive plasticity
pc - tensile plasticity reversed by compressive creep
cp - tensile creep reversed by compressive plasticity
cc - tensile creep reversed by compressive creep.

A complex structural response is considered as containing as many as three (3) of these damage modes. The usefulness of this method has been demonstrated by many researchers on isothermal test specimens subjected to complex loading histories (Ref. 6). Life prediction by Strain Range Partitioning requires basic life relationships ($\Delta\epsilon$ vs. Life) for the 4 generic damage modes of the material being considered. In addition, the inelastic strain components generated by the actual loading cycle in the component must be determined. For the louver, the predicted results at the end of the lip were used to define the magnitides of the damage modes. The thermomechanical response was assumed to contain only pp (tensile plasticity revised by compressive plasticity) and pc (tensile plasticity revised by compressive creep) damage. This is consistent with the assumption that all of the time dependent response is occuring at the higher temperature when the lip is in compression.

The generic pp and pc life lines used in the life prediction were generated from a separate Pratt & Whitney Aircraft funded fatigue test program. The program consisted of uniaxial, strain controlled tests of fine grained Hastelloy X material between 538°C (1000°F) and 982°C (1800°F). Fully reversed (pp) and compressive hold time (pc) tests were included. The strain rate used for the pp tests (0.1 min^{-1}) was considered to be fast enough to prevent any creep or relaxation during these tests. The majority of the pp tests were conducted at 871°C (1600°F), however, the limited number of specimens at the other temperatures did not indicate a strong temperature dependence on fatigue life. In establishing the pp life line, all of the pp data was considered as a single data set and a least squares fit used to define the life line. In the compressive hold time (pc) testing, the same transient strain rate (0.1 min^{-1}) was used to reverse the strain and a 1 minute strain controlled hold time imposed at the maximum compressive strain point. After reviewing the data, it was determined that the inelastic strain generated in these tests consisted of pp and pc damage ($\Delta\epsilon_{pp}/\Delta\epsilon_{in} \cong 0.5 - 0.75$). This required that the interaction damage rule and the pp life relationship be used to determine the pc component. A limited number of pc tests were conducted at 760°C (1400°F) and 871°C (1600°F). The results showed a stronger temperature dependence than in the pp tests, however, all data points were grouped as one data set to establish the pc life relationship. The pp and pc life lines determined from these tests are shown in Figure 43. Their equations are:

$$N_{pp} = \left(\frac{\Delta\epsilon_{pp}}{54.42}\right)^{-1/.68} \quad ; \quad N_{pc} = \left(\frac{\Delta\epsilon_{pc}}{9.68}\right)^{-1/.51}$$

The initial life prediction with the SRP method used the results from the 6th loading cycle of the non-linear analysis. The pp and pc components were determined from the amount of compression going plastic and creep strain as predicted by MARC. The inelastic strain components at the element integration point are $\Delta\epsilon$ pp = 0.025% and $\Delta\epsilon$ pc = 0.06%. Extrapolating the strains to the corner of the louver lip and using the above life relationships with the interaction damage rule produces:

$$\frac{1}{N_{total}} = \frac{Fpp}{Npp} + \frac{Fpc}{Npc}$$

$\Delta\epsilon pp$	=	.02947	$\Delta\epsilon pc$	=	.0705
Fpp	=	.294	Fpc	=	.706
Npp	=	10600	Npc	=	7850

N_{total} = 8500 cycles vs. 1000 – 1250 cycles observed life

This overprediction of the crack initiation life may be associated with uncertainty in the definition of the fatigue life relationships (particularly the pc component). Additional fatigue data could potentially reduce the predicted life, however, it appears that the SRP method would still overpredict the cracking by at least a factor of 2.

5.2.2 Pratt & Whitney Aircraft - Commercial Products Division Combustor Life Prediction Method:

Development of this method is fully described in Reference 7. It is conceptually the same as the Strain Range Partitioning method in that the material cyclic damage is assumed to be partioned into separate "types". For a combustor loading cycle the PWA system assumes that the damage contains only pp-(compressive plasticity reversed by tensile plasticity) and pc-(compressive creep reversed by tensile plasticity) components. The inelastic strain range - life relationships used are similar in form to the "ductility normalized" relationships proposed for SRP. They are:

$$Npp = \left(\frac{\Delta cpp}{.75 \times Dp}\right)^{-1/0.6} \quad ; \quad Npc = \left(\frac{\Delta cpc}{1.25 \times Dp}\right)^{-1/0.8}$$

where: N_{pp} - fatigue life produced by the pp component

$\Delta\epsilon_{pp}$ - pp component of inelastic strain range

Dp - temperature dependent tensile ductility

N_{pc} - fatigue life produced by the pc component

$\Delta\epsilon_{pc}$ - pc component of inelastic strain range

A linear damage rule is used to predict total life.

$$\frac{1}{N_{total}} = \frac{1}{Npp} + \frac{1}{Npc}$$

Prediction of the inelastic strain range components ($\Delta\epsilon pp$, $\Delta\epsilon pc$) for this method is based on the total mechanical cyclic strain range determined from a linear elastic analysis and two algorithms:

$$\Delta\epsilon pp = \Delta\epsilon_{TR} \quad \Delta\epsilon_{el} \quad ; \quad \Delta\epsilon pc = \frac{1}{E}\left(\frac{\Delta\epsilon_{TR}}{K_1}\right)^{1/m}\left[1 \quad \left(\frac{K_1}{Bt}\right)^{1/m}\right]$$

where: $\Delta\epsilon_{TR}$ - total strain range predicted from linear elastic analysis

$\Delta\epsilon_{el}$ - endurance limit strain range associated with a fatigue life of 10^8 cycles

E - Young's modulus

K_1 - temperature dependent constant used in stress- strain curve representation ($\epsilon = K_1\sigma^m$)

B_t - time and temperature dependent constant developed from creep data for prediction of relaxation response ($\epsilon_c = B_t\sigma^m$)

Prediction of the louver lip crack initiation life was based on the following values:

$\Delta\epsilon_{TR}$ = 0.401% - extrapolated total elastic hoop strain range at corner of lip

D_p = 38% - tensile ductility associated with maximum cycle temperature (982°C (1800°F))

$K_1 = 6.8 \times 10^{-7}$, $m = 3.1$

Bt = 5.7×10^{-5} - Based on strain hold time at 982°C (1800°F)

E = 18.4×10^3 KSI

$\Delta\epsilon_{el}$ = .18% - endurance limit strain range at maximum cycle temperature 982°C (1800°F)

The resulting quantities are:

$\Delta\epsilon_{pp}$ = .221%; $\Delta\epsilon_{pc}$ = .068%

Npp = 3300 ; Npc = 3600

Ntotal = 1720 cycles

This method predicts a life closer to the observed component life, however, the predicted inelastic strain range ($\Delta\epsilon_{pp} + \Delta\epsilon_{pc}$) is nearly 2.9 times as large as the inelastic strain observed in both the non-linear analysis and thermomechanical uniaxial speciment test. Reducing the inelastic strain range to the observed value increases the calculated life to approximately 8000 cycles, consistnt with the SRP prediction. In actual design practice calculation using this method would be used with experimental engine and field service data to determine an overall service life of the component.

Both of the above methods, based on the prediction of inelastic strain, overpredicted the louver cracking life. The fact that each is calibrated using isothermal fatigue and creep/fatigue data suggests that thermomechanical (varying temperature) cycling may produce fatigue damage at a faster rate than an isothermal cycle.

5.2.3 Continuous Damage Method:

The third crack initiation life prediction for the louver lip used the Continuous Damage Approach proposed by J.L. Chaboche (References 8 and 9). This method was selected for evaluation because it is sufficiently different from the previous two methods (P&WA-CPD Combustor Life Prediction Method and Strain Range Partitioning). The approach is similar in concept to the Ductility Exhaustion method used in the prediction of turbine blade creep/fatigue life at Pratt & Whitney Aircraft (Reference 10).

The Continuous Damage Method is a stress based approach which assumes a damage internal variable that defines the strength of a material. The prediction of life requires solution of differential damage equations which determine the evolution of this damage. The damage (D) is assumed to be 0 in the initial undamaged state and 1 at failure. For high temperature loading the damage consists of creep (time dependent) and fatigue (time independent) components.

The creep damage component follows the form of Kachanov (Ref. 11) and Rabotnov (Ref. 12) and is written:

$$dD = \left(\frac{|\sigma|}{A}\right)^{r} (1 - D)^{-k} dt$$

where: D = damage variable

A,r,k = temperature-dependent coefficients

t = time

The fatigue damage process is defined as:

$$dD = [\,1 - (1 - D)^{\beta+1}\,]\ \alpha(\sigma m, \bar{\sigma}) \left[\frac{\sigma m - \bar{\sigma}}{M(\bar{\sigma})(1 - D)}\right]^{\beta} dN$$

$$\alpha(\sigma m, \bar{\sigma}) = 1 - a\left[\frac{\sigma m - \sigma\ell^{*}(\bar{\sigma})}{\sigma u - \sigma m}\right]$$

$$\sigma\ell^{*}(\sigma) = \sigma\ell + \left[1 - b\left(\frac{\sigma\ell}{\sigma u}\right)\right] \bar{\sigma}$$

$$M(\bar{\sigma}) = Mo\left[1 - b\left(\frac{\bar{\sigma}}{\sigma u}\right)\right]$$

where:

a,b,Mo,β	=	temperature dependent coefficients
σ m	=	maximum stress in the cycle
$\bar{\sigma}$	=	mean stress in the cycle
σ u	=	ultimate tensile strength
σ l	=	fatigue limit under completely reversed loading
σ l*	=	fatigue limit for non-zero mean stress
N	=	cycles

This expression describes, for rapid cycle fatigue (no creep), the relationship between maximum stress and life including mean stress effects. Combining the two damage expressions results in the interaction equation:

$$dD = \left\{\frac{(1 - D)^{-k}}{(k + 1)Nc} + \frac{[\,1 - (1 - D)^{\beta+1}\,]^{\alpha}}{(\beta + 1)N_{f}(1 - \alpha)(1 - D)^{\beta}}\right\} dN$$

Integrating to determine total life:

$$\frac{N_R}{N_F} = \int_0^1 \left\{ \frac{N_F}{N_C} \frac{(1 \quad D)^{-k}}{(k+1)} + \frac{[1 \quad (1 \quad D)^{\beta+1}]^{\alpha}}{(\beta+1)(1-\alpha)(1 \quad D)^{\beta}} \right\}^{-1} dD$$

where N_R = total life

N_C = life in pure creep = $\frac{1}{N_C} = (k+1)\int_0^{\Delta t} \left(\frac{|\sigma|}{A}\right)^r dt$

N_F = life in pure fatigue = $\frac{1}{N_F} = (\beta+1)(1-\alpha) \left\{ \frac{\sigma m - \bar{\sigma}}{Mo[1 - b(\frac{\bar{\sigma}}{\sigma u})]} \right\}^{\beta}$

For the combustor louver lip life prediction, the Hastelloy X constants for the creep portion of the damage equation were determined from the high stress-short time creep tests discussed in Section 4.2.3. The constants associated with the fatigue portion of the life prediction were obtained from the previous strain controlled fatigue tests used to generate the $\Delta\epsilon pp$ vs. Npp life curve in the Strain Range Partitioning life prediction method. Here, the values of stress determined from the stabilized stress-strain loops were used to determine the constants. Several additional assumptions were made for the louver life prediction with this method, they are:

1. A mean stress has no effect on fatigue life for the louver thermomechanical fatigue cycle. This is based on limited data that suggests mean stress values < 138 MPA (20ksi) have little effect on life. This simplifies the fatigue equation allowing:

$$b = 0$$
$$\sigma\ell^* = \sigma\ell$$
$$M(\bar{\sigma}) = Mo$$

2. The creep (relaxation) damage is assumed to occur only between 871°C (1600°F) and 954°C (1750°F) in the louver cycle. Based on the creep testing, the constants A, r, K are temperature independent. No difference is assumed to exist between tension vs. compression and creep vs. relaxation damage.

3. For the case of a variable temperature history (thermomechanical fatigue), Chaboche proposes the idea of an effective temperature which is used to evaluate the constants in the fatigue equation. The effective temperature is determined by considering the thermomechanical fatigue cycle on a non-dimensionalized stress basis which results in the equation:

$$\frac{1}{N_F(P_{II}, \bar{I}_1, T^*)} = \frac{1}{2} \int_{cycle} \frac{\beta(T) \langle dI_2 \rangle}{|I_2 - \bar{I}_2| N_F(|I_2 - \bar{I}_2|, \bar{I}_1, T)}$$

$$P_{II} = \sqrt{\frac{2}{3}} \frac{\sigma m - \bar{\sigma}}{\sigma u} = \text{reduced stress amplitude}$$

$$I_2 = \sqrt{\frac{2}{3}} \frac{\sigma m}{\sigma u}$$

$$\bar{I}_2 = \sqrt{\frac{2}{3}} \frac{\bar{\sigma}}{\sigma u}$$

$$\bar{I}_1 = \frac{\bar{\sigma}}{\sigma u} = \text{reduced mean stress}$$

T = temperature

T^* = effective temperature

$N_F(|I_2 - \bar{I}_2|, \bar{I}_1, T)$ = isothermal fatigue life

$N_F(P_{II}, \bar{I}_1, T^*)$ = fatigue life under varying temperature

For a given stress-temperature history and isothermal fatigue life relationships the integral can be evaluated. The effective temperature (T^*) is then determined from the maximum stress amplitude (P_{II}) and the value of N_F (P_{II}, I_1, T^*). This approach has been demonstrated by Chaboche (Reference 9) on a high strength, fairly rate insensitive material (IN 100). Following

this procedure for the Hastelloy X isothermal fatigue tests produced a reduced fatigue curve (I_2 vs N) which was temperature independent which makes the concept of an effective temperature inappropriate for the Hasteloy X thermomechanical cycle. Furthermore, the stress levels obtained in the thermomechanical cycle are smaller than those observed in the rapid cycle (pp) fatigue tests. This is due to the high rate sensitivity of the material at these temperatures. Those results results, shown in Figure 44, suggest that the majority of the total damage in the louver cycle is associated with creep and not time independent fatigue. These observations raise some doubt as to the appropriation of this method for the thermomechanical fatigue of a material like Hastelloy X.

In the actual life calculation for the louver lip, several fatigue damage components were considered to determine the sensitivity of the calculation. The predicted 6th cycle stress-strain response at the end of the louver lip was used to establish the stress levels for the damage equations (see Figure 45). The creep damage is assumed to occur between -151.7 MPA (-22 KSI) and -27.6 MPA (-4 KSI) within 1 minute, an exponential die out of stress with time is used. The stress amplitude is chosen as 358.5 MPA (52 KSI) (the maximum tensile stress) and 510.2 MPA (74 KSI) (the total stress amplitude). The total fatigue damage is assumed to occur at either 538°C (1000°F) or 760°C (1400°F). A summary of the material constants and life predictions are shown below:

Hastelloy X Constants for Continuous Damage Approach

Temperature (°F)	σ_u (KSI)	σ_1 (KSI)	β	Mo
1000	86	42	8.92	219
1400	57	32	6.51	242
$A = 7.8 \times 10^7$	r = 0.23	K = 3.51	a = 1	b = 0

Stress Amplitude	Fatigue Life (cycles)	Creep Life (cycles)	Total Life (cycles)	Actual Life (cycles)
358.5MPA @ 538°C (52 ksi @ 1000°F)	128300	515	495	1000-1250
510.2MPA @ 538°C (74 ksi @ 1000°F)	600	515	250	1000-1250
358.5MPA @ 760°C (52 ksi @ 1400°F)	745	515	250	1000-1250

In all calculations the creep component was the limiting life component. Additional variations in the stress levels during relaxation did not significantly increase the predicted creep life. The conservative prediction of the louver lip cracking life suggests that the assumptions of the stress amplitude pro-

ducing fatigue damage and damage associated with compressive relaxation may not be appropriate for Hastelloy X at elevated temperature. This is further demonstrated when the Continuous Damage Method was used to predict the life of the isothermal strain controlled hold time tests. These are the same creep fatigue tests used to generate the $\Delta\epsilon_{pc}$ vs. N curve for the Strain Range Partitioning Method. For all tests (5), the Continuous Damage Method predicted life was approximately 15% of the actual life. This conclusion is consistent with the general SRP observation that a cp (tensile creep-compressive plasticity) is more damaging than a pc (tensile plasticity-compressive creep) type of cycle.

5.3 Crack Propagation Analysis:

A series of analyses were conducted using the linear elastic fracture mechanics method to predict the subsequent growth of fatigue cracks from the edge of the louver lip. Existing Hastelloy X sheet crack growth data was used to establish the crack growth law for the analyses. This data was obtained from isothermal, center cracked panel, load controlled (R = 0) tests which had been conducted at temperatures between 427°C (800°F) and 760°C (1400°F). Only the 760°C (1400°F) data was used in the analysis, since it represented the fastest available growth rate and would provide the most conservative prediction. This assumption is consistent with the louver lip stress-strain response since the highest tensile stresses occur during the thermomechanical cycle at temperatures between 760°C (1400°F) and 504°C (940°F). The louver lip was modeled as a semi-infinite plate with a through thickness edge crack. The prediction was based on an influence or weight function method described in References 13 and 14. This method allows for very general stress (strain) gradients to be simulated. The crack driving force (ΔK) is computed from the stress (strain) distribution in the uncracked part, along the plane of crack propagation. The effects of the cyclic stress range on the predicted growth rate was modeled by means of the R-ratio. The general equation for the crack growth rate used in the analysis is:

$$\frac{da}{dn} = c\left[\frac{\Delta K}{1-R}\right]^m$$

where: c,m = temperature dependent constants

R = R-ratio ($\sigma_{min}/\sigma_{max}$)

ΔK = stress intensity factor

The stress range ($\Delta\sigma$) and R-ratio in the analyses were determined from the 6th cycle of the louver non-linear analysis. The distribution of these quantities along the louver lip is shown in Figure 46. The results of three (3) calculations are compared to the measured rig crack growth data in Figure 47. In all calculations, an initial crack length of .0254 cm (.010 in) was assumed to

exist at 1050 cycles. Curves A and B are the predictions assuming R = 0 (considering the entire stress range as tensile loading). The difference in the two curves is associated with two representations of the crack growth law shown in the Figure. Curve A used the bilinear representation while B resulted from the extrapolation of the low ΔK values. This modification to the crack growth law was investigated because the steeper portion of the law (large ΔK) was associated with net section yielding ahead of the crack tip in the center cracked tests. Curve C s the result of including the predicted R ratio distribution along the lip in the crack growth law. The negative R-ratio reduces the growth rate (da/dn) for a given ΔK resulting in a much slower response than the R = 0 calculations. All 3 calculations predict an initial crack growth rate which is slower than the rig data. Curve A comes the closest to predicting the cyclic life, but the growth rate at crack lengths greater than .0508 cm (.060 in) is much steeper than the data. The effects of time dependent plasticity and the varying temperature cycle have not been included in these predictions. Under these conditions, the local stress at the crack tip, affected by closure and stress relaxation, may accelerate the predicted crack growth rate.

5.4 Sensitivity Analysis

A sensitivity analysis was conducted on the three crack initiation life prediction methods considered in Section 5.2. Variation in total mechanical strain range was selected as the key parameter for assessing the sensitivity of each of the life prediction methods. An increase in the mechanical strain range in the louver geometry is possible by perturbations of the temperature distribution and magnitude along the louver lip. The axisymmetric louver model previously used to establish the finite element mesh density along the lip, was used to predict the increase in circumferential (hoop) strain with these changes. Two variations in temperature distribution and a 100°F increase in maximum temperature were considered. Linear elastic analyses were performed using the 10 second transient temperature distribution as the baseline. This coincides with the point of maximum temperature gradient (strain) in the louver cycle. It was assumed that changes in the predicted strain at this point are directly related to changes in the mechanical strain range. The results of the analyses, (Figure 48) indicate that, as more of the temperature gradient is concentrated toward the edge of the lip, (profiles A and B), the predicted hoop strain increases relative to the baseline value. An increase in temperature of 100°F at the lip edge further increases the strain relative to the baseline. Although it is the more severe condition, profile B is least likely to occur due to heat conduction effects. Assuming a possible error of 100°F in the temperature measurement during the test and the "A" temperature profile, an increase in the total mechanical strain range at the edge of the louver lip of 20% seems reasonable for the sensitivity analyses.

The sensitivity of the three life prediction methods to a change in total mechanical strain range is shown in Figure 49. These calculations reflect only a change in the strain range, any change in temperature dependent parameters is neglected. Each method will be discussed separately.

PWA-CPD Combustor Life Prediction Method:

This method has a moderate sensitivity to a change in strain range. The 20% increase discussed above produces a 27% decrease in predicted life (1710 to 1240 cycles). The predicted inelastic strain range, determined by the two algorithms discussed in Section 5.2.2, increases by 29% of which most of the change is associated with $\Delta\epsilon$pp damage. A summary of the two calculations is shown below.

Baseline		120% of Baseline	
$\Delta\epsilon$ total	= 0.40%	$\Delta\epsilon$ total	= 0.481%
$\Delta\epsilon$ inelastic	= 0.289%	$\Delta\epsilon$ inelastic	= 0.373%
$\Delta\epsilon$ pp	= 0.221%	$\Delta\epsilon$ pp	= 0.301%
$\Delta\epsilon$ pc	= 0.068%	$\Delta\epsilon$ pc	= 0.072%
Npp	= 3299	Npp	= 1964
Npc	= 3592	Npc	= 3336
N_{total}	= 1710	N_{total}	= 1240

Strain Range Partitioning:

This method show a high degree of sensitivity to a change in strain range. The 20% increase produces a 65% decrease in predicted life (8500 to 3000 cycles). This is due to a 74% increase in the inelastic strain range which results from the assumption that all of the increase in total strain range is inelastic strain. This assumption is made because the cyclic plasticity in the Hastelloy X will not allow a significant increase in stress range with increasing strain range. The results of the uniaxial specimen testing shown in Figure 33 demonstrates this effect. These results emphasize the importance of an analysis technique and nonlinear material model that can accurately predict the inelastic strain range for a structural component. A summary of the two calculations are shown below.

Baseline		120% of Baseline	
$\Delta\epsilon$ total	= 0.372%	$\Delta\epsilon$ total	= 0.446%
$\Delta\epsilon$ inelastic	= 0.100%	$\Delta\epsilon$ inelastic	= 0.174%
$\Delta\epsilon$ pp	= 0.029%	$\Delta\epsilon$ pp	= 0.051%
$\Delta\epsilon$ pc	= 0.071%	$\Delta\epsilon$ pc	= 0.123%
Npp	= 10636	Npp	= 4700
Npc	= 7847	Npc	= 2640
N_{total}	= 8500	N_{total}	= 3000

Continuous Damage Method:

This method is assumed to be insensitive to strain range for the Hastelloy X thermomechanical cycle considered. This is based on the constant peak stress values related to a change in total strain range discussed for the SRP method. Actually, a small increase in the stress range would further decrease the predicted life, making the prediction more conservative relative to the data.

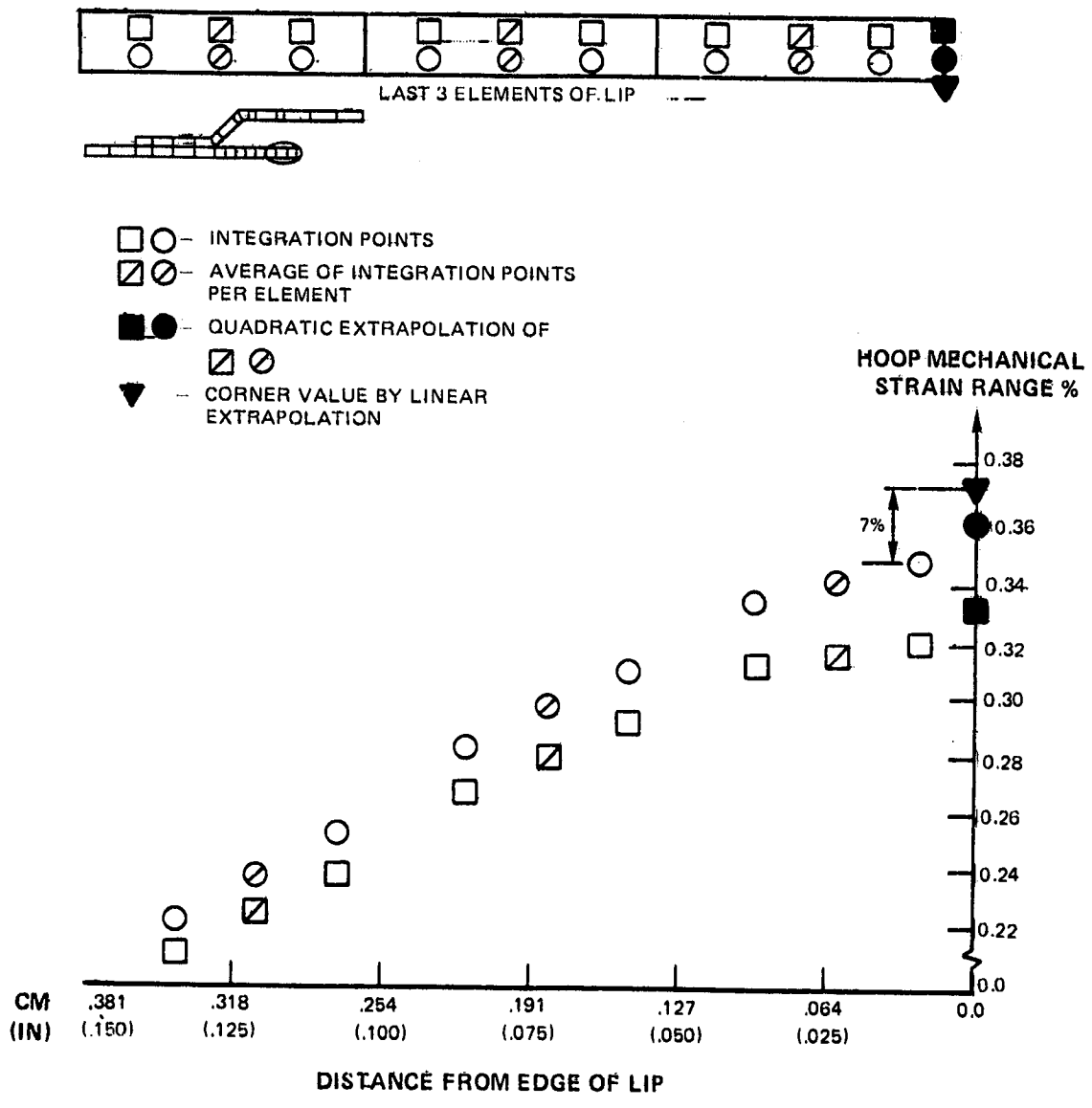

Figure 42 Extrapolation of Louver Lip Strain

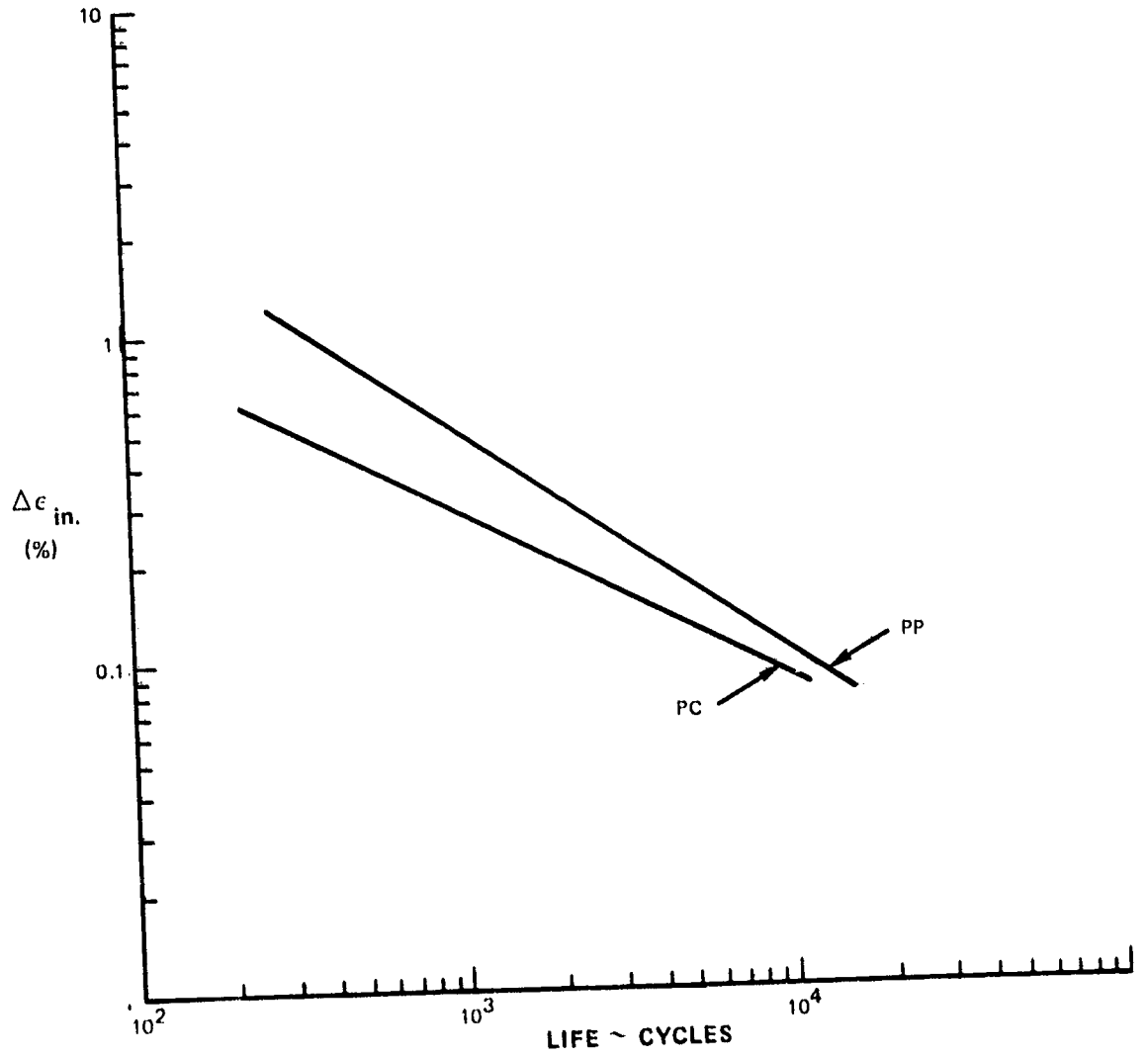

Figure 43 General Hastelloy X PP-PC Life Relationships for Strain Range Partitioning

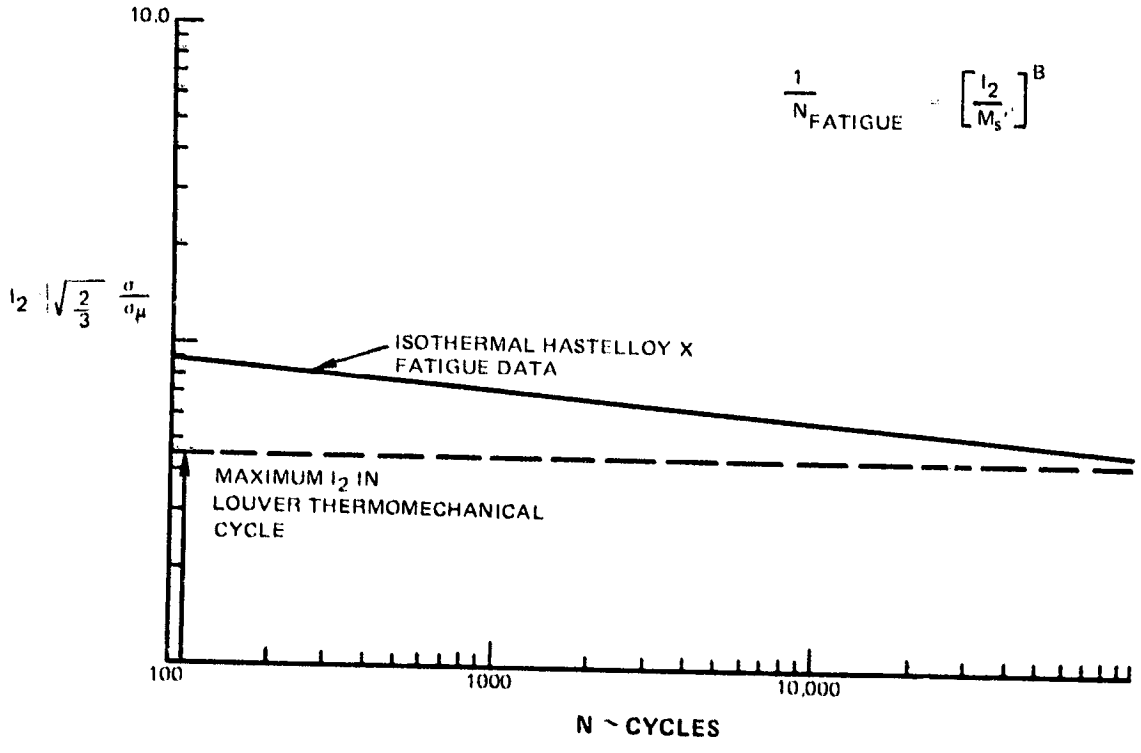

Figure 44 Fatigue Damage Component for Continuous Damage Method

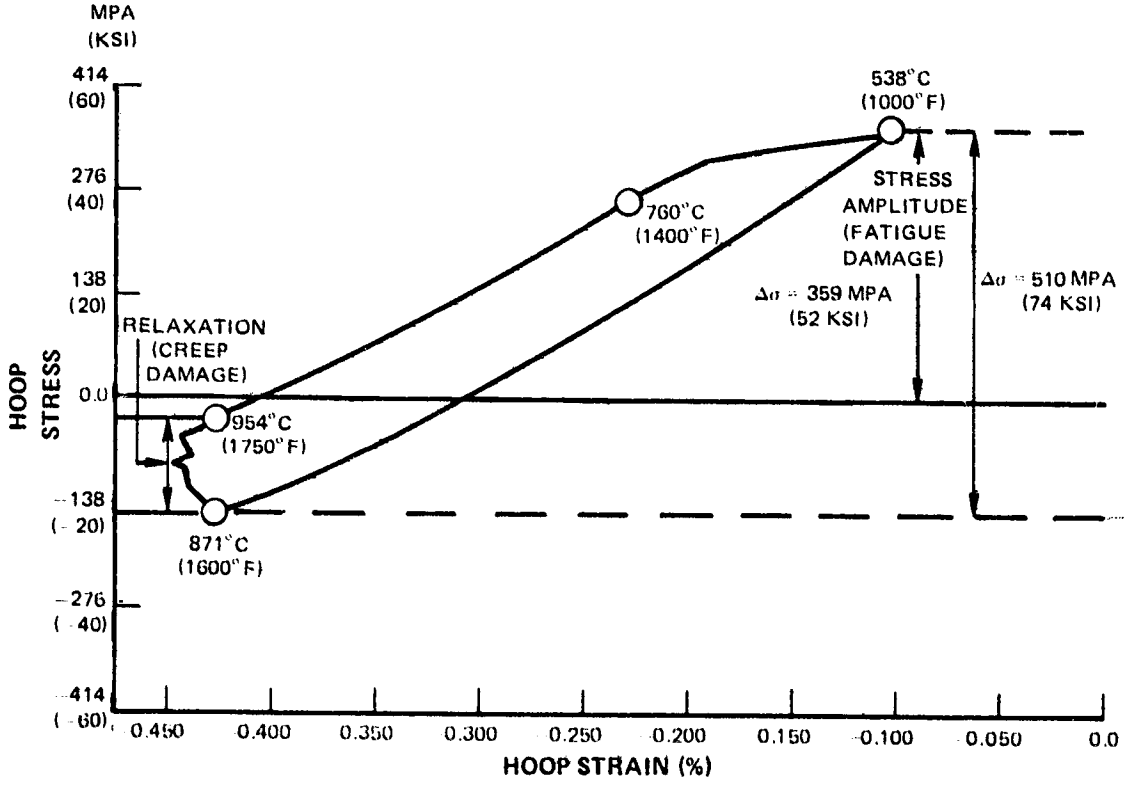

Figure 45 Stable Stress Response for Continuous Damage Method

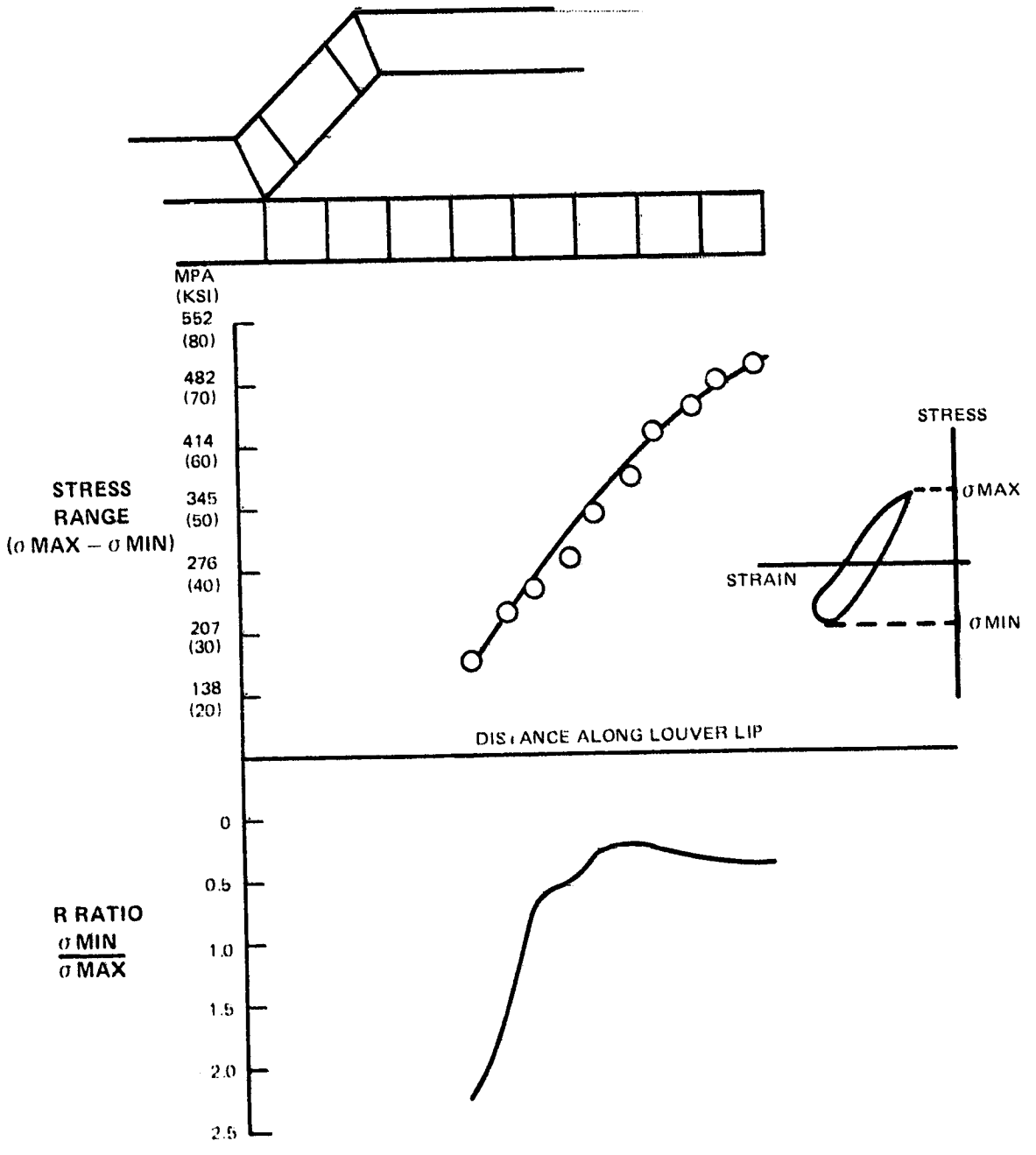

Figure 46 Stress Range and R Ratio Distribution along Louver Lip

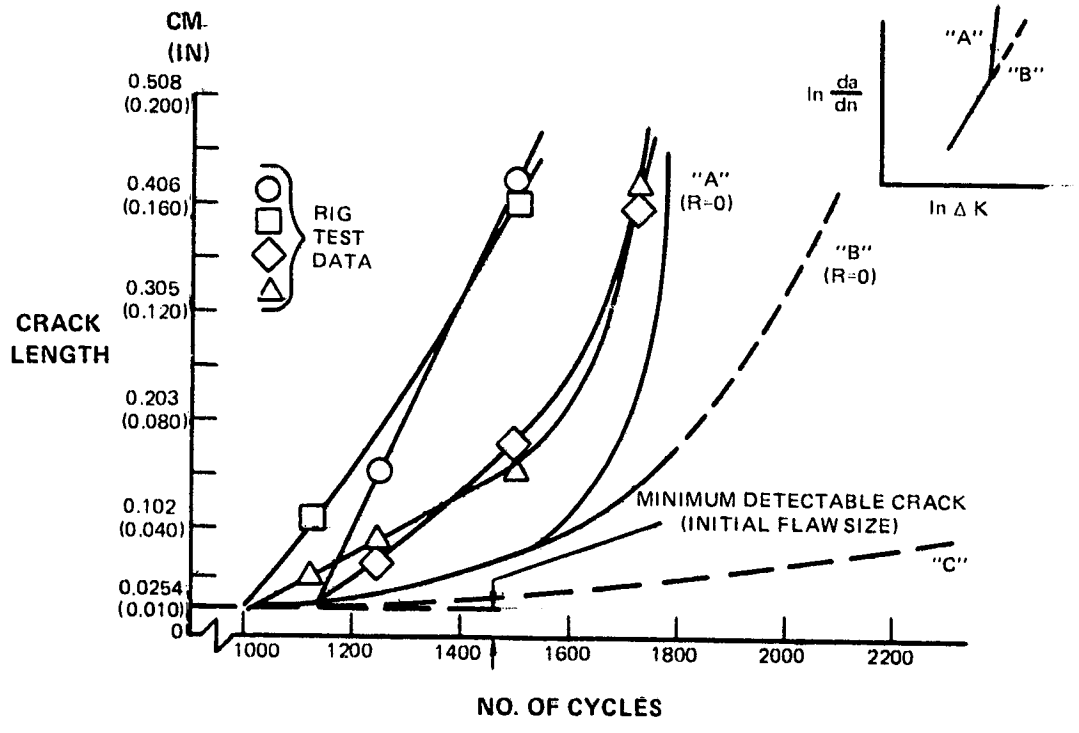

Figure 47 Comparison of Test Data and Crack Propagation Analyses

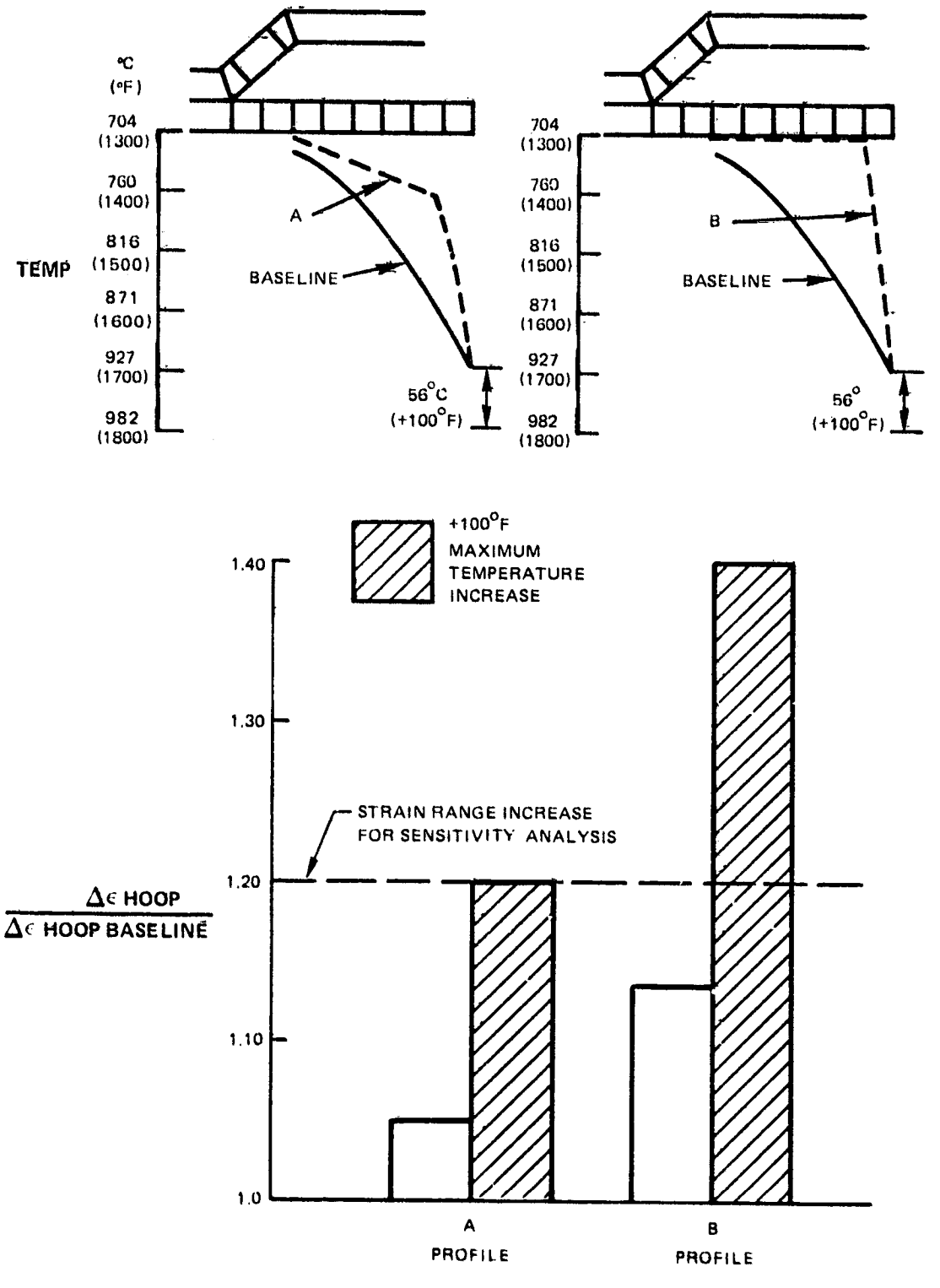

Figure 48 Effect of Temperature Distribution On Maximum Louver Lip Strain Range

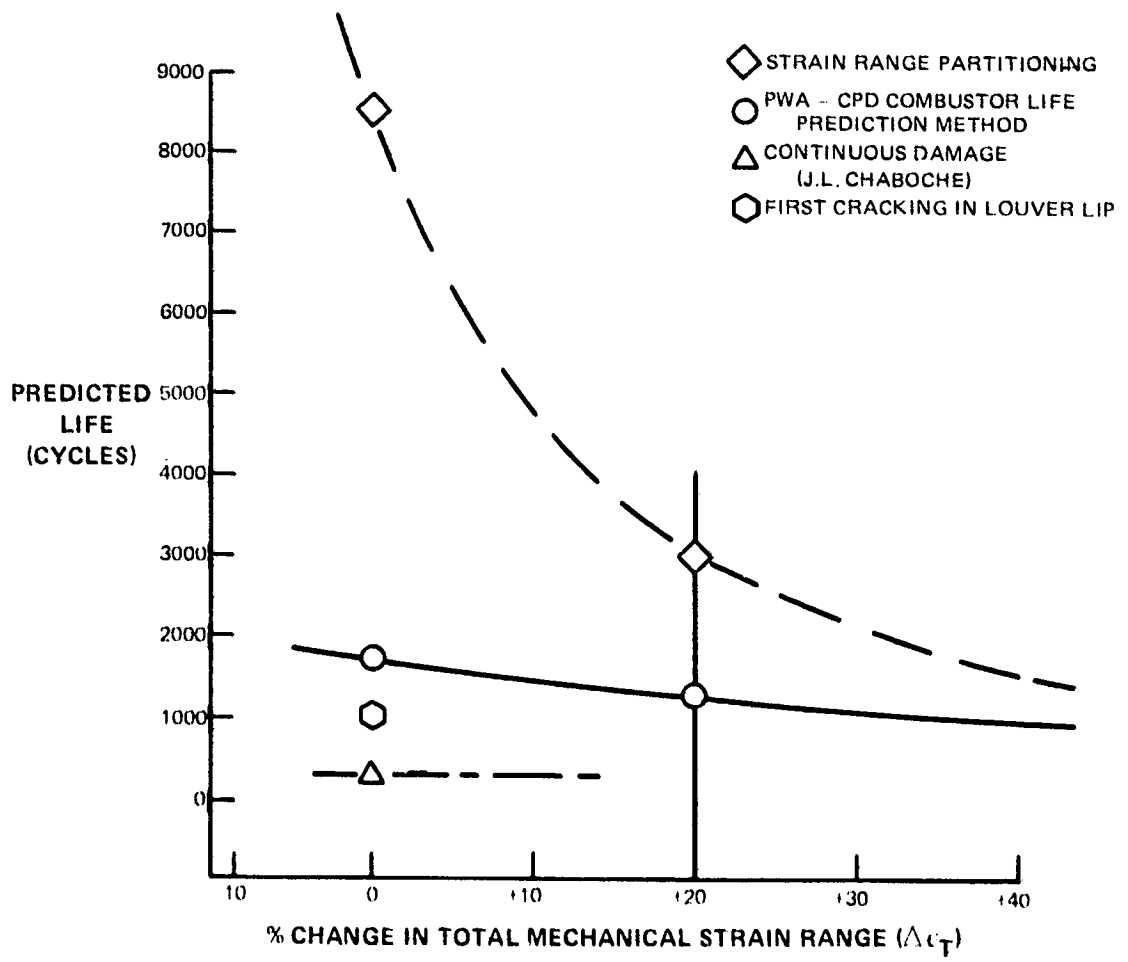

Figure 49 Sensitivity of Three Crack Initiation Life Prediction Methods

6.0 DISCUSSION OF RESULTS AND CONCLUSIONS

This program has addressed most of the disciplines associated with the design and analysis of gas turbine engine hot section structural components. The specific analyses have been performed on a well controlled simulated combustor liner test specimen. These results have identified a number of areas where further research and development would contribute toward the improved durability of these components. General conclusions and observations concerning this work are:

1. Hot section structural components are subjected to complex thermomechanical loadings. A well controlled source of benchmark data is a useful tool for the development and calibration of analytical and life prediction models.

2. The three dimensional finite difference heat transfer solution conducted for this program accurately predicted the louver steady state and transient temperature distribution.

3. The temperature predictions are highly dependent on the accuracy of the thermal boundary conditions. The greatest uncertainty in this analysis was in the calculation of the louver heat transfer coefficients.

4. The three dimensional spatial and temporal interpolation between the heat transfer and finite element structural meshes required a large amount of effort. The interpolation scheme used had difficulty in consistently selecting thermal nodes to determine a temperature for a structural integration point. A number of the temperatures were manually adjusted to agree with the temperature solution. Part of this problem may have been associated with the louver dimensions and the small included angle in the model. Potential improvements in this area would reduce the overall manpower to complete a thermal-structural analysis. One area suggested for investigation is the use of a finite element heat transfer solution. Use of a consistent element type and mesh would then eliminate the need for interpolation.

5 The combined (isotropic-kinematic) hardening rule can be used to model the isothermal Hastelloy X strain controlled cyclic response at a given strain rate.

6. A constant creep strain rate model developed from short time-high stress level creep tests accurately predicted Hastelloy X isothermal stress relaxation data.

7. Results of the nonlinear louver structural analysis indicated that the time independent plasticity model and the creep simulation did not accurately predict the cyclic thermomechanical response at the louver failure location. Tests of a uniaxial strain controlled specimen run with the same mechanical strain-temperature history as predicted at the failure location indicate that the stress-strain response stabilized within the

first few cycles. Simulation of this experiment with the Hastelloy X model discussed above showed continued cyclic hardening (increasing peak tensile stress and reduced inelastic strain range) after many cycles. Potential modification to the material model, including a multi-yield-surface concept, non-linear hardening or use of one of the rate dependent (unified) theories currently under development, may be required to improve the prediction for the varying temperature loading condition. Determination of correct thermomechanical response is important in the life prediction, and in determining the extent (number of cycles) of non-linear analysis required for a structural component.

8. The three (3) high temperature (creep/fatigue) life prediction methods considered are the Strain Range Partitioning, Pratt & Whitney Aircraft - Commercial Products Division Combustor Life Prediction, and Continuous Damage methods. All assume that time independent plastic and time dependent creep damage mechanisms are present at elevated temperature. Isothermal fatigue and creep rupture tests are used to define the material life relationships.

   The Strain Range Partitioning and PWA-CPD methods assume the existence of generic types of fully reversed damage cycles composed of combinations of the plastic and creep mechanisms. For purposes of this analysis, the combustor louver lip response contained only the pp(tensile plasticity reversed by compressive plasticity) and pc(tensile plasticity reversed by compressive creep) damage cycles.

   The Strain Range Partitioning method overpredicted the louver cracking life (8500 cycles vs. 1000 cycles). Part of this discrepancy may be associated with uncertainty in the definition of the generic pp and pc fatigue life curves. Better definition of the curves may reduce the predicted life (and improve the correlation), however, it appears that the SRP method will overpredict the cracking life by at least a factor of 2.

   The Pratt & Whitney Aircraft - Commercial Products Division method also overpredicted the louver cracking life (1700 cycles vs. 1000). This improved correlation (relative to SRP) is due, in part, to the fact that the inelastic strain range predicted by this method is larger than the observed inelastic strain in the louver. Equating the inelastic strain value results in a predicted life of 8000 cycles, which is similar to the SRP calculation. In actual design practice, this method is used with experimental and field service data to assess the overall service life of the component. These results suggest that a thermomechanical fatigue cycle may produce damage at a faster rate than a comparable isothermal cycle.

   The Continuous Damage Method predicts life based on the growth of a damage parameter (D) from the initial undamaged state (D = 0) to failure (D = 1). The method uses a non-linear accumulation of damage produced by the plastic (fatigue) and creep mechanisms. This method is a stress (rather than strain) based approach and has the general formulation to consider

mean stress effects in the fatigue cycle. In considering the stress range as the key fatigue damage producer, the method predicts that the louver thermomechanical cycle contains little fatigue damage. This is a consequence of the rate sensitivity of Hastelloy X at high temperature and raises some questions as to the applicability of this approach for highly rate sensitive materials. Initial calculations using this approach under predicted the louver lip cracking life by factors of 2 to 4. In all calculations the creep component was the controlling life component. The assumption that compressive stress relaxation (observed in the combustor cycle) is as damaging as tensile creep may be partially responsible for the conservative prediction.

9. Calculation of fatigue crack growth using the linear elastic fracture mechanics approach may not be appropriate for Hastelloy X thermomechanical loading. Analyses were conducted using a crack growth law generated from isothermal (760°C (1400°F)), load controlled (R=0), center cracked panel testing. Stress values were obtained from the 6th cycle nonlinear analysis. The use of load controlled data and predicted stress ranges was assumed to be valid for the small crack lengths considered. Two calculations were performed, 1) assuming that the total stress range was tensile loading (R=0), 2) using the global R ratio (min/ max) distribution determined from the louver analysis. Both analyses predict initial growth rates considerably slower than the observed values.

   Inelastic and time dependent effects were neglected in these calculations. The large region of inelastic response, relative to the small initial crack sizes, suggests that a nonlinear measure (e.g., J integral) may be a better correlating parameter. In addition, rapid stress relaxation observed in Hastelloy X suggests that the local R ratio near the crack tip is more important than the global R ratio effect.

7.0 REFERENCES

1. MARC General Purpose Finite Analysis Program, Users Manual-Volumes A - E. MARC Analysis Research Corporation, 1980.

2. INPUT B: A Thermal/Structural Data Interface Program for Two-Dimensional Interpolation, NASA-CR-144119, Boeing Aerospace Company.

3. Research and Development Program for Non Linear Structural Modeling With Advanced Time-Temperature Constitutive Relationships, Contract No. NAS3-22055, Pratt & Whitney Aircraft, 1980.

4. Hopkins, S. W., "Low Cycle Thermal Mechanical Fatigue Testing," Thermal Fatigue of Materials and Components, ASTM STP 612, American Society for Testing and Materials, 1976, pp. 157-169.

5. Manson, S. S., Halford, G. R., and Hirschberg, M. H.: "Creep-Fatigue Analysis by Strain-Range Partitioning", First Symp. on Design for Elevated Temperature Environment, Am. Soc. Mech. Engrs., 1971, pp. 12-28.

6. Characterization of Low Cycle High Temperature Fatigue by the StrainRange Partioning Method, AGARD-CP-243, Technical Editing and Reproduction Ltd., London, 1978.

7. Reliability Prediction for Combustors and Turbines, AFAPL-TR-77-8, 1977.

8. Chaboche, J. L., "Thermodynamic and Phenomenological Description of Cyclic Visco-Plasticity With Damage," European Space Agency Technical Translation, May, 1979.

9. Chaboche, J. L., Policella, H., Kaczmarek, H., "Applicability of the SRP Method and Creep-Fatigue Damage Approach to the LCHTF Life Prediction of IN-100 Alloy," AGARD-CP-243, Technical Editing and Reproduction Ltd., London, 1978, pp 4-1 to 4-20.

10. Polhemus, J. F., Spaeth, C. E. and Vogel, W. H., "Ductility Exhaustion Model for Prediction of Thermal Fatigue and Creep Interaction," Fatigue at Elevated Temperatures, ASTM STP 520, American Society for Testing and Materials, 1973, pp 625-635.

11. L. M. Kachanov, "Time of the Rupture Process Under Creep Conditions." Izv. Akad. Nauk. SSR, Otd Tekh. Nauk, No. 8, 1958, pp. 26-31.

12. Y. N. Rabotnov, Creep Problems in Structural Members, North Holland Publ. Comp., Amsterdam-London, 1969.

13. Bueckner, H. F., "Weight Functions for the Notched Bar," General Electric Company, Large Steam Turbine-Generator Department, Technical Report 69-LS-45, 1969.

14. Cruse, T. A. and Besuner, P. M., "Residual Life Prediction for Surface Cracks in Complex Details." Journal of Aircraft, Vol. 12, No. 4, 1975, pp. 369-375.